2024-04

Complementary classifications of aeolian dunes based on morphology, dynamics, and fluid mechanics

du Pont, SC

https://pearl.plymouth.ac.uk/handle/10026.1/22473

Complementary classifications of aeolian dunes based on morphology, dynamics, and fluid mechanics

Sylvain Courrech du Pont [*,1], David M. Rubin[2], Clément Narteau[3], Mathieu G. A. Lapôtre[4], Mackenzie Day[5], Philippe Claudin[6], Ian Livingstone[7], Matt Telfer[8], Jani Radebaugh[9], Cyril Gadal[10], Andrew Gunn[11], Patrick Hesp[12], Sabrina Carpy[13], Charles Bristow[14], Andreas C. W. Baas[15], Ryan C. Ewing[16], and Giles Wiggs[17]

[1]Laboratoire Matière et Systèmes Complexes, Université Paris Cité, CNRS, Paris, France
[2]Dept. of Earth and Planetary Sciences, University of Santa Cruz, Santa Cruz, USA
[3]Institut Physique du Globe de Paris, Université Paris Cité, CNRS, Paris, France
[4]Det of Earth and Planetary Sciences, Stanford University, Stanford, USA
[5]Dept. of Earth, Planetary, and Space Sciences, University of California Los Angeles, Los Angeles, USA
[6]Laboratoire de Physique et Mécanique des Milieux Hétérogènes, CNRS, ESPCI Paris, PSL Research University, Université Paris Cité, Sorbonne Université, Paris, France
[7]The Graduate School, The University of Northampton, Northampton, UK
[8]SOGEES, University of Plymouth, Plymouth, UK
[9]Dept. of Geological Sciences, Brigham Young University, Provo, USA
[10]Institut de Mécanique des Fluides de Toulouse, Université de Toulouse, CNRS, Toulouse
[11]School of Earth, Atmosphere and Environment, Monash University, Clayton, Australia
[12]College of Science and Engineering, Flinders University, Bedford Park, Australia
[13]Laboratoire de Planétologie et Géosciences, CNRS, Nantes Université, Université Angers, Le Mans Université
[14]Dept. of Earth and Planetary Sciences, Birkbeck University of London, London, UK
[15]Dept. of Geography, King's College London, London, UK
[16]Dept. of Geology and Geophysics, Texas A&M University, College Station, USA
[17]School of Geography and the Environment, University of Oxford, UK

September 21, 2023

Contents

---

*sylvain.courrech@u-paris.fr

Abstract

Dunes form where winds blow over a bed of mobile sediment grains – conditions that are common in our solar
system. On Earth, dunes abound in arid continental interiors and along sandy coastlines. Dune fields have also
been recognized on other planetary bodies, including Venus, Mars, Saturn's moon Titan, and Pluto. Despite the
relatively basic conditions required for their formation, dunes adopt a rich diversity of shapes, sizes, and behaviors
in response to their boundary conditions and other environmental forcings. Thus, people around the globe and over
centuries have developed a rich vocabulary to describe dunes and their complexity. In addition, many studies have
been devoted to link dune shape to environmental forcings, usually by means of correlations. As a result, existing
dune nomenclature often includes redundant terms with differing definitions across scientific communities. Although
a worthy first step, correlation-based classifications can be misleading if not based on an underlying mechanics and
if dune morphogenetic classes are not uniquely defined. Here, we synthesize existing dune terminology and put the
last two decades of research on dune morphodynamics in perspective in proposing three simplified dune classification

schemes based on the state-of-the-art understanding of dune morphology, morphogenetic processes and coupling between sand bed, fluid flow and sediment transport. Together, these classifications provide a unified framework for geomorphologists, sedimentologists, geographers, physicists, and others to describe windblown sand dunes on Earth and beyond through their shape, dynamics, and size as a response to winds and boundary conditions.

1 Introduction – Previous Classifications and Aims

Dunes propagate and develop through the action of wind, constrained by other factors such as topography and vegetation. They are not only the result of present winds, but can integrate the history of winds including seasonal wind cycles and longer-term changes. This property helps to explain the richness of shapes and scales observed, and makes dunes witnesses of past winds and conditions. On Earth, dunes are used to study paleoclimates and test global circulation models [1, 2, 3]. The sedimentary structure, shape and orientation of dunes are also used to constrain climate models and the history of celestial bodies such as Venus, Mars and Titan, for which little climate data are available but where dunes are observed [4, 5, 6, 7, 8, 9, 10, 11, 12, 13, 14].

The discovery of planetary dunes and the use of comparative geomorphology make it increasingly necessary to define a dune in terms of physical processes, in particular to compare their sizes in different environments. Such physical definitions are especially critical when, for example, the scales and morphologies of different types of bedforms may overlap.

While sand transport mechanisms, sizes, and characteristic times may be different from one environment to another, dune shapes are similar (Fig. 1). General formation processes seem insensitive to the details of sediment transport, and such over-arching processes tend to prevail in the establishment of dune shape and the development of dune patterns and arrangement within fields. This area of research has advanced considerably in recent years through a combination of field studies, laboratory experiments, and models, and it is now possible to quantitatively relate wind regimes to dune shapes and dynamics.

The purpose of classification is to describe the relationship between different objects in such a way as to simplify these relationships and facilitate generalization [16]. Despite the overwhelming variety of terms used to denote dune types (table 1), there is an assumption that this variety collapses to a much smaller number of common groups, and often that dunes not only look different from each other, but are formed in different ways. Thus classification may help us to use a name to convey morphology and thereby comprehend dune formation processes and dynamics. Defining the categories into which dunes should be classified, however, is challenging. The debate is an old one, and very closely analogous to the long-standing biological taxonomic debates, using Charles Darwin's terms, between 'lumpers' (those that seek to classify into as few categories as possible, allowing for more variability within each class) and '(hair) splitters' (those that tend to permit more categories, but allow for less variability within a class). An ideal classification scheme should be comprehensive, mutually exclusive, internally consistent, unambiguous and easy to use, with morphology providing information about genesis. These ideals can be hard to reconcile when dealing with natural phenomena.

Often, different terms have developed in separate geographical locations for essentially the same phenomenon. In the early days of the study of dune geomorphology, this was perhaps more understandable, as the true global extent of some landforms would have been unknown, and thus locally-used terms were applied to landforms which were new to the eyes of (largely European) science; hence, for instance, the abundance of terms derived from the Arabic language (*e.g.* seif, draa). Yet, in some instances, regional terminology has persisted. For instance, the English-language term 'pyramid dune' (to describe a large dune with multiple crestlines, typically leading to a central highpoint) recently has been used almost exclusively in the Chinese-based literature, and the synonymous term 'star dune' is found more commonly elsewhere.

Early classifications of dunes were based primarily on field-based research, and thus were generally based on work in specific geographical locations, such as Sokolow's work in Russia [22], Melton's work in the High Plains, USA [23], Smith's work in Nebraska [24] and Cooper's work along the west coast of the USA [25, 26]. Some of these early classifications were reviewed by Mainguet [27], but in general remained regional in scope and therefore sometimes lacked more general application. That said, Aufrère did attempt some more global qualitative synthesis, based not only on his own studies in the Algerian Sahara, but also on the work of Vaughan Cornish and Richard Oldham (India), Sven Hedin (central Asia) and Cecil Madigan (Australia) [28]. From the outset, there were frequent endeavours to link formative factors to landform, and one of the first to attempt this semi-quantitatively was Hack, based on his work in northern Arizona, USA [29]. The resultant ternary diagram, based on wind strength, sand supply and vegetation
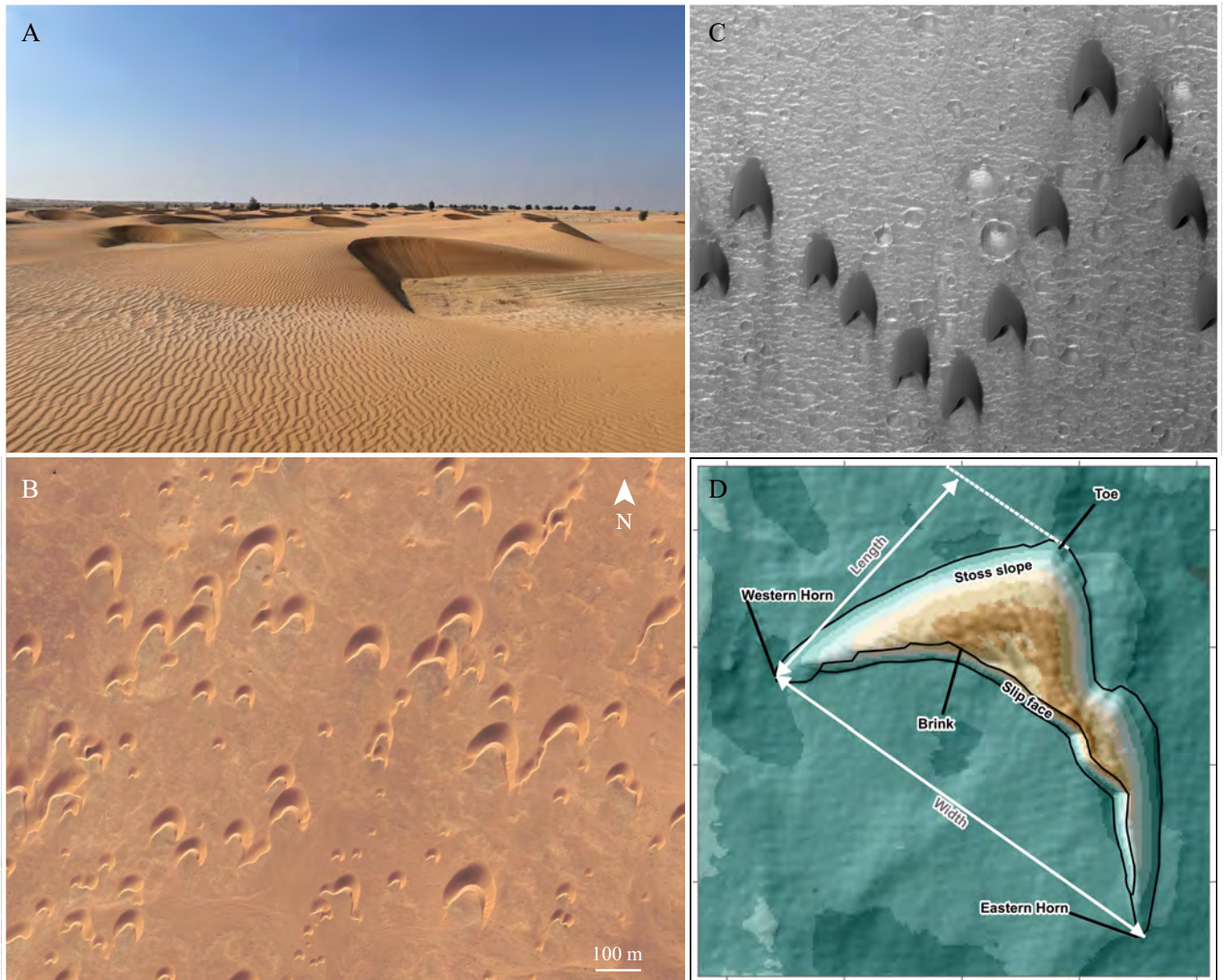
Figure 1: Barchan dunes in different environments. A: Barchan dunes in Oman (20.75°N, 57.611°W). B: Barchan dunes in in Occidental Sahara (26.758°N, 13.378°E), date: 11/2021. C: Barchan dunes on Mars. D: Bathymetry image of a marine barchan dune off the east coast of the UK in the North Sea from [15]. The width scale of the image is 410 m. Credits: M. Lapôtre (A), Maxar Technologies (B), NASA/JPL-Caltech/University of Arizona (C), [15] (D).

cover worked well in that region, but lacked global applicability.

Developing a global (and possibly universal) classification required the global scope that satellite-borne remote sensing provided. The first attempt at a general characterisation of dune forms from global examples was that of McKee and co-workers [18] facilitated by the global coverage of Landsat imagery that became available in the 1970s. McKee also brought a body of work on the internal structure of dunes to this study, which was used to identify sand dune types based on their process of construction. Various versions of the McKee scheme have been subsequently adopted particularly in desert and aeolian geomorphology textbooks (*e.g.* [30]). McKee also introduced a terminology to allow for the co-existence of dunes at different scales [18]: *simple dunes* – single dunes or a single dune type; *compound dunes*, dunes of the same type at two or more scales; *complex dunes*, dunes of more than one type, usually at different scales.

While McKee's classification distinguished a number of fundamental forms on the basis of morphology and internal structure, other classifications, often developed as pedagogic tools for textbooks, have used a branching (dendritic) structure to show the interrelationships between dune types. The first of these was developed by Pye and Tsoar ([19],

abyssal	aklé	anchored	barchan	barchanoid
blowout	chaots	chequerboard	chevron	clay
clifftop	climbing	complex	compound	coppice
crescentic	demkha	dome	draa	echo
ellipsoidal	elongating	embryo	falling	foredune
free	frontal	ghourd	hairpin	hummock
lee	linear	longitudinal	lunette	megadune
nail	nebkha	network	oblique	obstacle
oghroud	pancake	parabolic	parallel	pyramidal
phytogenetic hillock	polygonal	precipitation ridge	raked	relic/relict
retention ridge	rhourd	sand massif	sand mountain	sand ramp
shadow	seif	simple	snow	source-bordering
star	stellate	straight-crested-asymmetric	teardrop	terminal
transverse	true	unvegetated	vegetated	zalib
zibar				

Table 1: Dune type terminology. Terms are drawn from a number of English-language sources, although some terms used in English originate from other languages. Key sources for terms are [17, 18, 19, 20, 21].

p.162, Fig 6.7) and was subsequently modified by Cooke *et al.* [31] and then by Livingstone and Warren [17]. Each of these versions uses the distinction between *free* and *anchored* dunes as a starting point. *Free dunes* (called "true dunes" by Bagnold ([32] p.188) exist because of a lack of inhibition to the movement of particles. These are fundamental bedforms. Conversely, *anchored dunes* (which Bagnold termed "sand shadows and sand drifts") owe their existence to the presence of an inhibition to particle movement, most usually topography or vegetation (see review by Hesp and Smyth p. 157-178 in [17]).

At the heart of geomorphological studies of dune form is the relationship between morphology and wind regime. The work of Wasson and Hyde [33], evaluated by Bullard and Livingstone [34], was a first attempt to use empirical data (largely from Australia) to distinguish dunes on the basis of available sand (measured by Wasson and Hyde as an estimate of the depth of available sand if spread as a sheet of uniform thickness) and the directional variability of the wind regime. Although this pioneering work provided a useful scheme for future studies, the limited data (largely from Australia), resulted in restricted ranges of dune type. Consequently, the results suggested that longitudinal dunes were restricted to areas with little sand. Using the same general approach, Livingstone and Warren [17] and Bishop et al. [35] revised this conclusion and showed that linear dunes can form where sand coverage is extensive. This scheme was subsequently adapted as the basis for a classification by Lancaster who added his own data from a wider range of sand seas to that of Wasson and Hyde [36, 37]. Lancaster added "other key parameters" to sand supply and wind regime.

Although many schemes have related dune form to the 'resultant' wind directions or sand-transport directions, Hunter *et al.* [38] and Rubin and Hunter [39, 40] were keen to point out that terminologies, and therefore classifications, implying those relationships were problematic. Their contention was that dunes can form with orientations that are neither parallel nor perpendicular to the resultant transport direction. Thus, it is misleading to use terms such as longitudinal and linear interchangeably: *linear* denotes a form in which one planform dimension greatly exceeds the other and is therefore a morphological description, whereas *longitudinal* implies an orientation that is approximately parallel to net sand transport. Many linear dunes are not aligned with the resultant transport directions but are oblique, *i.e.*, the planform long axis is at 15-75 degrees from the resultant sand transport direction [38]. Rubin and Hunter showed that dune orientation where the bed is fully covered with sand does not depend on the resultant transport direction, but on what they termed gross bedform normal transport [40]. The more recent experimental and theoretical work of Courrech du Pont et al. bridged the gap between the older studies that classified dunes at least partially on the basis of sand availability, and the new studies that showed that dune orientation is controlled by two mechanisms, one of which dominates where the bed is fully covered with sand and the other where the bed is partially starved [41].

Although many of the classification schemes discussed so far owe their origins to inland desert dunefields, throughout this period there was also development of an understanding of coastal dunes, as well as increasingly sophisticated work

from the physics community aimed at understanding fluid entrainment, transport and deposition of granular materials and their coupling with the topography. Despite the fundamental process similarity between coastal and desert environments highlighted by the physical modeling of dunes, some differences in nomenclature had begun to emerge. Thus, whilst parabolic and transverse dunes were frequently discussed in both desert and coastal literature, the term *foredune* is reported almost exclusively from the coastal dune domain (*e.g.* [42]). Conversely, the term *source-bordering dune* [43], common in the desert literature to refer to a dune owing its existence to an immediately adjacent sediment supply – which might be said to apply to any coastal dune if it evolves from the backshore like foredunes – is almost absent from the coastal literature.

The observation in the early 1970s of dunes on Mars, tentatively from Mariner 6 [44] and more definitively from Mariner 9 [45], opened new opportunities and challenges in dune classification. The subsequent discovery of aeolian bedforms on at least six other solar system bodies (the process of their discovery is reviewed in [46]) emphasizes the seeming near-ubiquity of dunes and other bedforms – indeed, they have so far been found on every solid planetary body with an atmosphere, and some where the 'atmosphere' is at best extremely tenuous. There is something of an irony in that in each case, landforms were identified as dunes by analogy with identified, and classified, terrestrial dunes, and yet in some instances, the planetary dunes have thrown up additional complications for classification. For instance, on Mars, barchans were one of the first types of dunes to be identified, and yet we now know there is greater morphological diversity of Martian barchans than those on Earth, and some Martian dune morphologies do not readily fit into McKee's, or subsequent, classifications [47].

This study aims to provide a comprehensive classification of dunes that can form the basis for a nomenclature that can be used both with terrestrial and extra-terrestrial systems, building on recent advances in the understanding of those systems. We propose a new classification of dunes through three distinct and complementary classification-tree diagrams that when combined should answer the fundamental questions of how to describe a shape, relate dune shape and size to the external constraints (the wind regime, the environment and the boundary conditions), and infer the dune dynamics. The first tree is based on dune morphology where a step-by-step recognition of shapes, possibly interacting with their surroundings, discriminate the main dune types (Section 2). This tree is connected to the second tree, which is based on mechanisms of dune growth and dynamics that links the shapes to external constraints through morphogenetic processes (Section 3). The third tree is based on the fluid mechanics and sediment transport, which set the characteristic scales and the range of possible sizes that can occur in different planetary environments (Section 4). We illustrate the practical use and relevance of those three classifications through several case studies and examples (Section 5). These different classifications involve many concepts and parameters. We present the main ideas as necessary in the description of the trees and refer to appendix (Section 7) for detailed development and explanation. It is our intention that together these classifications will lead to a convergence in understanding dune-forming processes and dynamics and will provide a platform and nomenclature for future dune studies on Earth and beyond.

2 Classification of aeolian dunes based on dune morphology

2.1 Purpose and approach

The morphology of a dune encompasses the three-dimensional geometry defined by the bedform surface. The readily observable characteristics of dune morphology have been the bedrock of previous dune classification schemes (Section 1) and can be investigated either from the ground level, or using aerial photography or satellite imaging. Importantly, classifications based on dune morphology do not require *a priori* knowledge of the local winds. We assembled here a morphology-based dune identification tree (Fig. 2) that aims to assist in the categorization of a given dune based on its observable shape, including crestline morphology in plan-view, and environment. The tree is structured with the goal that someone with introductory training in geography, geomorphology, geology or other related disciplines could identify dune type by answering the series of questions posed in the tree. We attempted to keep the number of questions to the minimum necessary to discriminate between the different types of dunes.

The categorization tree in Figure 2 is appropriate to the majority of dunes found in nature. Rather than encompassing all possible cases, including niche situations or exotic environments, the classification tree aims to broadly categorize and include the very large majority of the dune types found on Earth (Section 2.3.1 for discussion of planetary applications and special cases).

Sandy Surface

Are there distinct shapes?

No — Sand sheet

Yes — Dune

Is there more than one fundamental shape?

Yes — Superimposed (*compound, complex*). Iterate classification for each scale starting with the largest.

No

Is there an association with vegetation, obstacle, or pan/playa?

No — Free dune. *Usually associated with ergs, sand seas, or transgressive dunefields*

What is the form?

- Long | Arcuate — Barchan dune (*crescentic*)
- Round/Hemispheric — Dome dune
- Mesh/Lattice — Network dune (*aklé, chequerboard, chaot, polygonal*)
- Stellate — Star (*pyramid*)

What is the shape of the cross section?

- Symmetry or low asymmetry — Linear dune
- Strong asymmetry with full slipface

  Is the crest sinuous?
  - Yes — Barchanoid dune
  - No — Straight-crested asymmetric dune

- Low relief, no slipface, coarse grained? — Zibar

What is the orientation of the crest with respect to the net sand flux direction?
- Perpendicular — Transverse dune
- Oblique — Oblique dune
- Parallel — Longitudinal dune

Yes

- Vegetation

  Does the dune have a discrete plant at its core?
  - Nebkha (*coppice*)

  Formed in continuous vegetation on the backshore? — Foredune

  Is there an erosional hollow with depositional lobe attached? — Blowout

  Does the dune have trailing ridges? — Parabolic dune

- Pan/playa — Lunette (*clay dunes*)

- Obstacle — Obstacle dune

  Is it on a slope?
  - Yes

    Does it extend up or down slope?
    - Up — Climbing dune
    - Down — Falling dune

  - No

  Where is it in relation to the obstacle?
  - On top — Clifftop dune
  - Up-wind — Echo dune
  - Down-wind — Lee dune (*shadow dune*)

No knowledge of wind regime required
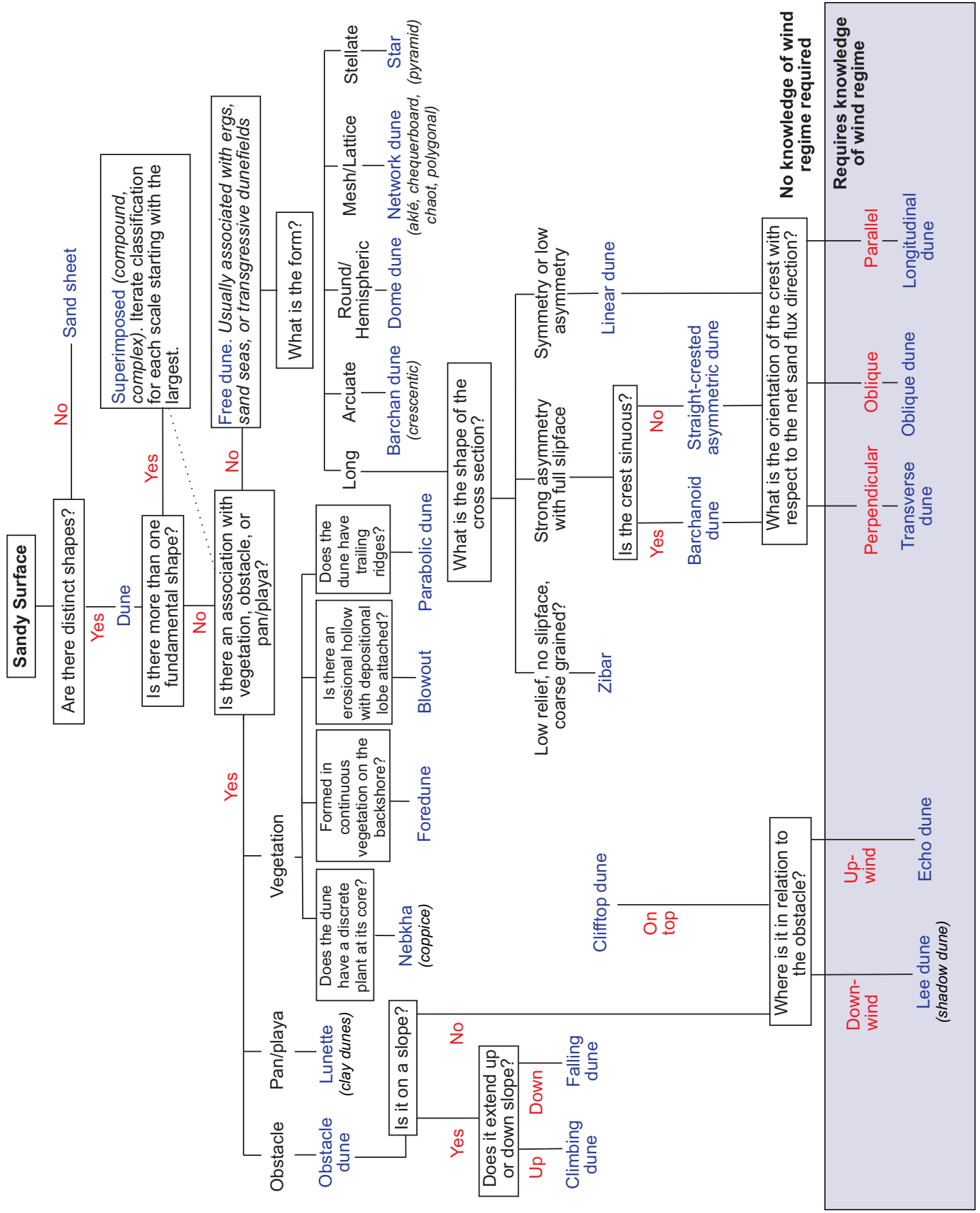
Requires knowledge of wind regime

Figure 2: Identification tree for dune classification based on morphology.

7

2.2 Tree description – Selection of dune type from shape and interactions with surrounding landscape

Below is a walkthrough of the tree in Figure 2, highlighting some nuances in the classification where additional description is helpful. We start by requiring a sandy surface, and immediately differentiate between dunes and non-dunes (*e.g.*, sand sheets) using the presence of distinct shapes, and from there use observations about the morphology in plan-view to determine dune type. Although the vertical morphology of dunes holds important information, the plan-view morphology of dunes exhibits more significant global variability and is both more diagnostically useful and more convenient in part because planform morphology is readily visible in remotely sensed images. In addition, we refer to the crestline of a bedform, which loosely follows the planform morphology. Crestlines are defined by topographic high points along a dune's upper surface and along with brinklines (*i.e.*, the often sharp transition from stoss to lee face), can be easily observed in aerial images. Once the dune type has been identified, it may imply information about the local wind regime. The inferred wind direction and/or variability is based on previous research and helps connect the identification in this tree to the growth mechanisms and fluid dynamics outlined in the other two classification trees in this work. Dunes may occur in desert sand seas and ergs [48, 49], on beaches of all kinds (*e.g.* on ocean shores, lake shores, playas, rivers and estuaries), and on coastal transgressive dunefields (coastal sand seas or ergs). For sandy surfaces with distinct shapes (dunes), the classification is intended to be applied to a single one of these shapes (morphologies). In many cases, these shapes are likely repeated in the immediate vicinity to form a dunefield. Dunes exhibiting similar shapes at different scales or multiple shapes at different scales are considered compound or complex dunes, respectively, and each morphology and scale can be interrogated separately.

Dune types are differentiated by the immediate non-dune boundary conditions that influence the dune morphology. Dunes whose morphology is integrally related to the presence of a local obstacle, vegetation, or playa are differentiated from dunes not directly related to such specific boundary conditions. Although any dune is influenced by boundary conditions such as local topography, water table, and vegetation [50, 51, 52, 21], we only consider dunes where these local conditions are clearly related to or control the morphology, and consider all other dunes *free dunes*. The former are more commonly found in local settings (*e.g.*, coastal systems, lakes, estuaries, rivers, playa margins), whereas the latter are more likely to populate extensive dune fields, ergs, and sand seas (*e.g.*, as seen in the Rub' al Khali [18, 53], or Taklimakan deserts [54] and in many coastal transgressive dunefields [42]).

2.2.1 Free dunes

Free dunes (Figs. 1 & 3) are further subdivided based on their plan-view shape. Stellate morphologies with many arms in radial patterns are considered *star dunes*. Mesh or lattice patterns in dune crests indicate *network dunes*. Many other terms for this morphology also exist, but their defining characteristic is always a network of dune crests crossing one another, commonly at near perpendicular angles and at similar scales. Isolated dunes with arcuate shapes, sometimes called crescent- or half-moon shapes, are *barchan dunes*. Mound-shaped, round, and hemispheric sand bodies are called *dome dunes*. Round landform structures may also develop on sand sheets in early stages of development. These proto-dunes are differentiated from dome dunes by low heights and attachment to a sand sheet source. Proto-dunes are not included in the categorization tree because as transitional features between sand sheets and dunes they may not be identifiable as distinct shapes. However, we note them here for disambiguation and completeness [55, 56, 57, 58].

The remaining categories of free dunes are all morphologically 'long', meaning their length to width ratio is high and the crestline continuity in plan-view is large with respect to the bedform width or wavelength. The term 'elongate' was avoided given the use of the term in the dynamical process-based dune classification (Section 3). To differentiate between dune types with long morphologies in plan-view, additional information is needed on the shape of the cross section and in particular on its symmetry with respect to the crest line. Dunes with a symmetrical or slightly asymmetrical normal-to-crest profile are referred to as *linear dunes*. In dunes with some slight asymmetry in cross section, a slip face may be locally present. Linear dunes by definition exhibit long, straight-crested morphologies. Dunes whose cross section has a strong asymmetry with an extended slip face on one side are *barchanoid dunes* if the crest line is sinuous and simply *straight-crested asymmetric dunes* if not. Long dunes with low relief and coarse grains not developing a slipface are termed *zibars* [59, 60, 61].

Morphologically long dunes can be further classified according to their orientation with respect to the net transport direction. We note that the wind direction discussed when categorizing aeolian dunes should refer specifically to the direction of sand-transporting winds, as sub-threshold winds will not contribute to the mobilization of sand or, therefore, dune development (Section 7.2). Dunes whose crest is perpendicular to the net transport direction are
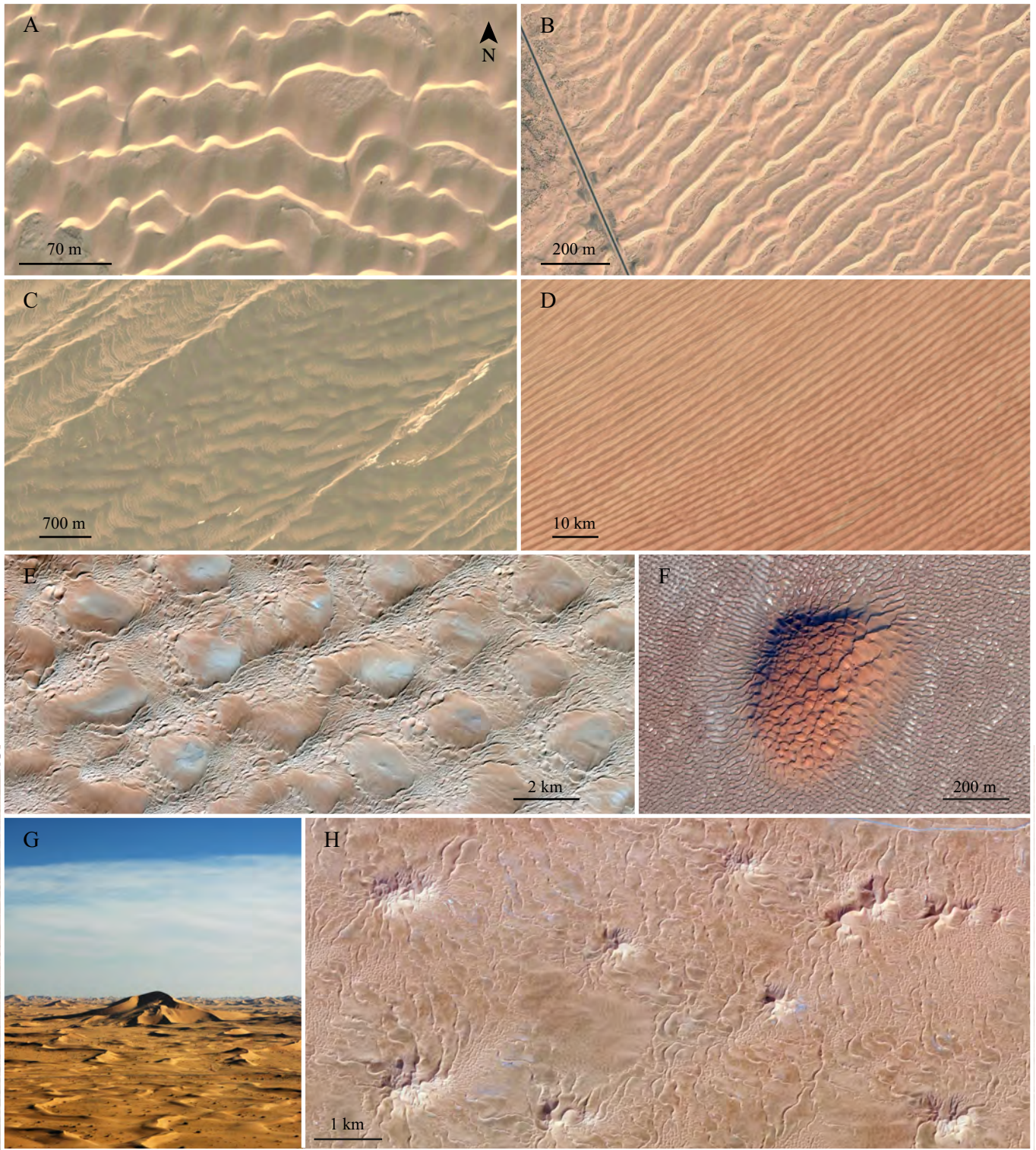
Figure 3: Free dunes. A: Barchanoid ridges in Occidental Sahara (27.166°N, 13.29°E), date: 11/2018. B: Straight-crested asymmetric dunes in the Mu-Us desert in China (38.756°N, 107.936°E), date: 3/2011. C: Zibars (low relief dunes between linear dunes) in the Kumtagh desert in China (40.33°N, 92.655°E), date: 3/2021. D: Linear dunes in the Rub' al Khali desert (18.39°N, 48.058°E), date: 12/2016. E: Network dunes in Libya (25.136°N, 13.082°E), date: 9/2016. D: Dome dune in Oman (18.522°N, 53.549°E), date: 11/2014. G,H: Star dunes in Algeria (31.427°N, 7.302°E), date: 8/2012 (H). Credits: Maxar Technologies (A, B, E, F, H), CNES/Airbus (C), Landsat Copernicus (D), P. Claudin (G).

termed *transverse*. Those that are oriented parallel are referred to as *longitudinal*. *Oblique* dunes are in between. Previous work proposed that oblique dunes be defined differing from parallel or perpendicular orientations by more than 15 degrees [38, 40]. Such denominations are not morphological in nature. However, linear dunes typically develop in wind regimes that are bi-modal to multi-directional and have parallel or oblique orientations (Section 5.2.2) [40, 62, 63, 41, 64]. In some singular cases as in reversing flows, their orientation may be transverse analogous to wave ripples or tidal sand waves [65]. Typical barchanoid or straight-crested asymmetric dunes are transverse and develop slipfaces along some or all of the downwind side of their crests, allowing for identification of the dominant sand-transporting wind direction from aerial photograph/satellite images or surface observation.

2.2.2 Dunes coupling to their surroundings

Dunes not considered as free dunes (*i.e.*, those with morphologies controlled by local material boundary conditions) are subdivided into morphologies related to vegetation (Fig. 4), obstacles, or playas and pans (Fig. 5).

Although any dune type can become vegetated (*e.g.*, the Nebraska Sand Hills [66] and most coastal dune systems [42]), here we specifically require that the vegetation be morphologically intrinsic to the dune [67, 68, 42, 21]. For example, *nebkha dunes* form with a core of vegetation and develop as the vegetation traps sand by slowing winds while also continuing to grow in place [69, 70]. Various other terms have been used to describe discrete dunes formed in isolated plants such as coppice dunes, bush mounds, nabkha, phytogenetic hillocks, and others [70]. Dunes that are formed by aeolian sand deposition in semi-continuous to continuous vegetation in coastal backshore systems are considered *foredunes* [71, 72]. Note that nebkhas commonly form along the backshore of semi-arid to arid coasts and may also be considered foredunes in these systems [73, 74]. Dunes that form principally by erosion within vegetation forming erosional bowls, troughs, saucers (and other shapes) are called *blowout dunes* (or simply *blowouts*) [75, 72]. Blowouts normally display downwind attached depositional lobes thereby fulfilling the definition of a dune; defined by Bagnold [32] as 'a mound or hill of sand which rises to a single summit" (p. 188). Note that erosional depressions in the absence of a depositional lobe may also be referred to as blowouts, but then do not meet the definition of a dune. *Parabolic dunes* develop when vegetation stabilizes the lateral margins of the depositional lobes, causing them to develop U- or parabola-shaped (sometimes V-shaped) crestlines and plan view shapes. Parabolic dunes display short to long trailing ridges whereas blowouts do not have trailing ridges [21]. The trailing ridges in the parabolic dunes point in the opposite direction to the avalanche face, rather than in the same direction, as is the case with barchan dunes.

Although dunes are almost exclusively formed from sand-sized grains, dunes may form with significant clay and silt fractions along the margins of playa, salt lake, and evaporitic pan systems. Much of the clay and silt can occur as sand-sized aggregates that behave dynamically as sand grains. These dunes are intrinsic to the pan/playa and have been termed *clay dunes* and *lunette dunes* [76, 77, 78]. The term lunette is preferred here.

Finally, wind and, therefore, aeolian sediment transport respond to topographic obstacles, sometimes generating dunes with morphologies tied to that topography. We refer to these collectively as *obstacle dunes* and differentiate between them using the underlying slope, proximity to an obstacle, and direction of the wind [80]. As with some free dunes discussed earlier, assessing the sub-type of an obstacle dune requires either knowledge of the sand-transporting wind direction, or an inference based on the morphology of the dune. *Climbing-* and *falling dunes*, found on slopes less steep than the angle of repose, may or may not exhibit slip faces, but develop in response to sediment transport up- and down slope, respectively. Note that the use of 'climbing' in the geomorphic classification of dunes is distinct from the stratigraphic use of the term (*e.g.*, climbing ripple structures, or bounding surfaces with an angle of climb) which refers to bedform migration accompanied by net deposition. Depending on the local boundary conditions, dunes can also form immediately upwind, downwind, or on top of a topographic obstacle that diverts the wind. Once the position of the dune with respect to the wind direction and the obstacle is known, the dune can be identified as either an *echo dune* (upwind of the obstacle, and approximately echoing the planform or morphology of the adjacent feature), *lee dune* (downwind of the obstacle), or *clifftop dune* (on top of the obstacle). We note that the obstacles controlling dune development in this case are broadly defined. For example, echo dunes might form at the base of scarps, in front of and along the margins of small to large boulders or obstacles, and lee dunes (including shadow dunes) form downwind of obstacles (including vegetation and nebkhas). However, climbing-, falling-, and clifftop-dunes all require topographic slopes to form.

10
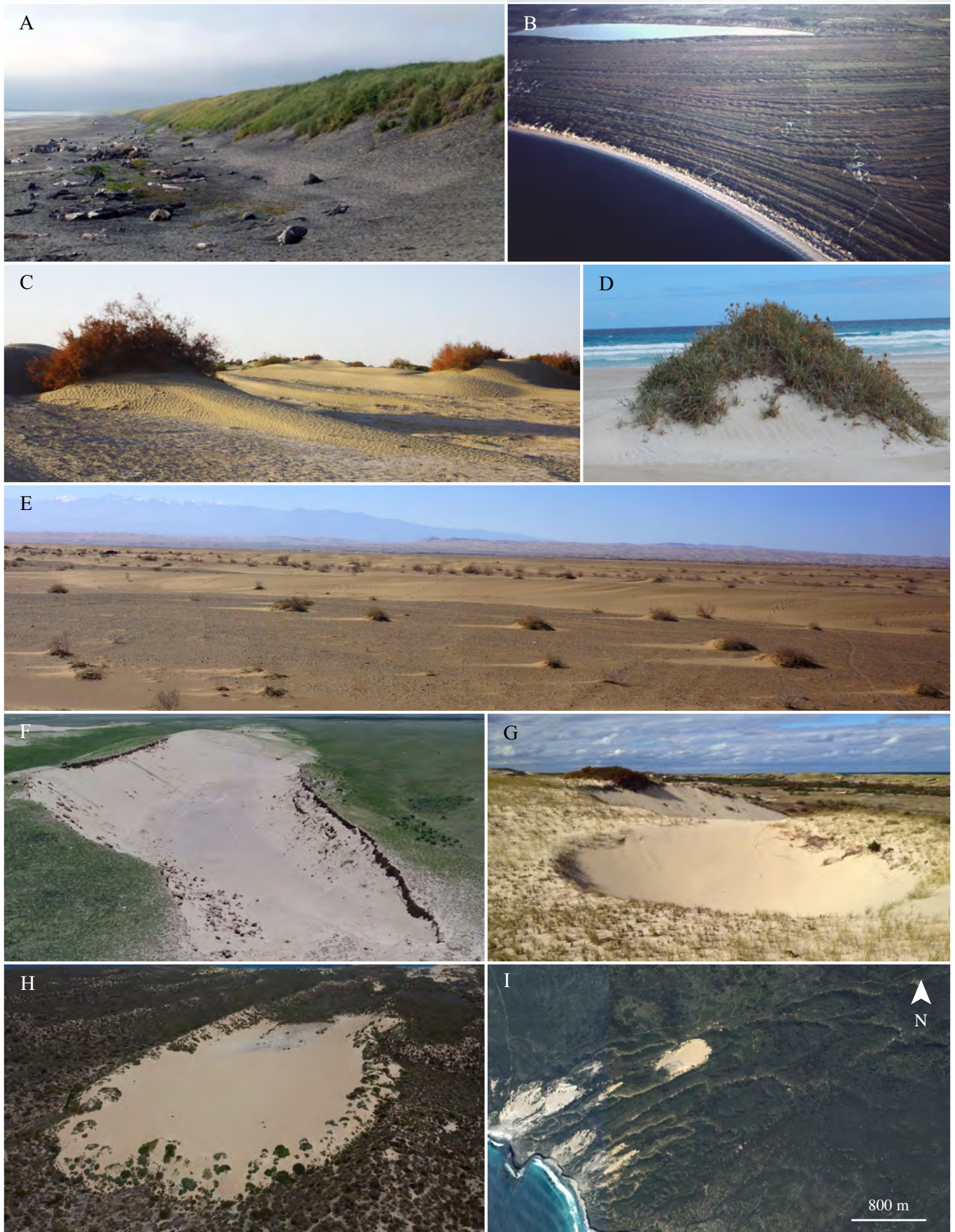
Figure 4: Dunes associated with vegetation. A: Foredune at Fort Steven, Oregon (46.182°N, 123.982°W). B: Foredune plain comprising multiple foredunes formed by coastal progradation. C-E: Nebkhas. F: Trough blowout 12 m deep and 600 m long on the Tibet plateau (35.992°N, 100.415°E). G: Bowl blowout 3 m deep at Cape Cod (42.075°N, 70.189°W). H & I: Parabolic dune in south Australia (34.912°S, 135.89°E) in 9/2016 (I) . Credits: C. Bristow (A), P. Hesp (B, D, F, G, H), C. Narteau (C, E), CNES/Airbus (I).
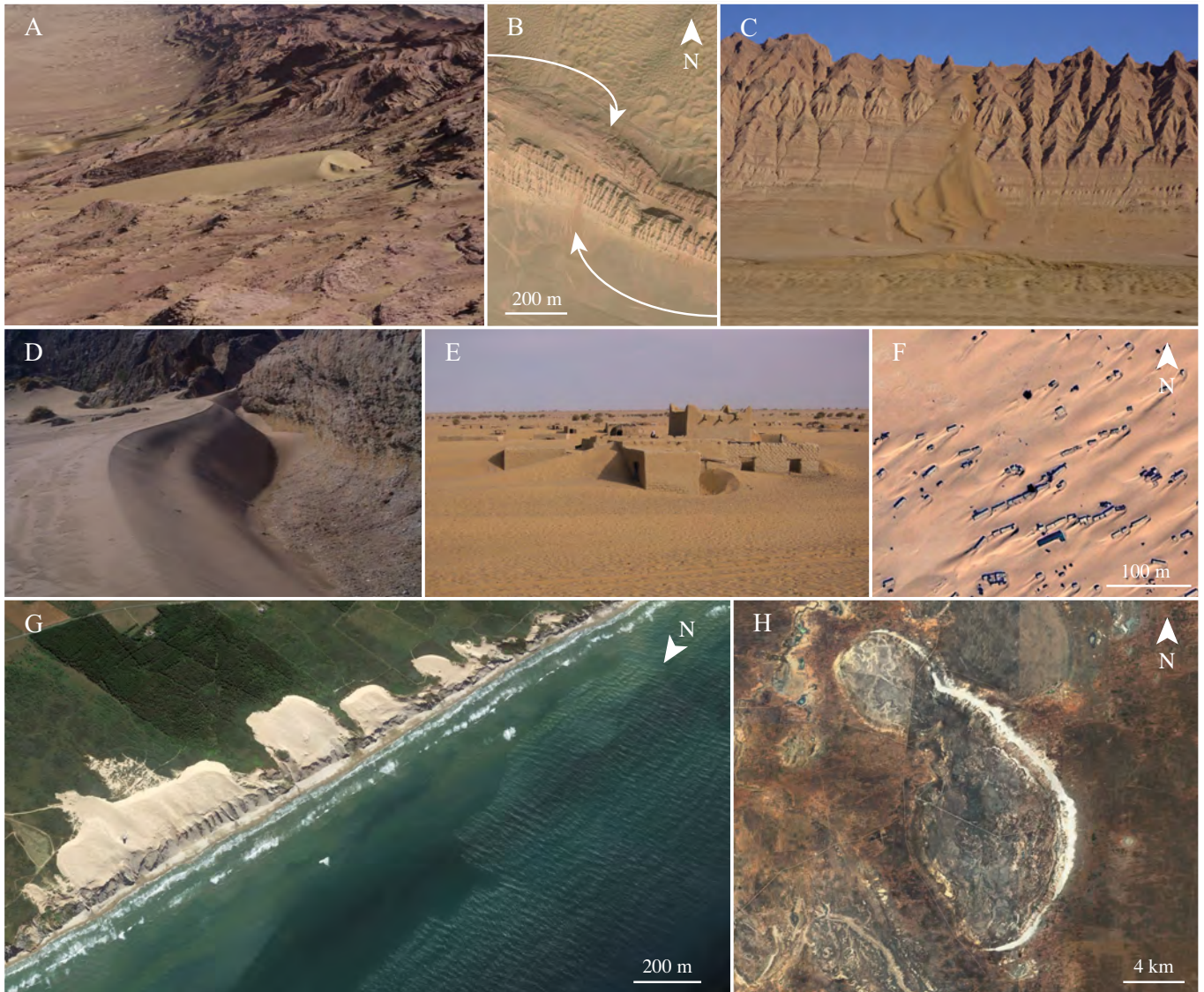
Figure 5: Dunes in association with an obstacle or pan. A-C: Climbing (A) and falling (C) dunes on either side of Mazartagh mountain range (38.676941°N, 80.378328°E) (B, date: 09/2019). D: Echo dune at Castlepoint, New Zealand (-40.9°, 176.23°), date: . E: Lee (downwind, left) and echo (upwind, right) dunes on either side of a building from Kouba Olanga in Chad, date: 2005. Panel F shows the context (15.75°N, 18.3°E), date: 01/2006. G: Cliff-top dune in Rubjerd Knude, Denmark (57.439336°N, 9.768589°E), date: 07/2021 [79]. H: Lunette dune bordering (now dry) Lake Mungo in Australia (33.74°S, 143.13°E), date: 02/2023. Credits: C. Narteau (A, C), CNES/Airbus (B, H), P. Hesp (D), C. Bristow (E), Maxar Technologies (F), Terra Metrics (G).

2.3 Discussion

2.3.1 Scope of the morphology-based classification

The morphology-based identification tree in Figure 2 is intended to encompass the majority of aeolian dune types observed on Earth. Other aeolian bedforms, including many varieties of ripples (*e.g.*, impact ripples, megaripples, granule ripples) are not included. Not every name for every type of dune is represented in the geomorphology tree. In a perusal of recent literature, we identified more than 50 different terms for types of dunes (table 1). Many of these terms were duplicative, or specific to niche environments or localities. To combat some of the confusion that arises from so many terms, in Figure 2 we note some equivalent terms in black below the dune identification in blue. In the future, we encourage the community to converge on the use of a single term for a given dune type, but here we

include the duplicative names in this work for reference. Because dune type recognition can be aimed to infer wind regimes and environmental constraints, we avoided using dynamical properties or we included them at the end of the classification. For example, we did not include the commonly used term *reversing dunes*. This term can be added to further define a dune. A dune undergoing and integrating successive inversions generally does not have a fully developed avalanche face on one side only.

Although the geomorphic dune identification tree was developed with terrestrial aeolian dunes and dune examples in mind, the tree can be applied to dunes in any system or on any planet. Aeolian bedforms are known to develop on many planetary bodies in our solar system, including Venus, Earth, Mars, Titan, Pluto, Io, and Comet 67P [8, 81, 46, 82, 83, 84]. In most cases the morphologies of dunes observed on other planetary bodies are similar to those observed on Earth [7, 85, 86, 82] and the tree in Figure 2 can be easily applied to these systems. Some planetary aeolian bedforms have debatable analogs on Earth. For example, transverse aeolian ridges [87, 88] and large ripples [12, 89] are both abundant on Mars, but bedforms of similar scales and morphologies are comparatively uncommon on Earth. Large martian 'ripples' have no known direct analog among the many kinds of aeolian ripples on Earth, none of which are included in this geomorphology-based classification tree. However, transverse aeolian ridges (TARs) on Mars can be several meters high and would be considered by this classification to be transverse dunes, though dynamically the processes forming each might be quite different. The application of the geomorphology tree to planetary systems must be done with appropriate caution and context. Together with the other two trees, the tree based on dune morphology will facilitate interplanetary comparison in future research and limit terminological confusion in the literature.

2.3.2 Wind direction and variability inferred from morphology

The classification based on dune morphology does not require prior knowledge of the local wind direction, except in some cases when it is needed to disambiguate between sub-types. However, decades of research studying the relationship between dune morphology and local winds has allowed us to make inferences about the local wind direction when a given morphology is observed (*e.g.*, [32, 40, 62, 90, 41, 64]). As noted above, slipfaces develop on the net downwind side of dunes, providing a morphological indicator of the leeward side of dunes with slip faces that are fully developed on one side only.

Asymmetry in planform or cross-section in the morphology of a dune can also provide some information about the local wind variability. For example, barchan dunes with dissimilar horn lengths form when two winds with an obtuse divergence angle have differing strengths [91, 92, 64, 93, 94]. In barchanoid dunes, lee-side spurs that are asymmetric in plan form (skewed rather than transverse to the main dune) indicate the main dune is asymmetrically oriented relative to the winds (*i.e.*, not entirely transverse). Similarly, lee-side spurs that are perpendicular to the main crests but are asymmetric in cross-section (having a steep lee side and gentle stoss side) indicate net transport parallel to the lengths of the main dunes, thereby demonstrating that the main dunes are not perfectly transverse. Net transport parallel to the crests of the main dunes can also be inferred from orientation of asymmetric peaks, saddles, or superimposed dunes enabling significant complexity to be disentangled from observed dune morphologies [95, 39, 40, 96, 41]. Superimposed dunes are common on linear dunes that can form with kilometer-scale wavelengths and large enough widths to host subordinate dunes on their surfaces [97]. Specifically for long-crested dunes, the transverse and longitudinal symmetry/asymmetry indicates whether the transverse and longitudinal net transport, respectively, is zero or greater than zero.

This general approach has been applied to identification of deposits of transverse, oblique, and longitudinal dunes in the stratigraphic record [95, 39, 98]. Stratigraphically, the approach is applied by determining whether the main dunes migrated laterally or aggraded in place and whether or not the superimposed topographic features such as dunes, spurs, peaks, and saddles migrated in a preferred direction along the lengths of the main dunes. Deposits of a perfectly transverse dune preserve migration of the main dune without a preferred along-crest migration direction of superimposed features; perfectly longitudinal dunes aggrade in place with superimposed features migrating consistently in the same along-crest direction; and deposits of oblique dunes preserve both lateral migration of the main dune and consistent along-crest migration of superimposed features.

Here we suggest that the same general approach can be used to distinguish transverse, oblique, and longitudinal dunes using asymmetry rather than stratification to infer migration of the main dune and superimposed features (Table 2.3.2). This approach comes with three limitations. First, it can only be applied where the main dune has superimposed topography. Second, both the main dune and the superimposed bedform must integrate the wind regime. Although some dunes are small enough to re-form seasonally, here we are restricted to dunes that coexist and persist through complete cycles of flow [99]. Third, the determination of dune type may not necessarily match the definition of Hunter, Richmond, and Alpha [38]. Specifically, dunes that meet the geomorphic criteria of oblique dunes (Table 2.3.2) might have orientations outside the defined range of 15°to 75°relative to the net transport direction.

Nevertheless, this approach can identify dunes that are qualitatively neither transverse nor longitudinal, and it can do so using only morphologic criteria as shown in Section 5.3. The same information required to classify dunes as transverse, oblique, and longitudinal can be used to infer the net sand transport direction relative to the main dunes. Where dunes meet the geomorphic criteria of transverse or longitudinal dunes, the net sand transport direction is perpendicular or parallel to the dune crests, respectively. Where dunes are oblique, the net transport direction is constrained to the quadrant bounded by the migration direction of the main dunes and the direction of migration of superimposed features along the crests of the main dunes. These directions of migration are derived from the dip direction of the slipfaces. Note that these two migration directions are only used to constrain the net transport direction; the two migration directions do not necessarily correspond to two formative winds.

Across-crest (transverse) symmetry or asymmetry (identified by cross-section profile)	Along-crest (longitudinal) symmetry or asymmetry (identified by symmetry or asymmetry of superimposed topographic features such as peaks, saddles, crest sinuosities, spurs, or superimposed dunes)	
	Along-crest symmetrical	Along-crest asymmetrical
Across-crest symmetrical	Zero net transport in both the across-crest and along-crest directions suggests formation by opposed equal winds; singular conditions with zero net transport (analogous to some wave ripples)	Longitudinal dunes (net along-crest transport with no net across-crest transport)
Across-crest asymmetrical	Transverse dunes (net across-crest transport but no net along-crest transport)	Oblique dunes (net across-crest and along-crest transport)

Table 2: Identification of transverse, oblique, and longitudinal dunes based on symmetry/asymmetry of main dune and superimposed features.

When considering multiple related dune morphologies, perhaps occurring at different scales, it is important to consider the timescales of formation and how they compare to the time period of the wind regime. Smaller dunes migrate faster than larger dunes, and change morphology in response to a change in wind regime faster than larger dunes [32, 100]. The most recent winds are reflected by the smallest bedforms (all the way down to wind ripples), and larger and larger dunes reflect wind regimes as integrated over longer and longer timescales. Different scales also frequently differ in orientation or morphology for reasons other than changes through time in wind regime. The larger dunes may modify the apparent winds for smaller superimposed or adjacent dunes, or the different scales may interact [99, 101]. Often, the different scales experience different boundary conditions. For example, the main dune may extend on bedrock while the superimposed ones develop on the underlying main dune, *i.e.* a sand bed. Orientation and morphology of both the main dune and the superimposed ones then provide information about winds and potentially help differentiate between longitudinal and oblique dune types [41, 102]. Additional discussion of the relationship between morphology and process is provided in Section 3.

2.3.3 Dunefield patterns and changes in dune type

The geomorphological identification tree deals with individual dunes and their morphology, but dunes in nature are rarely found in isolation. More commonly, many dunes form a field, and that field may vary spatially in the morphology and size of individual dunes. Boundary conditions that change spatially (*e.g.*, sediment supply, antecedent topography, water table, vegetation) can cause variability in the morphology of the dunes [103, 104, 21]. Similarly, dunefield patterns mature spatially and in time, with dunes becoming larger and more widely spaced as they develop and migrate downwind [105]. With time, almost all dunefields and dune systems can be fully stabilized and many other dune forms can develop as a result of vegetative stabilization [106, 107, 42, 108]. Dunefield patterns are fundamentally constrained by these local boundary conditions, but changes in that pattern are also driven by time and interactions between the bedforms [109, 110, 111]. These interactions can act at different scales and be of different kinds, *e.g.*, aerodynamic in nature, a dune modifying the flow in its vicinity, or concern directly the mass exchange (sand loss and capture or collisions) [112, 113, 100, 114]. For example, in barchan dune fields, smaller dunes migrate faster than larger dunes, resulting in small upwind dunes colliding with slower downwind dunes. When colliding, dunes may split or merge leading to size regulation and spatial organization within the field as in dune corridors [113, 114, 115, 100, 116, 117, 118].

14

Barchan dunes may also link together to form barchanoid ridge dunes, which is an overall change in the morphology of dunes in the field. It is rare to find a dune field composed of a single dune morphology in deserts, although it does occur more frequently in coastal dunefields (*e.g.*, on Earth there are multiple examples of foredune plains, and parabolic dunefields), and just as the morphology of a single dune can help determine information about the local winds and sediment state, interpreting the dune morphologies of a field in aggregate, the spatial succession of forms and types, can yield important information about the larger system [119, 120], as exemplified by the case study in Section 5.

3 Classification of aeolian dunes based on dune dynamics

3.1 Purpose and approach

Aeolian dunes exhibit a wide variety of forms, and geomorphologists have wondered for more than a century what processes control this variability. The goal of this classification is to link the various dune types (bottom row in Figure 6) with the formative processes in a dune field (upper rows in Figure 6). Specifically, we propose a tree structure to identify the dynamical processes by which dunes are built and aligned according to wind regime, sand availability, and other boundary conditions. This dynamics-based tree diagram thus links dune type to the sediment and wind conditions, allowing for both forward modeling of dune morphologies in specified conditions (top-to-bottom) or inverse interpretation of observed dune morphologies (bottom-to-top). The case studies in section 5.2 complete and illustrate this classification based on dune dynamics and link it to the classification based on morphology (Figure 2).

The dynamics-based classification reflects the state of the art of the physical understanding of dune morphodynamics derived from field observations, laboratory experiments, numerical simulations, and theoretical studies. Based on these physical insights, environmental conditions are intentionally simplified or conceptualized, and cannot cover the whole range of complexity observed in nature. In such a process-based approach to dune classification, we consider that dunes types and general morphologies are in dynamic equilibrium with environmental conditions. Other factors such as interactions between dunes, *e.g.* collisions, modify these general morphologies. Such morphological properties, which are usually local and transient, are beyond the scope of this classification. As a first step, we focus on free dunes composed of loose sand. Cohesion between grains and vegetation are not taken into account. We expect that this diagram will evolve as the understanding of the formative conditions and processes progresses.

3.2 Tree description – Selection of dune shape and crest orientation from formative processes

The tree in Figure 6 classifies dunes depending on the dominant dynamics. The dune morphodynamics are controlled by spatial variations of the sand flux. The bed is eroded where sand flux increases and aggrades where sand flux decreases. Those spatial variations can make a dune (i) grow in height, (ii) migrate (propagation perpendicular to crest), and (iii) elongate (increasing the length of the crest line). Growth in height, migration, and elongation correspond to dune dynamics in the three dimensions: vertical, horizontal across-crest, and horizontal along-crest, respectively. Growth in height generally corresponds to an overall increase in dune cross-sectional area so that the dune transverse length increases accordingly. In a multidirectional wind regime, these three dynamics are present to different degrees. Depending on boundary conditions and wind regimes, one of these dynamical processes may prevail and drive the overall dune shape and orientation. The orientation of the dune with respect to the different sand fluxes further determines the secondary dune dynamics, which ultimately set the dune type.

One first has to choose the dune's length scale or time period to address, the two being linked (Section 7.1). The tree describes dunes of a given length scale. When different scales are present, each scale can be described by going down the tree separately. The first decision relates to a boundary condition through the question: Is the bed made of mobile sand ? A dune may strongly interact with the surrounding sand bed, *e.g.*, growing from the erosion of the interdune. Conversely, the interaction may be limited like for a barchan, which evolves on a starved floor. Bed mobility has a strong influence on dune dynamics and shapes. We recognize the floor as a mobile sand bed when the granular medium that composes the dune and the bed surface are similar.

3.2.1 Mobilized sand bed – Growth in height prevails

Where the bed is made of loose sand, dunes develop from the destabilization of the bed by the wind. We call this growth mechanism the *bed instability*, and growing in height is the prevailing dynamics. The resulting dunes are long
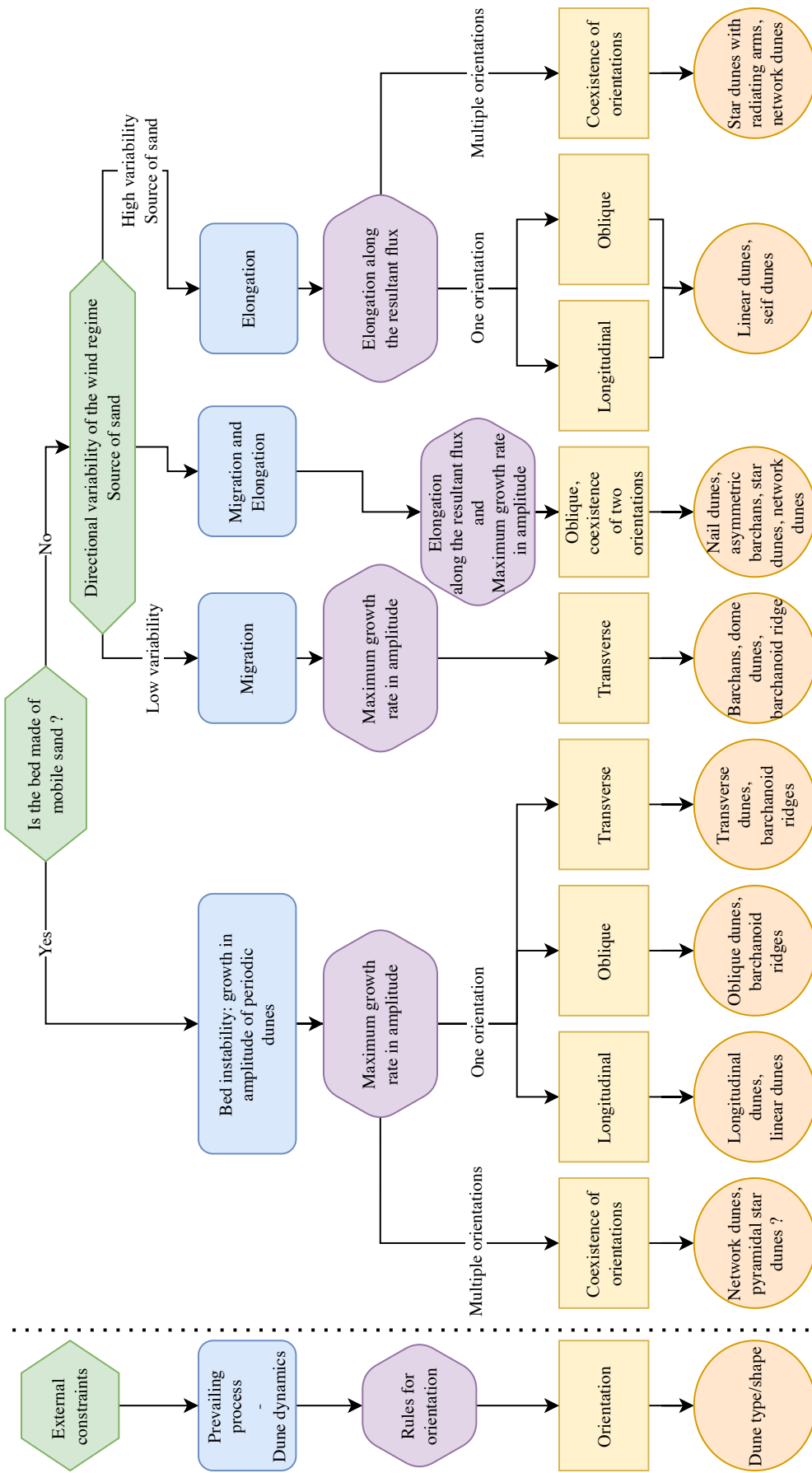
15

Figure 6: Identification tree for dunes classification based on dune dynamics.

ridges generally organized periodically. In accordance with an instability mechanism, the observed pattern, and in particular its orientation, is such that the growth rate in height is maximum [40, 41, 121]. Dunes are built up by normal-to-crest sand fluxes. In a multidirectional wind regime, sand fluxes of opposite directions both contribute to build the dune, so that dune orientation maximizes the *gross bedform-normal transport*, which, depending on the wind regime, can be transverse, oblique, or longitudinal with respect to the resultant drift direction, *i.e.*, the direction of the net transport on a flat bed. For some specific wind regimes, multiple orientations can coexist, resulting in intricate patterns that may be defined as network or star dunes.

The shape of dunes is then modulated by the two other processes and by migration in particular. Migration tends to promote the development of sinuous crestlines. In contrast, along-crest sand flux promotes dune straightness [65].

3.2.2 Non-mobilized bed – Migration and elongation prevail

When large areas of the bed cannot be mobilized by the winds (but sand is still piled up by the winds), the growth in height of a periodic pattern is inhibited due to sand supply limitation. Consequently, *migration* and/or *elongation* prevail in determining the dune type and orientation [41]. Although dunes may be arranged periodically, dunes can be isolated objects unlike in the case of a sand-covered bed. They persist because capture of free sand flux and losses balance out, or slowly evolve such that their shape and size are quasi-static.

What controls the relative dominance of migration and elongation remains largely unknown to date. Elongation can be promoted over migration by some boundary conditions that 'pin' part of the dune. Generally, the dune would grow from a localised sand source, behind an obstacle that acts as a sand trap for example. A part of the dune may also be so large that it barely moves during the time it takes to develop extensions, such as the core of a star dune [90]. If part of the dune is pinned, the dune cannot propagate but only elongate in the direction of the sediment net transport [41, 64]. We recognize elongation as another growth mechanism. For most wind regimes, a dune would migrate and elongate if not pinned. The boundary condition can force elongation and prevent migration, but only if such dunes are stable. An elongating dune cannot form in a unidirectional transport regime [122]. Although it extends in the direction of transport, its growth in height and sustainability requires that it is subjected to components of wind perpendicular to its crest line. Because the direction of elongation is generally different from that of the bed instability [41, 64], secondary superimposed patterns in the bed instability mode are likely to develop on an elongating dune [41]. An isolated dune parallel to the direction of the net transport, therefore, eventually destabilizes into migrating dunes if its growth rate in height is not sufficiently large relative to that of the superimposed patterns in the bed instability mode [122, 64].

Elongation prevails If elongation prevails, dunes have a ratio of length (along crest) over width (across crest) much larger than unity and extend in the direction of the net transport if they do not migrate [63, 122, 41, 64]. The orientation of such elongating dunes can be longitudinal or oblique to the resultant drift direction (RDD) because the dune topography modifies the transport (Section 7.2.3) [41]. In a multidirectional wind regime, the topography may change the relative magnitudes between the different transport directions, so that the dune experiences a direction of net transport different from that over a flat sand bed, the RDD. Some specific wind regimes allow multiple elongation directions, which may produce star dunes with radiating arms. Arms of adjacent dunes may connect to form network dunes.

Migration prevails Migration does not directly select dune orientation because only dune growth mechanisms do, *i.e.* growth in height (cross-section) and growth in crest line length, or elongation. However, migration mutes elongation, so when migration prevails, we expect dune crest orientations to maximize growth rate in height, as in the bed instability mode. The archetypical migrating dune is the barchan dune. As variability in wind directions increases, the width of the slipface decreases from the full width of the dune (barchan) to a restricted region, and then finally disappears completely (dome dune) [122, 123]. Although they may correspond to transitional regimes, we also classify isolated barchanoid ridges in this branch. Experiments under water [122] and numerical simulations [124, 125] have shown that an isolated straight-crested transverse dune subjected to a monodirectional flow is unstable when migrating on a non mobile sand bed and without being fed by an incoming free flux. A perturbation in height or in streamwise length leads to a perturbation in the migration velocity and to the redistribution of sand towards where the avalanche face is concave, which amplifies the perturbation. The transverse dune transforms into a barchanoid ridge and eventually breaks into a row of barchans. In light of those studies, barchanoid ridges on beds of non-mobile sand correspond to transient dynamics. Because they might be stable in different conditions and because this instability is driven by migration, we recognize these dunes as being shaped by migration.

17

Concurrent migration and elongation If boundary conditions and/or sand supply do not force the development of an elongating dune from a point source, a dune is likely to migrate except in some specific symmetric wind regimes, *e.g.*, two transport directions with an obtuse divergence angle and equal magnitudes [63, 122]. Most multidirectional transport regimes should involve both dynamics. The transition between elongation and migration is not sharp but a continuum. As such, when neither migration nor elongation fully dominates, the orientations and morphologies associated with these two dynamics coexist, leading for example to asymmetric barchans, nail dunes or raked linear dunes [91, 92, 64, 126].

3.3 Future refinements

Here, we classify dunes in broad classes and determine their orientation according to the prevailing formative dynamical processes. The ideal classification would not only address the dune orientation but also the detailed dune morphology in a quantitative way, *e.g.*, the straightness of linear dunes or the sinuosity of their crest line, the curvature of the avalanche face of barchans, or their asymmetry like the relative size of their horns. Many of those properties should depend on the competition between the three processes, which are all at work at different degrees in multidirectional flow regimes. How much a morphologically long dune migrates relative to its growth in height or elongation should for example control the dune straightness as conceptually proposed in [65]. Growth in height and elongation should favor the spatial coherence of the dune, while migration destabilizes it [122, 124, 125]. Periodic transverse dunes in the bed instability mode being subject to migration are often barchanoid ridges. However, all these morphological properties not only lack unified predictive models but also quantitative measurements. The quantitative prediction of dune orientation is an important step to the quantitative prediction of dune types as it is a prerequisite to evaluate the components of sand flux associated to the different dynamics.

Other boundary conditions associated with obstacles or confining factors could be added to the tree, *e.g.*, a dune may interact with a cliff to form an echo dune. Finally, the role of cohesion and vegetation is another challenge that could provide additional understanding if incorporated in a dynamics-based classification.

In Section 5.2, we apply this dynamics-based classification to various characteristic dune types on Earth, using observed wind regimes to evaluate the dynamical processes in a simple way, and giving rules to select the prevailing dynamics and to calculate crest orientations.

4 Classification of aeolian dunes based on fluid mechanics and sediment transport

4.1 Purpose and approach

Dunes are observed at a variety of scales that differ from one environment to another. The purpose of the following classification, based on fluid and sediment-transport mechanics, is to define the different dune-formation regimes, which determine the range of possible dune sizes. As environmental and boundary conditions vary from one planetary body to another, Earth and extraterrestrial dunes sample these different formation regimes, such that predictions from theory can be compared with observations returned by planetary exploration missions (Section 5.4).

For simplicity, we consider the case of a steady, unidirectional wind blowing over a cohesionless granular bed with unlimited sediment supply, at wind velocity above the threshold of transport. Under these conditions, a flat bed may become unstable, leading to the growth of a periodic dune pattern with a characteristic wavelength, $\lambda_{\min}$. Specifically, dunes form from a positive feedback between fluid flow, sediment transport and bed topography as sketched in Figure 7. Spatial variations of sand flux drive erosion and deposition through conservation of mass (Exner equation [127, 128, 129]). A dune grows with time if sand is, on average, deposited at its top, *i.e.*, if the sand flux peaks upwind of the dune top and decreases further downwind from the top. Conversely, a peak in flux downwind of the dune top leads to dune flattening. The minimum possible dune wavelength corresponds to the size at the threshold between a negative and a positive feedback of the instability, *i.e.*, when loci of maximum sand flux and maximum topography coincide. This minimum wavelength is very close to the wavelength of incipient dunes that would form from an initially flat sand bed, which formally is the wavelength for which the feedback is maximum.

The response of the fluid flow to a positive topographic perturbation is characterized by an increase of the fluid velocity (speed-up) above the bump and a space shift between the fluid velocity close to the ground, the shear velocity, and the bed elevation profile. For a sinusoidal elevation profile, the space shift corresponds to a phase shift,
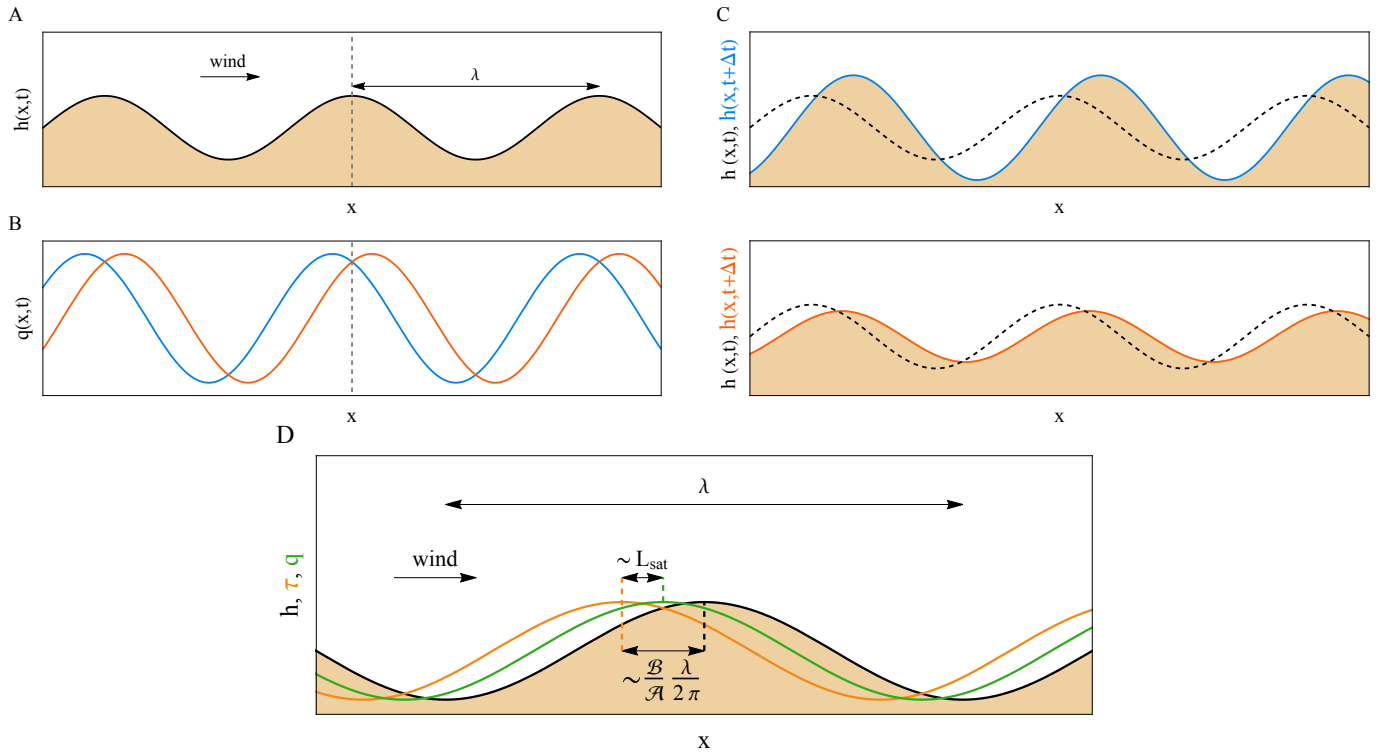
18

Figure 7: Formation of periodic dunes. A. Sand bed with a sinusoidal elevation profile $h(x)$ of wavelength λ at time t. B. Sand flux q along the bed profile. The sand flux peaks upwind (blue) or downwind (orange) of the maximum of topography. C. Evolution of the sand bed depending on how the sand flux is shifted with respect to the bedform. D. Basal shear stress is shifted - here upwind (positive) shift - with respect to bedform by a distance $(\mathcal{B}/\mathcal{A})\lambda/(2\pi)$. Sand flux lags with respect to shear stress by a distance L_{sat}.

$\phi = \arctan(\mathcal{B}/\mathcal{A})$ (see sec. 7.4.1). In turn, the maximum possible sand flux, called saturated sand flux, increases with shear velocity, or equivalently, with wind shear stress on the bed. However, the flux itself lags spatially as it responds to a change in shear stress. It peaks at some distance downwind of the locus of maximum shear stress. This relaxation distance is called the saturation length, L_{sat}, and is defined as the characteristic length over which sediment flux adapts to a change in transport conditions. The spatial shifts between the basal shear stress and the topography, and between the sand flux and the shear stress are the two key parameters that determine the formation of dunes from a flat sand bed. If the shear stress is maximum downwind of the peak in topography, dunes cannot develop. If the shear stress is maximum upwind of the topography, so could be the sand flux. If the saturation length is short enough for the flux to peak upwind of the crest, a dune grows. Conversely, if the saturation length is so long that the flux would still increase at the dune top, a dune cannot form.

The sign of the phase shift between shear stress and bed topography (positive if shear stress peaks upwind of the topography, negative otherwise) is controlled by the aerodynamic roughness of the bed. In turn, saturation length for wind saltation has been measured on Earth in the field [130, 131] and in wind tunnels [132] but still lacks a robust mechanistic model for predictive capabilities. Current empiricism suggests that it depends on three dimensionless numbers, which compare the density of sand grains with that of the fluid (s), the fluid force to the apparent weight of grains (the Shields number Θ) and gravitational to viscous effects (the Galileo number $\mathcal{G}$). The mechanics of a turbulent flow over a corrugated soil and sand transport are further discussed in sections 7.4.1 and 7.2.1, respectively.

Dunes migrate as they develop. This migration forces interactions (such as collisions) between dunes, which leads to the coarsening of the dune pattern, *i.e.*, an increase in dune wavelength. The mechanism by which this coarsening process stops, limiting the size of giant dunes, is debated, possibly involving a limit in sand availability of the bed, flow confinement, or a change in flow regime (Section 7.5).

In Figure 8, we describe how the minimum and maximum dune wavelengths are determined depending on fluid and transport conditions, and discuss the different scenarios below. Dunes have been observed on a variety of planetary

19

bodies, which we discuss in section 5.4. Several parameters that control dune wavelength are currently unknown, and theoretical knowledge gaps still exist, offering exciting avenues for future research and investigation.

4.2 Tree description – Selection of dune size from flow regime and sediment transport

4.2.1 Turbulent flow above the bed - Aerodynamic roughness

The response of the flow to a topographic perturbation is sensitive to the bed's *aerodynamic roughness*, which affects the turbulent mixing and the surface drag ([133], fig. 2 in [134]). The roughness length scale, r, is a property of the bed surface at a much shorter length scale than the bedform wavelength, λ. Depending on the specific bed, flow, and transport conditions, r can be controlled by grain size, d, the thickness of the transport layer (fig. 23 in [135]), or by the height of smaller bedforms like ripples. How this length scale compares with the viscous length scale, ν/u_* (where u_* is wind shear velocity and ν the kinematic viscosity of the fluid), has a critical impact on dune formation. Two regimes can be distinguished based on a roughness Reynolds number, $\mathcal{R}_r = ru_*/\nu$ (see Section 7.4.1).

Above $\mathcal{R}_r \simeq 100$, shear stress peaks upwind of maximum topography regardless of dune wavelength. This is the *aerodynamically rough regime*, favorable to the onset of the dune instability.

For $\mathcal{R}_r$ values lower than ~ 10, the spatial shift between shear stress and topography strongly depends on the wavelength, λ, of the bedform perturbation. This regime is called the *aerodynamically smooth regime* and allows for shear stress to peak downwind of the topography maximum for a range of λ, preventing the formation of dunes at these scales, *i.e.*, a *dune gap* [134, 136, 137]. We refer to this particular response of the flow to the bedform perturbation as the *Hanratty anomaly* [138]. This peculiar flow regime is predicted from extrapolation of a model built on a few measurements (sec. 7.4.1) and is supported by observations of bedforms on Mars [139] as well as dissolution and melting patterns in nature (sec. 7.4.2).

For intermediate $\mathcal{R}_r$ values ($\sim 10 - 100$), some effects of the Hanratty anomaly are detected but the physics essentially remains that of the rough limit [134].

4.2.2 Minimum wavelength selection

Rough flow   The first branch of Figure 8 we consider is that of aerodynamically rough conditions. In this case, assuming that the flow is virtually unconfined in the vertical direction, the minimum wavelength, $\lambda_{\min}$, is found, to a first approximation, to scale with the saturation length, L_{sat}, multiplied by a prefactor that is controlled by the fluid mechanics, *i.e.*, the spatial shift between the topography and the shear stress, which is roughly constant in this regime, *i.e.*, $\lambda_{\min} \propto (\mathcal{B}/\mathcal{A})L_{\text{sat}}$ [140, 141, 105] (Section 7.4.1).

Smooth flow   In the aerodynamically smooth regime, shear stress peaks downwind of the topography for a range of wavelengths that is determined by the viscous length. Dunes with those wavelengths cannot develop, creating a dune gap that extends over an order of magnitude around $\lambda_{\text{g}} \simeq 10^4 \nu/u_*$. As a result, the minimum wavelength for dunes can either be set by the viscous length, as for λ_{g}, or by the saturation length. A saturation length-based Reynolds number $\mathcal{R}_L = L_{\text{sat}}u_*/\nu$, allows for comparisons of these two length scales.

When $\mathcal{R}_L$ is large enough (*i.e.*, $L_{\text{sat}} > \lambda_{\text{g}}$, $\mathcal{R}_L \gtrsim 10^4$), saturation length is the limiting factor like in the rough regime and the most unstable wavelength scales as $\lambda_{\min} \propto (\mathcal{B}/\mathcal{A})L_{\text{sat}}$ [137].

For $\mathcal{R}_L \lesssim 10^3$, *i.e.*, $L_{\text{sat}} < \lambda_{\text{g}}$, bedforms with two distinct populations of wavelengths can coexist, either independently or as a superimposed pattern. They are scale-separated by the dune gap around λ_{g}. The minimum wavelength is thus either λ_{g} for dunes above the gap, or is controlled by L_{sat} for dunes under the gap. In the latter case, the minimum wavelength scales with $\lambda_{\min} \propto L_{\text{sat}}/\mathcal{R}_L^\alpha$, where $\alpha \simeq 0.4$ [12, 102, 142, 139, 83, 137].

4.2.3 Maximum wavelength selection

Once initiated, dunes migrate, interact, and coarsen leading to an increase in wavelength. The size of giant dunes in the solar system, however, appears to be limited, with a maximum wavelength, $\lambda_{\max}$. The upper limit on dune wavelength could be set either by the boundary conditions, introducing another characteristic length scale, or by the lower bound of the gap (*i.e.*, λ_{g}) for dunes initiated below the gap in the aerodynamically smooth regime. The smallest of those scales sets the maximum wavelength for dunes.

A first potential size limitation comes from the sediment supply and availability, which can lead to stalling dune growth [143]. Another possible limitation arises from flow confinement. In the case of a non-confined flow, *i.e.*, a deep flow, a dune perturbs the flow above it over a characteristic height proportional to the dune's wavelength. An

What is the minimum wavelength, $\lambda_{\min}$, in unconfined flow conditions ?

How does bed roughness compare with viscous length ?
(Is the flow regime rough or smooth ?)
$\mathcal{R}_r = r u_* / \nu$

♀ ?

Smooth regime
$\mathcal{R}_r \lesssim 10$

dune gap

λ_g λ

$\lambda_g \sim 10^4 \dfrac{\nu}{u_*}$

Rough regime
$\mathcal{R}_r \gtrsim 10^2$

— **Fluid dynamics** —

- roughness r
- viscous length ν/u_*

How does saturation length compare with the dune gap length scale ?
(Is the flow response to topography laminar or turbulent ?)
$\mathcal{R}_L = L_{\text{sat}} u_* / \nu$

♇ ?

Laminar response
$\mathcal{R}_L \lesssim 10^3$
Dune gap splits range of possible wavelengths
into two distinct populations

Turbulent response
$\mathcal{R}_L \gtrsim 10^4$
No gap in possible dune
wavelengths

— **Sediment transport** —

- saturation length L_{sat}

Controlled by :
    - density ratio s
    - Shields number Θ
    - Galileo number $\mathcal{G}$

☄ ♂

$\lambda_{\min} \propto L_{\text{sat}} / \mathcal{R}_L^\alpha$
range of $\lambda < \lambda_g$

♂

$\lambda_{\min} \propto \lambda_g$
range of $\lambda > \lambda_g$

♁   ♄

$\lambda_{\min} \propto L_{\text{sat}}$

What is the maximum reachable wavelength, $\lambda_{\max}$?

How does confinement height compares
with the dune gap length scale ?
$\Delta = \Lambda / \lambda_g$

unconfined
$\Delta > 1$

confined
$\Delta < 1$

— **Flow confinement** —

- flow height Λ
- flow Froude number $\mathcal{F}$

Controlled by :
    - capping/surface
    - flow stratification

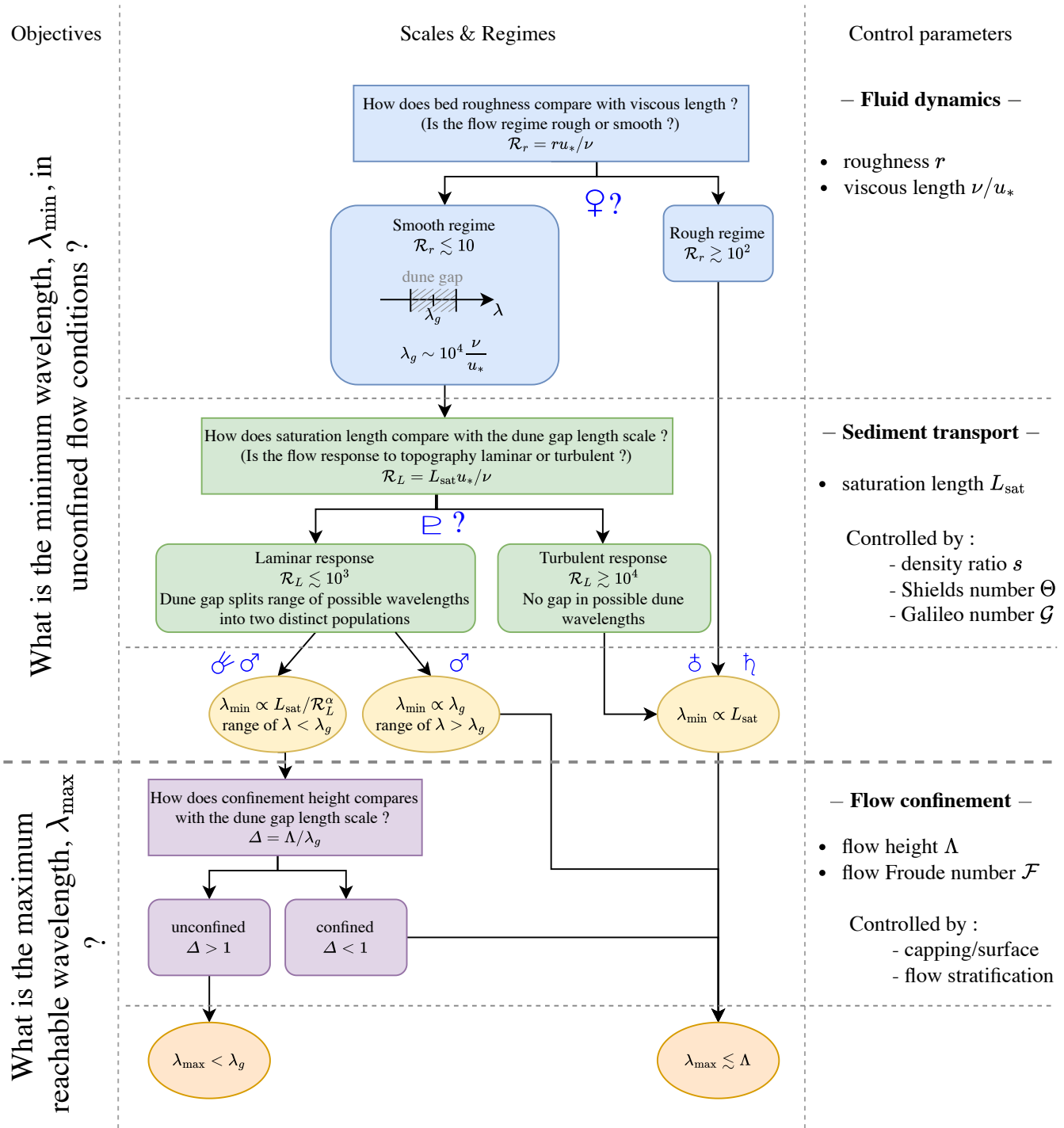$\lambda_{\max} < \lambda_g$

$\lambda_{\max} \lesssim \Lambda$

Figure 8: Identification tree for dune classification based on fluid mechanics and sediment transport. Notations: roughness length scale r, shear velocity u_*, fluid kinematic viscosity ν, fluid to particle density ratio $s = \rho_f/\rho_p$; Shields number $\Theta = u_*^2/[(s-1)gd]$ where g is the gravitational acceleration and d is the grain size, Galileo number $\mathcal{G} = \sqrt{(s-1)gd^3}/\nu$. Several Froude numbers can be associated with flow confinement or stratification, e.g. $\mathcal{F} = U/\sqrt{g\Lambda\Delta\rho_f/\rho_f}$ where U is the flow velocity and $\Delta\rho_f$ is the fluid density jump, both evaluated at altitude Λ. Blue symbols: astronomical representations of planetary bodies (♀ Venus, ♁ Earth, ♂ Mars, ♄ Titan, ♇ Pluto, ☄ comets (*e.g.*, 67P/Churyumov-Gerasimenko).

upper wall or a free surface confining the flow to a comparable or thinner height than dune wavelength would affect the flow above the dune and the sediment transport. Whereas the influence of a free surface is clear in rivers, it remains debated for planetary atmospheres, which are density stratified and do not exhibit a sharp interface. It was proposed that the thickness, Λ, of the atmospheric boundary layer (ABL) could act as a confinement scale, stalling dune coarsening at $\lambda_{max} \simeq \Lambda$ (see sec. 7.5) [144]. This hypothesis, showing a correlation between the size of giant dunes on Earth and calculations of Λ, was challenged by another data set, in which the size of giant dunes on Earth were compared with satellite measurements of Λ [145]. The question of the confining role of the ABL remains debated to date and may lack a good estimate or proxy of the characteristic thickness, Λ, which depends on time and space.

5 Case study

Here we analyse different dune fields in light of our classifications, demonstrating their complementarity and practical utility to describe and understand the observed patterns and untangle their complexity. We provide keys and methods for approaching pattern interpretation and their evolution through space and time. These also emphasize remaining open questions in fully predictive classifications and models.

5.1 Spatial and temporal changes in dune morphology as markers of evolution in external forcing and boundary conditions

5.1.1 Framework

Although dunes are dynamical patterns that interact with each other and continuously grow, migrate, elongate, or reorganize within the field, equilibrium dune types are entirely determined by external forcing and boundary conditions, which include bed mobility, sand and vegetation coverage. Some changes in equilibrium dune type occur as discontinuous jumps when a factor varies. Perhaps the best known example is the change associated with the abrupt switch in dune orientation of periodic pattern on a mobile bed from transverse to longitudinal that occurs where the divergence angle between equal bimodal winds changes from less than to more than approximately 90°, as has been studied by experiments, simulations, and theory [40, 63, 122]. Other changes in dune morphology vary along a continuum, such as where increasing dispersion of wind directions produces dome dunes rather than barchans [123].

Just as external forcing and bed conditions can cause differing equilibrium dune morphologies—either abrupt or along a continuum—dune type and morphology can also vary spatially or evolve temporally as forcing or bed conditions change through space or time. Typical changes in external forcing include environmental, climatic, and tectonic (*e.g.*, [51]). These manifest as changes in wind regime (speed and direction), sediment supply, substrate type or geology, topography, vegetation cover, or moisture (*e.g.*, water table). In today's vast active sand seas on Earth, dune types are, in most cases, in approximate equilibrium with current conditions [41] (Figs. 12 - 20). However, shifts in winds on millennial scales change dune morphology [146] and can create generations of superimposed dune morphologies [147, 148]. Larger dunes incorporate so much sand and inherit so much environmental history that to rearrange their morphology could indeed require millennia (*e.g.*, [119, 147]). In a multidirectional wind regime, dune type can also vary with dune size at the same location because they respond with different time scales to a change in wind direction. On the other hand, dunes formed in drier, windier climates may now be fully vegetated because of a climate shift. One example is the Nebraska Sand Hills, which were once characterised by active megabarchans and large barchanoid ridges during the Pleistocene but are now fully vegetated relict dunes [149].
Environmental factors and bed conditions typically vary over 100's km length scales across vast sand seas, or across a few kilometers' length scales, as with small dune fields that develop from beaches and extend inland. Migrating dunes can experience varying conditions, and the larger dunes may then inherit morphology from upwind, thereby lagging the local conditions in which they are observed.

As far as equilibrium dune types are concerned, changes in space or time are interchangeable. In transitional zones or periods, however, dunes are likely out of equilibrium. In case of migrating dunes, spatial morphologic and size changes in a dune field could still reveal what would be an autogenic temporal evolution. Ageing and coarsening of dune pattern, the arrangement of dunes within a field and response to changes in external forcing or boundary conditions are generally driven by the autogenic process of dune interactions such as dune collision, linking or repulsion, which may result in recognizable dune patterns that are inherently transitional. In the simplest case, merging and linking of barchan dunes results in transient barchanoid ridges (*e.g.*, [115]). Blowouts and, to a lesser extent, migrating

Figure 9: The Porto do Mangue, Northeast Brazil coastal transgressive dunefield illustrating downwind development as the areal coverage of sand increases. The middle of the image lies at (5.05°S, 36.83°W). Credit: Maxar Technologies.

parabolic dunes may be other examples. Some dune types also correspond to specific boundary conditions, *i.e.*, to a transitional zone. This is the case for foredunes or lunettes, for example.

These examples paint a complex picture of dune equilibrium, where understanding the morphologic and dynamic richness of such dune fields relies first and foremost on recognizing changes in dune type and size along with potential external factors that influence these changes [50].

5.1.2 Field examples

Here we first discuss two examples of spatial evolution of dune type within fields where sediment enters the system from an upwind source (*e.g,*, beach [50]). These examples illustrate the interplay between spatially varying external drivers and autogenic processes occurring at different stages of dune development. Then, we show how the observation of dunes in continuously varying environments can be extrapolated to the time evolution of dunes. We use examples that show evolutionary sequences that result in parabolic dunes, but the trajectory to the parabolic state differs due to varying boundary conditions within the fields.

Where sediment enters a dune system from a margin (*i.e.*, not from excavation of substrate alone) such as a beach or a playa, dune morphological evolution generally follows a characteristic morphologic evolutionary sequence that largely reflects a decrease in flux that drives an increase in sand cover and dune growth through dune-dune interactions. Boundary conditions including water table and feedbacks from vegetation growth can also play a role.

Figure 9 illustrates a coastal example from NE Brazil where sand sheets and stringers evolve downwind across a deflation plain into barchans and barchanoids, and then sinuous transverse dunes. This change in dune types is correlated to a change in bed surface cover, which suggests that the wind is weakening inland.

It is also common to observe active mobile dunes such as barchans, barchanoids, and transverse dunes evolve into parabolic dunes downwind in both continental and coastal environments [29, 26, 120, 150, 151] as observed in the White Sands dunefield shown in Figure 10. White Sands is a gypsum dune system in New Mexico, which formed in the late Pleistocene to early Holocene ($\sim 9 - 12$ kya), and which provides a type-example of spatial changes in dune
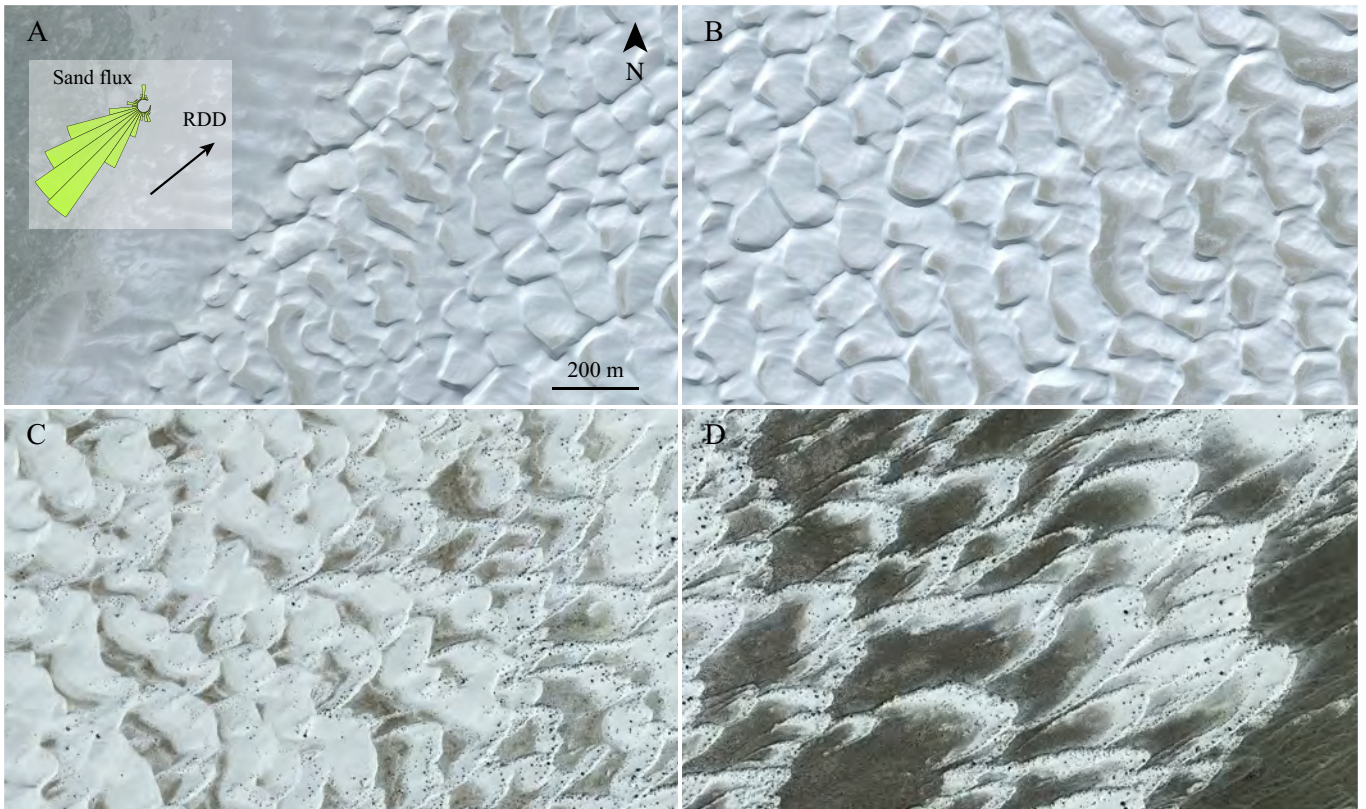
Figure 10: A west-to-east along-RDD (30°N of East) evolutionary sequence across the White Sands dunefield starting at (32.802°N, 106.302°W) and ending at (32.848°N, 106.204°W), which corresponds to a distance of approximately 11 km. Sand sheets and proto dunes (A) evolve into transverse barchanoid dunes (B) and downwind into parabolic dunes (D). Scale is the same for all snapshots. Sand flux rose points upstream. See Sections 7 for details of calculations. After the publication [105], we used a density $\rho_s = 2300\,\mathrm{kg.m^{-3}}$ and a grain diameter $d = 670\,\mu\mathrm{m}$ in the calculations for this particular case. Credit: Maxar Technologies.
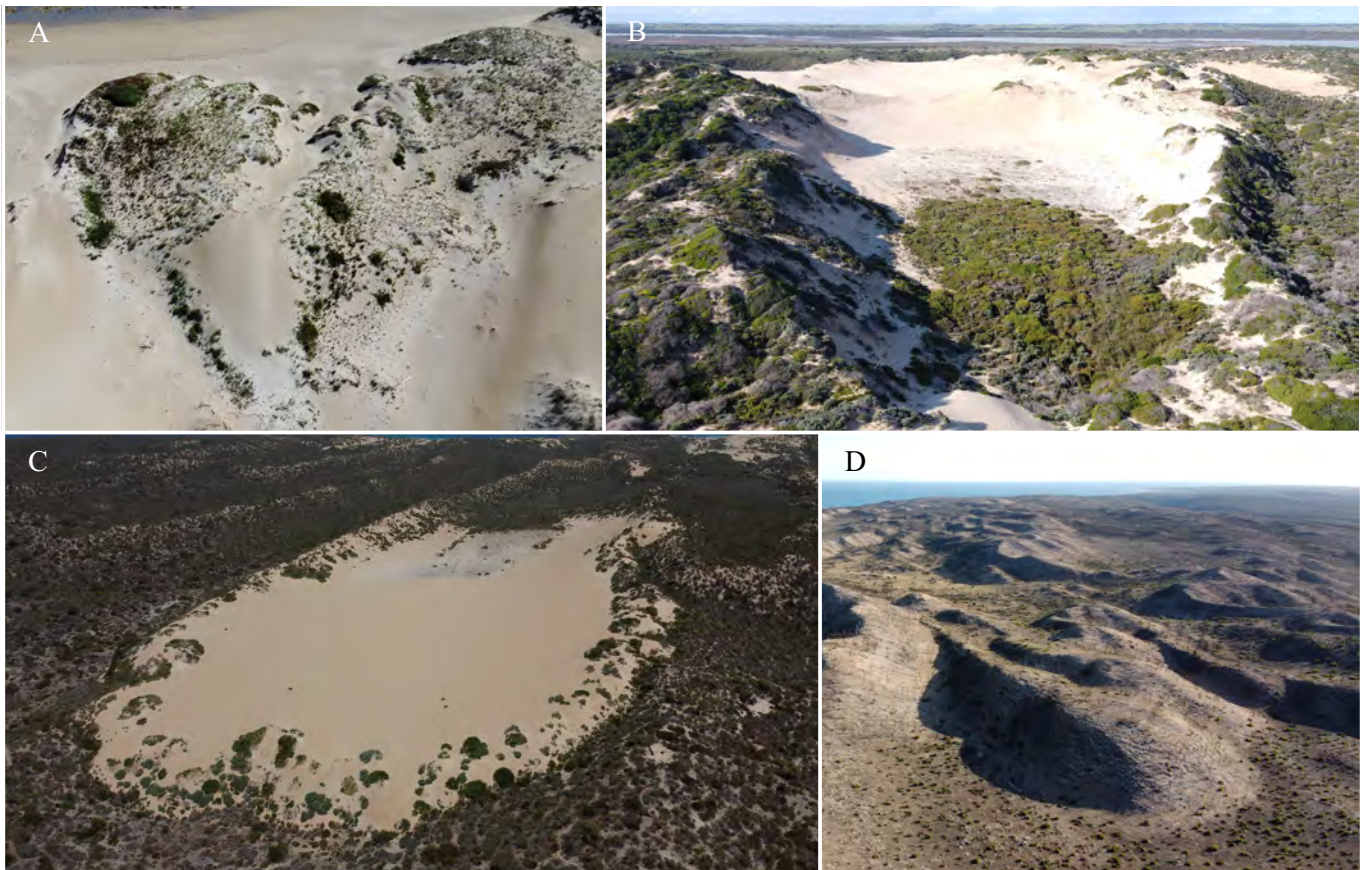
Figure 11: A: Blowout at Maurpetuis Bay, Kangaroo Island, South Australia. B: Parabolic dune near Cantara, Younghusband Peninsula, South Australia. C: Long-walled parabolic dune near Port Lincoln, South Australia. D: Nested, long-walled parabolic dunes at Snake lagoon, Kangaroo island, South Australia. Credits: P. Hesp.

morphology from an upwind sediment source [152, 153, 154, 155, 156]. Sand sheets and proto dunes emerging from the playa margin (Fig. 10 A; [157, 105]) develop into sinuous transverse dunes (also termed crescentic dunes), then more complex barchanoids (Fig. 10 B), to sub-parabolic and then parabolic dunes (Figs. 10 C and D) as vegetation takes root and expands [158, 50, 159, 160]. The evolution from incipient dunes at the playa margin to stagnant parabolic dunes downwind occurs over a distance of approximately 10 km. This transition has been explained by changes in field-scale aerodynamics and a reduction in groundwater salinity [160, 161]. In the aerodynamic model, vegetation growth becomes more favorable downwind as the dune roughness relative to the playa reduces near-bed wind speed and therefore sediment transport [160, 162]. The barchan-parabolic transition occurs 8 km downstream of the field margin over a characteristic distance of 2 km and is correlated with an increase in plant density (number per dune) and a drop in the groundwater table [160]. The change in morphology begins with vegetation stabilizing the margins and horns of the mobile barchan dunes. The edges being held while the central and larger volumetric portion of dunes continue to advance, the dunes switch to a parabolic morphology [159, 158].

Different from the transition described above, parabolic dunes may instead develop directly from blowouts forming above the backshore of beaches or within continental dune fields where vigorous vegetation growth is supported [163, 164, 74]. The driving external factors affecting the transition are sediment transport rate and supply, and climate (*e.g.*, rainfall) [21, 70]. Figure 11 shows dunes at different stages of interaction with vegetation, suggesting what might be the typical evolution of a dune from its initiation on a foredune to its complete stabilization by vegetation as it migrates inland. This scenario may apply to the coastal dunefield in South Australia shown in Figure 4 I, for example. In Figure 11 A, a 50-m long blowout is beginning to develop incipient trailing ridges (note the vegetation stabilizing the edges of the depositional lobe), and if the depositional lobe continues to migrate downwind will evolve into a parabolic dune. Figure 11 B shows a large 750-m long parabolic dune with a well vegetated deflation basin. In

semi-arid environments, nebkha often form on the depositional-lobe margins as shown in this photograph. Figure 11 C illustrates an older, long-walled (2.3-km long) parabolic dune with pronounced nebkha development around the lobe and trailing ridges. Trailing ridges are eventually stabilized by nebkha development and vegetation cover of the inside trailing ridges. Deflation basins and plains are colonised by vegetation once the deflation has occurred down to a base level fixed by the water table (*e.g.*, Figure 11 B), or hard surfaces (*e.g.* Pleistocene calcrete in Figure 11 C). Parabolic dunes eventually stabilise due to running out of sediment or due to climate changes (*e.g.*, higher rainfall, lower wind speeds). Figure 11 D illustrates an example where a later parabolic dune phase has created a nested parabolic dune system.

The changes in dune morphology described herein present a basis for interpreting environmental conditions and processes through space and time. The characteristic spatial changes in morphology from an upwind source reveal the direction of the source area, sediment flux gradient, bed conditions, and the presence, absence, and feedbacks of vegetation in the system. The trajectory of the morphologies toward vegetated parabolic dunes from differing initial states highlights the strong control vegetation has on dune morphology. These systems also show the time-varying characteristics of dune morphological evolution that has only been revealed through long-term observations, field-scale experiments, and scaled laboratory experiments [122, 165, 157]. Understanding these as time-varying morphological characteristics provides a foundation to interpret the recent and future climatic changes that could affect dune morphology [148].

5.2 Revealing dune patterns on Earth from dynamical processes

The dynamic-based classification aims to quantify dune morphodynamics according to environmental forcing. Dune type and orientation result from the competition between three dynamical processes, which are growth in height, elongation, and migration. The prevailing dynamics and the balance between the three depend on boundary conditions and on the regime of sand transport the dune experiences, *e.g.* the distribution of sand flux orientations, the magnitude and the sequence of transport events. In order to quantify this concept, three different sand flux components are defined in the reference frame of the dune crest. (i) The crest-normal component of sand flux, $Q_\perp$, is associated with dune migration. (ii) The crest-parallel component of sand flux, $Q_\parallel$, is associated with dune elongation. (iii) The growth in height is quantified through the gross bedform-normal transport, *i.e.*, the absolute value of crest-normal component of sand flux, $|Q_\perp|$. Following the mass conservation principle, the rates of growth in height, of migration, and of elongation correspond to the divergences of $|Q_\perp|$, $Q_\perp$, and $Q_\parallel$, respectively. Growth in height depends on gross transport (absolute value) rather than net transport, because transports in both directions across the crest contribute to dune growth [40, 41]. Before presenting analysis for various common dune types on Earth, we review the different parameters that allow us to evaluate the dynamical processes and calculate their relative importance from wind data.

5.2.1 Parameters for the characterization of the sand transport regime and dune dynamics

Sand transport regime Using wind data from the last decade [166, 167], we calculate the instantaneous shear velocities, u_*, with Equation 6, and saturated sand flux vectors on a flat sand bed, $\vec{Q}_0$, with transport law Equation 2 using a transport threshold velocity, u_t (Appendix Section 7). We then characterize the sand transport regime at a given location using the time-averaged $\langle u_* \rangle$, $\langle \vec{Q}_0 \rangle$, and $\langle \|\vec{Q}_0\| \rangle$. The mean shear velocity, $\langle u_* \rangle$, is averaged over the duration of active transport, *i.e.* when $u_* > u_t$, so that the ratio $\langle u_* \rangle / u_t$ is a proxy for the average intensity of transport when it occurs. Because norms of individual sand flux vectors, $\vec{Q}_0$, correspond to the saturated values of sand fluxes, the norm of the time averaged sand flux is equivalent to the resultant drift potential, $\left\| \langle \vec{Q}_0 \rangle \right\| = \mathrm{RDP}$, and its direction is the resultant drift direction, RDD. The time averaged norm of instantaneous sand flux is equivalent to the drift potential, $\langle \|\vec{Q}_0\| \rangle = \mathrm{DP}$, so that the ratio RDP/DP is a measure of the directional variability of sand transport [168, 169]. RDP/DP $\to 1$ where sand transport tends to be unidirectional; RDP/DP $\to 0$ indicates high directional variability resulting in a small net transport compared with what it would be if all transport events were in the same direction.

Sand transport over dunes Dune dynamics are evaluated with the time-averaged components of the characteristic sand flux over dunes, $\langle \vec{Q}_c \rangle$, in the reference frame of dune crest: $\langle Q_\perp \rangle$, $\langle Q_\parallel \rangle$, and $\langle |Q_\perp| \rangle$, which we calculate using the same transport law as for Q_0, but including the effect of *wind speed-up*, *i.e.*, the increase in wind shear velocity induced by dune topography. For this purpose, we reduce dunes to straight and symmetrical ridges of constant orientation

and cross-section, *i.e.*, the cross section is constant along the dune and neither the size nor the slopes of the dune change over time. This simplification is valid within the limit of very large dunes that fully integrate the wind regime (Appendix Section 7.1). Following the approach of Jackson and Hunt [170], we assume that the relative increase in wind velocity is proportional to the dune slope (increase in elevation with distance) along a wind streamline. It is maximum when wind is perpendicular to dune crest. Wind speed-up modulates the norm of each instantaneous sand flux, $\left\|\vec{Q}_c\right\|$, as a function of the angle between the wind and the dune crest. Therefore, the direction and magnitude of the time averaged sand flux the dune experiences, $\langle\vec{Q}_c\rangle$, depend on dune orientation in a multidirectional transport regime. $\langle Q_\perp\rangle$, $\langle Q_\parallel\rangle$, and $\langle|Q_\perp|\rangle$ can be evaluated for any potential dune orientation, α. The functions $\langle Q_\perp\rangle(\alpha)$, $\langle Q_\parallel\rangle(\alpha)$, and $\langle|Q_\perp|\rangle(\alpha)$ allow us to predict the orientation of dunes according to the prevailing dynamical process.

Evaluating dune orientation   When growth in height prevails, as in the bed instability mode where dunes develop from a loose sand bed, the selected orientation of dunes, α_H, maximizes the growth rate in height, σ, or equivalently the gross bedform-normal transport, $\langle|Q_\perp|\rangle$ (Section 7.3.3). In a multidirectional wind regime, this orientation can be transverse, oblique or parallel to the RDD. α_H is also the expected crest orientation when migration prevails. When elongation prevails, and when dunes elongate without migrating, dune crest orientation, α_E, corresponds to the direction of elongation, which in this case is also the direction of the mean sand flux on the dune, $\langle\vec{Q}_c\rangle$, such that $\langle Q_\perp\rangle(\alpha_E) = 0$ (no migration), and $\langle Q_\parallel\rangle(\alpha_E) > 0$ (elongation).

Sand flux depending on dune orientation   We use these predicted dune orientations to determine the averaged characteristic sand flux experienced by dunes in the two modes of orientation: $\langle\vec{Q}_H\rangle = \langle\vec{Q}_c(\alpha_H)\rangle$ of direction θ_H for dunes whose orientation maximizes growth in height, and $\langle\vec{Q}_E\rangle = \langle\vec{Q}_c(\alpha_E)\rangle$ of direction $\theta_E = \alpha_E$ for dunes that elongate without migrating. Except in singular situations, dunes whose orientation maximizes growth in height migrate according to the resultant crest-normal component of sand flux of norm $\left\|\langle\vec{Q}_M\rangle\right\| = |\langle Q_\perp(\alpha_H)\rangle| = \left\|\langle\vec{Q}_H\rangle\right\||\sin(\theta_H - \alpha_H)|$ and direction θ_M, which is perpendicular to the dune orientation, α_H. The characteristic migration velocity equals $\left\|\langle\vec{Q}_M\rangle\right\|/H$, where H is dune height. Similarly, the elongation rate of a non-migrating dune can be evaluated with $\left\|\langle\vec{Q}_E\rangle\right\|/H$ [171, 126].

Competition between dynamics   We argue that the orientation of dunes depends on the prevailing growth mechanism and that dune type depends on the competition (relative balance) between the three dynamical processes. The main factor selecting the prevailing growth mechanism for dune orientation appears to be the mobility of the sand bed and the boundary conditions. The variety of shapes within a given regime of orientation, as the balance between migration and elongation on a starved bed, must depend on the wind regime alone when all boundary conditions are fixed. Aiming at a fully predictive phase diagram of dune type and equilibrium shape, we propose and review from previous studies several dimensionless ratios built from the different sand fluxes just discussed to assess the competition between the three dynamics. For each of the two dune orientations, the three sand fluxes, $|\langle Q_\parallel\rangle|$, $|\langle Q_\perp\rangle|$, and $\langle|Q_\perp|\rangle$, associated with the three dynamics, elongation, migration, and growth in height, can be calculated. Because dunes in the elongation mode do not migrate ($\langle Q_\perp\rangle(\alpha_E) = 0$), this makes 5 different fluxes ($2 \times 3 - 1$), with which we can build 4 independent dimensionless ratios, *i.e.*, that cannot be built as a combination of the others. We chose 3 ratios that allow us to compare dynamics of dunes in a given mode of orientation: $|\langle Q_\parallel(\alpha_H)\rangle/\langle Q_\perp(\alpha_H)\rangle|$ and $|\langle|Q_\perp(\alpha_H)|\rangle/\langle Q_\perp(\alpha_H)\rangle|$ for dunes whose orientation maximizes growth in height, and $|\langle|Q_\perp(\alpha_E)|\rangle/\langle Q_\parallel(\alpha_E)\rangle|$ for dunes in the elongation mode of orientation. In addition, we select one ratio that compares the two different modes of orientation: $\langle|Q_\perp|(\alpha_E)\rangle/\langle|Q_\perp|(\alpha_H)\rangle = \sigma_E/\sigma_H$, the ratio between growth rates in height of dunes under the two modes of orientation. In the simplified framework we developed, these 4 ratios fully define the parameter space associated with wind forcing.

σ_E/σ_H varies between 0 and 1, and has been proposed to evaluate the stability of elongating dunes when they develop from a point source [64]. The stability of dunes elongating on a starved bed from a sand source in bimodal flow regimes was numerically studied in [64]. Depending on the parameters (divergence angle and transport ratio between alternate flow directions), an elongating linear dune or a train of propagating asymmetric barchans is observed. The ratio σ_E/σ_H was found to discriminate between the two morphologies ; elongating dunes are observed when σ_E/σ_H is larger than 0.6. This result reflects the fact that perpendicular flows are required to build a dune, regardless of its orientation. Note that in experiments under water with a bimodal flow regime, a linear dune elongating from a point

Figure	12	13	14	15	16	17	18	19	20		
Bed surface	CB	CB	CB	SB	SB	SB	SB	SB	PSB		
Shear velocity											
$\langle u_* \rangle$ (m s^{-1})	0.243	0.24	0.229	0.218	0.227	0.288	0.238	0.236	0.226		
u_t (m s^{-1})	0.153	0.153	0.153	0.153	0.153	0.153	0.153	0.153	0.153		
$\langle u_* \rangle / u_\mathrm{t}$	1.585	1.56	1.498	1.425	1.484	1.879	1.56	1.544	1.47		
Flux on a flat sand bed											
DP = $\langle \|\vec{Q}\| \rangle$ (m^2 yr^{-1})	39.1	37.2	31.8	25.1	43.8	118.9	39	30.2	29.5		
RDP = $\|\langle \vec{Q} \rangle\|$ (m^2 yr^{-1})	33.8	8.3	14.9	14.4	19.2	100.5	28.7	15.4	2.5		
RDP/DP	0.86	0.22	0.47	0.57	0.44	0.85	0.74	0.51	0.08		
RDD (deg., mod 360°)	48.6	294.9	337.5	214.1	226.6	253.1	88.5	219.4	62.7		
Dune orientations and flux at the crest											
α_H (deg., mod 360°)	136.6	51.6	148.2	144.2	111.4	162.9	168.9	110.2	127.7		
α_E (deg., mod 360°)	45.2	272.5	328.8	202.9	237.4	251.5	90.3	222.3	30.8	119.7	253
$\|\langle \vec{Q}_\mathrm{H} \rangle\| = \|\langle \vec{Q}_\mathrm{c}(\alpha_\mathrm{H}) \rangle\|$ (m^2 yr^{-1})	151.0	29.4	42.9	68.1	87.6	393.7	142.1	67.5	9.1		
θ_H (deg., mod 360°)	48.2	292.4	329.3	223.8	220.1	253.3	86.4	212.2	112		
$\|\langle \vec{Q}_\mathrm{M} \rangle\| = |\langle Q_\perp(\alpha_\mathrm{H}) \rangle|$ (m^2 yr^{-1})	150.1	25.7	0.87	67	82.9	393.7	140.8	66.1	2.45		
$\|\langle \vec{Q}_\mathrm{E} \rangle\| = \|\langle \vec{Q}_\mathrm{c}(\alpha_\mathrm{E}) \rangle\|$ (m^2 yr^{-1})	57.1	18.5	42.9	41.4	44.2	144.3	46.7	37.4	11.6	7.7	3.8
$\Delta\alpha = \alpha_\mathrm{H} - \alpha_\mathrm{E}$ (deg.)	88.6	40.9	0.7	58.7	53.9	88.7	78.5	67.9	86.9	10	54.7
$\Delta\theta = \theta_\mathrm{H} - \alpha_\mathrm{E}$ (deg.)	3.0	19.9	0.5	20.9	-17.3	1.84	3.9	-10.2	81.2	-7.7	-141
Competition between dynamics											
$\sigma_\mathrm{E}/\sigma_\mathrm{H}$	0.18	0.67	1	0.61	0.67	0.18	0.23	0.4	0.23	0.98	0.48
$|\langle Q_\|(\alpha_\mathrm{H}) \rangle / \langle Q_\perp(\alpha_\mathrm{H}) \rangle|$	0.03	0.56	49.4	0.18	0.34	0.01	0.13	0.21	0.03		
$|\langle |Q_\perp(\alpha_\mathrm{H})| \rangle / \langle Q_\perp(\alpha_\mathrm{H}) \rangle|$	1.09	5.9	115	1.54	1.88	1.07	1.18	1.83	54.05		
$|\langle |Q_\perp(\alpha_\mathrm{E})| \rangle / \langle Q_\|(\alpha_\mathrm{E}) \rangle|$	0.51	5.5	2.31	1.51	2.38	0.53	0.81	1.31	2.7	17	16.8

Table 3: Wind velocity, sand flux, and dune orientation calculated from wind data at the different locations shown in Figs. 12 - 20. Orientations are with respect to the east. Bed surface: CB, SB, and PSB stand for sand covered bed, starved bed, and partially starved bed, respectively. α_H is the dune orientation that maximizes growth rate in height. α_E is the dune orientation in the elongation mode. θ_H is the direction of mean sand flux at dune crest for dunes whose orientation is α_H.

source on a starved bed turns into a highly asymmetric barchan with an oblique arm if the sand source shuts off so that the dune is free to migrate [93]. The sand source helps to mute dune migration. As such, the ratio $\sigma_{\mathrm{E}}/\sigma_{\mathrm{H}}$ cannot be used to distinguish the prevailing dynamics for dune orientation under different boundary conditions, including bed mobility. This could be the case if the boundary conditions were specifically taken into account in the calculations, which is not the case here.

When dunes develop on a sand covered bed, growth in height prevails and the orientation of the dune crest is α_{H}. Within given boundary conditions, the variety of shapes should then depend on the two dimensionless ratios $\left|\langle Q_{\parallel}(\alpha_{\mathrm{H}})\rangle/\langle Q_{\perp}(\alpha_{\mathrm{H}})\rangle\right|$ and $\left|\langle|Q_{\perp}(\alpha_{\mathrm{H}})|\rangle/\langle Q_{\perp}(\alpha_{\mathrm{H}})\rangle\right|$. The ratio between the crest-parallel and the crest-normal components of sand flux, $\left|\langle Q_{\parallel}(\alpha_{\mathrm{H}})\rangle/\langle Q_{\perp}(\alpha_{\mathrm{H}})\rangle\right|$, was conceptually proposed to quantify the impact of a wind regime on straightness and sinuosity of morphologically long dunes [65]. The crest-parallel component should favor straightness whereas the crest-normal component, causing migration, should favor sinuosity. We note, however, that crest-straightness could be favored by the gross crest-parallel component instead of the crest-parallel component of resultant, so that the ratio $\left|\langle|Q_{\parallel}(\alpha_{\mathrm{H}})|\rangle/\langle Q_{\perp}(\alpha_{\mathrm{H}})\rangle\right|$ could be more appropriate. Growth in height also building the spatial coherence of a dune, the ratio $\left|\langle|Q_{\perp}(\alpha_{\mathrm{H}})|\rangle/\langle Q_{\perp}(\alpha_{\mathrm{H}})\rangle\right|$ may be relevant as well to evaluate dunes straightness.

For dunes migrating on a starved bed, which also have an orientation that maximizes growth in height, the migrating direction, θ_{M}, does not necessarily correspond to the resultant transport direction, θ_{H}. This asymmetry in sand fluxes must drive an asymmetry in dune morphology that the ratio $\left|\langle Q_{\parallel}(\alpha_{\mathrm{H}})\rangle/\langle Q_{\perp}(\alpha_{\mathrm{H}})\rangle\right|$ may account for.

For dunes elongating without migrating, the crest-normal component of sand flux is constant and null, so that the ratio $\left|\langle|Q_{\perp}(\alpha_{\mathrm{E}})|\rangle/\langle Q_{\parallel}(\alpha_{\mathrm{E}})\rangle\right|$ alone should allow us to distinguish between morphologies.

Finally, since the very existence of a dune relies on the ability of winds to raise it in height, the competition between migration and elongation for selecting dune orientation on a starved bed could be assessed by comparing the two ratios $\left|\langle|Q_{\perp}(\alpha_{\mathrm{H}})|\rangle/\langle Q_{\perp}(\alpha_{\mathrm{H}})\rangle\right|$ and $\left|\langle|Q_{\perp}(\alpha_{\mathrm{E}})|\rangle/\langle Q_{\parallel}(\alpha_{\mathrm{E}})\rangle\right|$. A mode should be promoted when it favors the growth in height over migration or elongation.

Although only a few of these parameters have been tested in previous studies, and that their calculations are based on numerous simplifications, they formalize a framework for studying dune morphology based on dune dynamics. We already remarked that fully predictive parameters should take into account boundary conditions, which affect sand supply and the divergence of sand flux at the dune scale. Some parameters, such as free flux, may be difficult to infer remotely. For example, the migration velocity of an isolated dune like a barchan decreases and its size may increase when it captures an incoming free flux. More importantly, useful predictive parameters should involve the temporal sequence of transport directions and the relative size of dune to transport capacity of individual wind events. For example, experiments in water and simulations have shown that a dune initially turns over before migrating when subjected to an abrupt change in flow direction [172, 41, 173, 174, 175]. Furthermore, in bidirectional wind regime, numerical simulations show that the ratio between the time period of wind reversal and the characteristic turnover time of dune controls the crest sinuosity [63, 176].

5.2.2 Example analyses for various characteristic free dune types on Earth

Different types of free dunes from the geomorphological classification 2 are shown in Figures 12-20. The sand transport parameters for characterization of their formative processes and orientation according to the dynamics-based classification are gathered in Table 3. Transport parameters are calculated from wind data provided by the ECMWF ERA5-Land reanalysis [166, 167] from January 1, 2010 to December 31, 2020.

Periodic long-crested dunes on sand covered beds Periodic long-crested dunes on sand covered beds can form with orientations that are transverse (Fig. 12), oblique (Fig. 13), or longitudinal (Fig. 14) with respect to the RDD. The expected prevailing process on a sand bed is the growth in height of a periodic pattern (bed instability) with dunes forming in the orientation that maximizes the gross bedform-normal transport, *i.e.* $\langle|Q_{\perp}|\rangle$, which is well verified in these three examples. Where the wind regime tends to be unidirectional, long transverse dune patterns develop with an asymmetric shape showing a clear difference between gentle stoss side and steep lee face (Fig. 12). Under bimodal wind regimes, long-crested dune patterns with more symmetric slopes are observed. As predicted from theory, they are usually oblique in orientation (Fig. 13), and only tend to be longitudinal where the transport ratio between the two main wind directions is close to one (Fig. 14) [65, 41]. Transverse dune patterns in Fig. 12 show a range of sizes with smaller dunes either being superimposed on larger ones or spatially separated. Subjected to an almost unidirectional flux regime, they must migrate as predicted by the net sand flux associated with migration, $\langle Q_{\mathrm{M}}\rangle = |\langle Q_{\perp}(\alpha_{\mathrm{H}})\rangle|$. In these examples, the ratios $\left|\langle Q_{\parallel}(\alpha_{\mathrm{H}})\rangle/\langle Q_{\perp}(\alpha_{\mathrm{H}})\rangle\right|$ and $\langle|Q_{\perp}(\alpha_{\mathrm{H}})|\rangle/|\langle Q_{\perp}(\alpha_{\mathrm{H}})\rangle|$ increase by more than two orders of magnitude as the predicted dune orientation goes from transverse, to oblique, to longitudinal. This may explain why
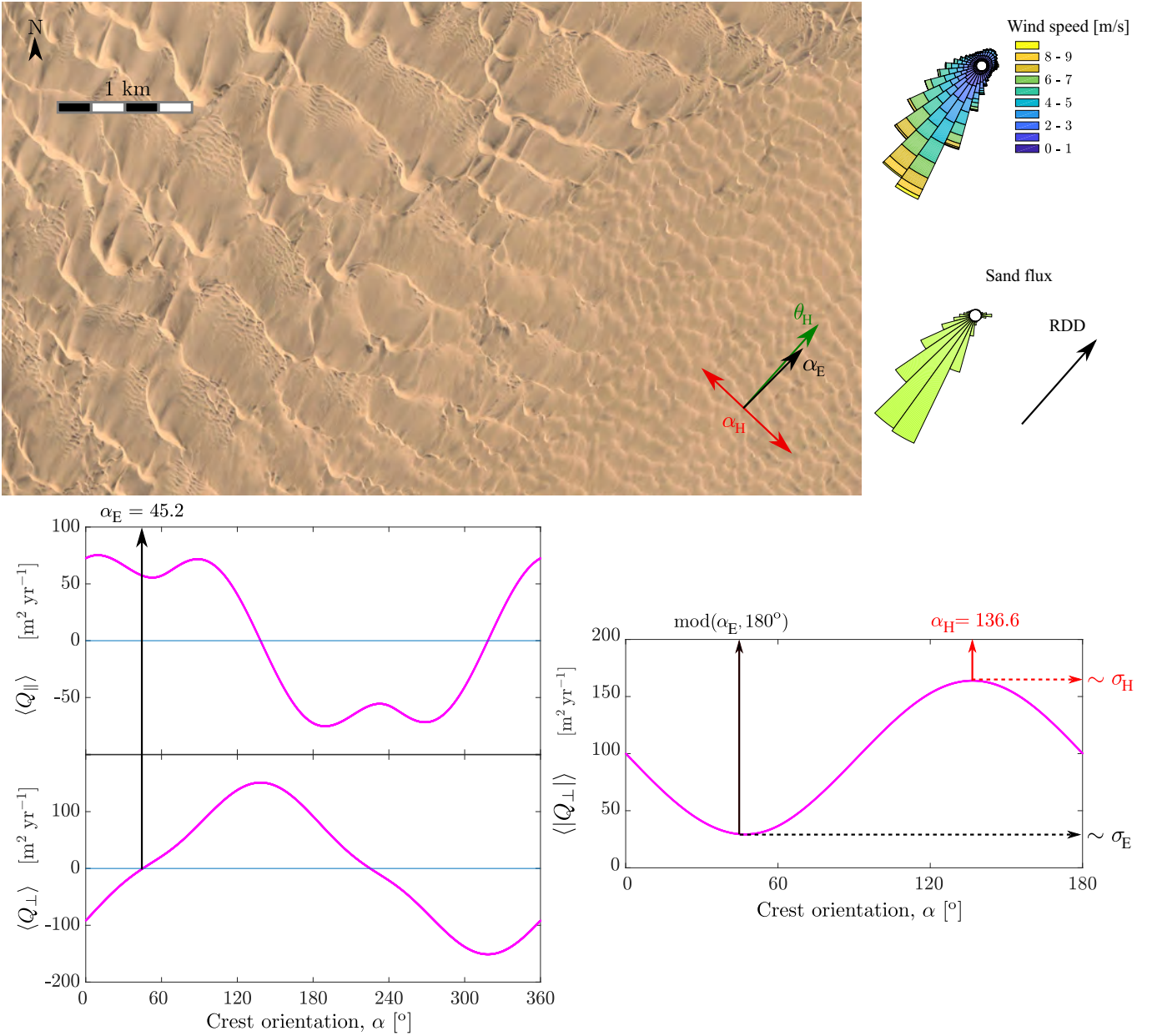
Figure 12: Transverse long-crested dunes on sand-covered bed in the Moçâmedes desert in Angola (16.6°S, 11.9°E). Roses, which point upstream, show the wind regime and the corresponding sand flux regime from 2010 to 2020. See Sections 5.2 and 7 for an explanation of parameters and details of calculations. Graphics show the calculated characteristic sand flux components $\langle Q_\perp \rangle$, $\langle Q_\parallel \rangle$ and $\langle |Q_\perp| \rangle$ over a dune with orientation α. Angles are measured relatively to east direction. The dune orientation α_I that maximizes $\langle |Q_\perp| \rangle$, the dune direction α_E for elongation ($\langle Q_\parallel \rangle > 0$) without migration ($\langle Q_\perp \rangle = 0$) and the direction of the sand flux θ_I over a dune of orientation α_I are shown by arrows in the image.

transverse dunes in Fig. 12 resemble barchanoid ridges, whereas oblique dunes in Fig. 13 are straighter. Although these ratios are even larger for longitudinal dunes in Fig. 14, crests are not straight. However, we observe that in this region, sand transport directions are much more widely distributed. Here, the amplitude of variation of gross bedform-normal transport as a function of crest orientation, $\langle |Q_\perp| \rangle(\alpha)$, varies by a factor 1.4, compared to a factor 3 for transport regimes in Figures 12 and 13. This smaller value may lead to a weaker selection of a well defined orientation, especially at small scale, explaining the greater variability in crest alignment observed for the longitudinal dunes in Fig. 14.
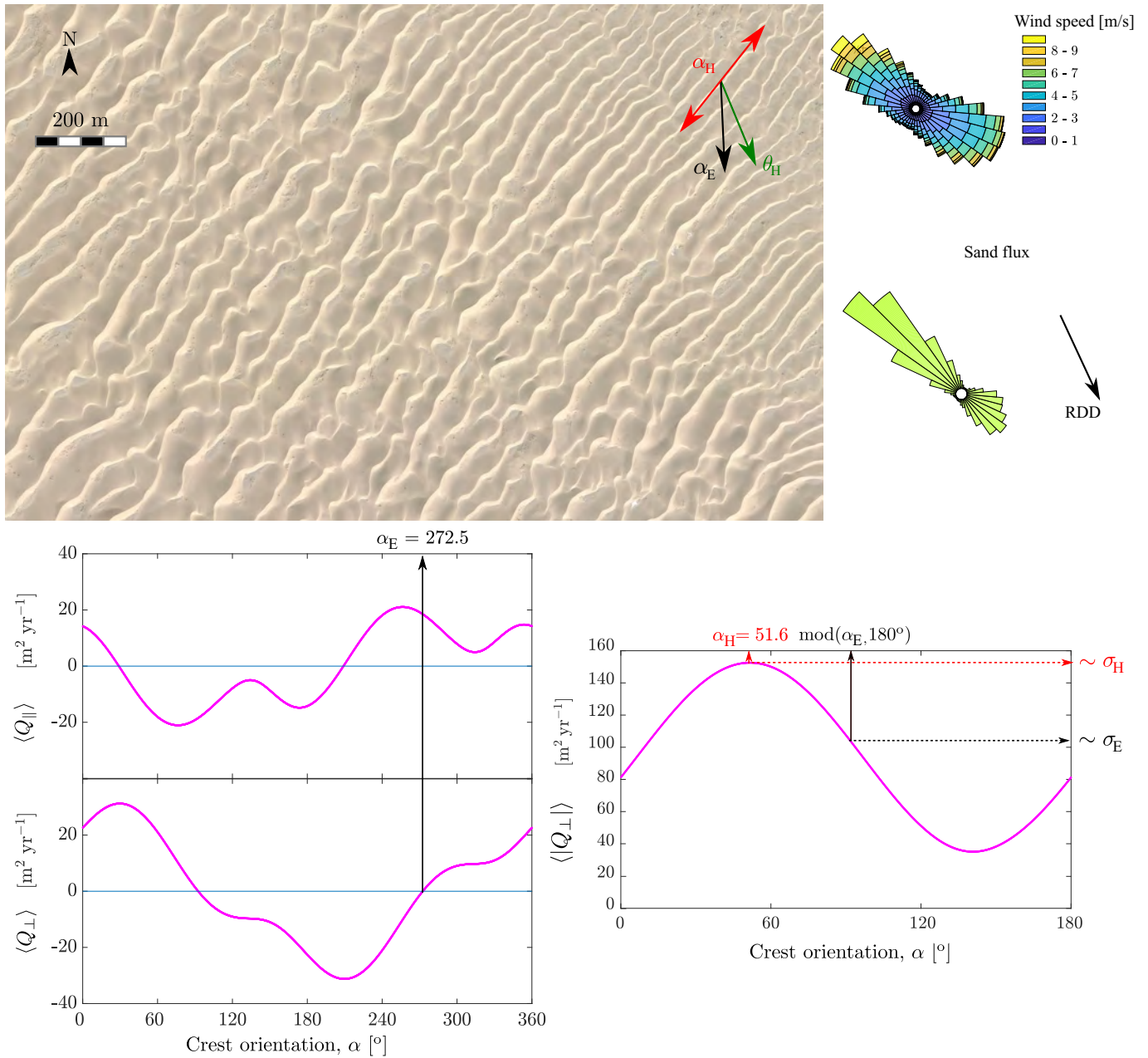
Figure 13: Oblique long-crested dunes dunes in the Tengger desert in China (37.7°N, 105.1°E). See caption of fig. 12 for an explanation of parameters and plots.

Dunes on starved beds Starved interdunes should promote elongation or migration. Elongation without migration can be favoured by boundary conditions such as a localized sand source, which inhibits migration. Extended lee dunes are good candidates, like the isolated linear longitudinal dune extending downwind from a large obstacle shown in Figure 15. The predicted orientation for elongation without migration, α_E, corresponds to the observed orientation of this dune and is significantly different from the oblique alignment predicted for dunes whose orientation maximizes growth in height, α_H. In a different bimodal wind regime, the larger periodic linear longitudinal dunes shown in Figure 16 also exhibit an orientation that corresponds to the elongation mode. Longitudinal linear dunes, because they can elongate along the sand flow paths, are the most likely to extend over long distances. These massive dunes follow a major sand flow path that extends from southwestern Algeria to Mauritania. Unlike the bed instability, experiments and numerical simulations have shown that the elongation process does not directly determine dune size or wavelength [41, 177]. The periodicity and sizes are instead imposed by boundary and initial conditions, which,
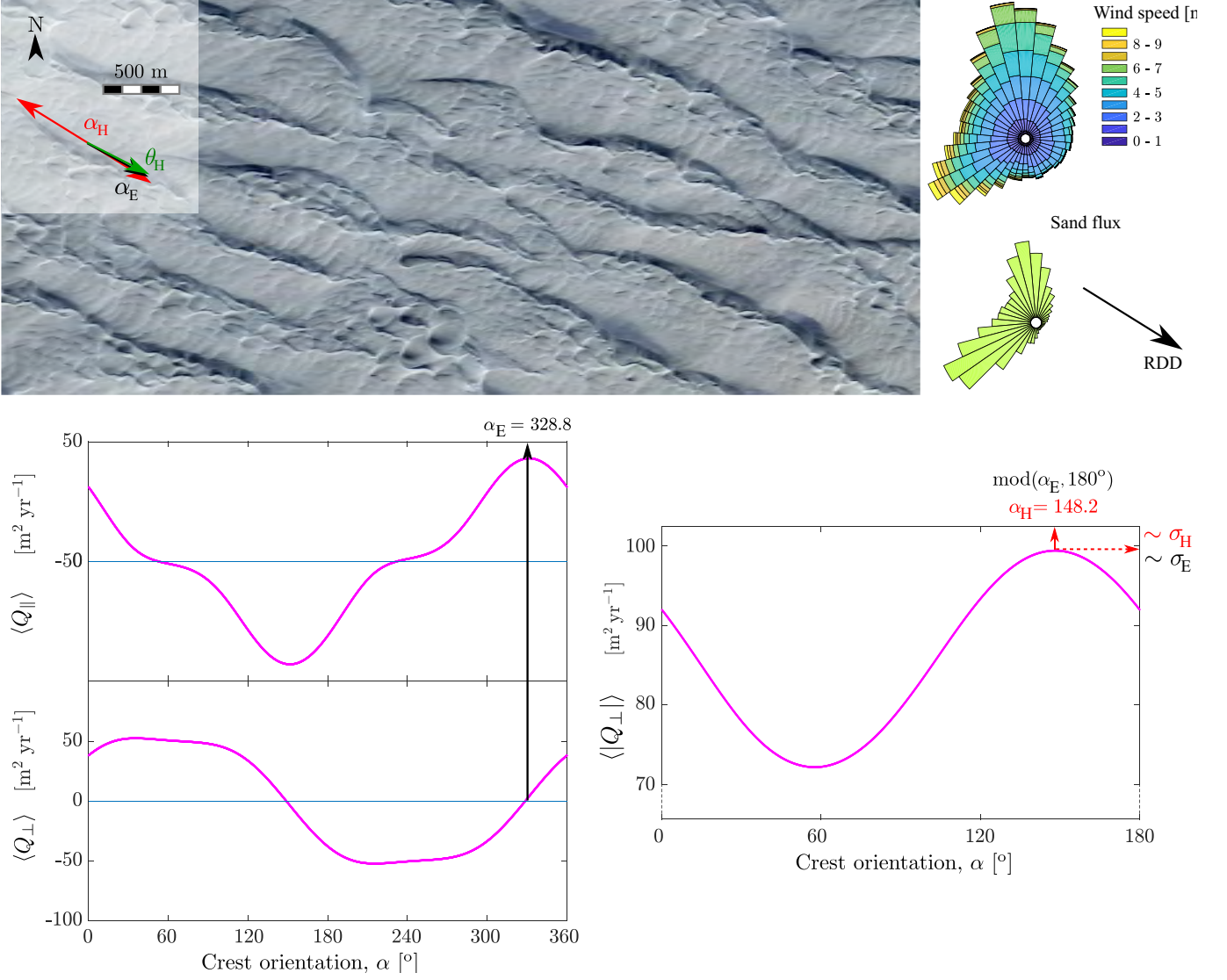
Figure 14: Longitudinal long-crested dunes on sand-covered bed in the Northern Sinai in Egypt (30.9°N, 33.1°E). See caption of fig. 12 for an explanation of parameters and plots.

with self-organization, are possible explanations for the periodic pattern in the elongation mode observed in this field. However, we note that the ratio σ_E/σ_H is quite large (0.67 when the largest possible value is 1), and, according to [64], this enables dunes in this region to be oriented in the elongating mode, as shown by the isolated linear dune shown in Fig. 15 ($\sigma_E/\sigma_H = 0.61$).

Barchan dunes, such as those observed in the Western Sahara (Fig. 17), are the archetype of migrating dunes. Here, and most often for symmetric barchans, the sand flux regime is unidirectional. Barchan slip faces are oriented perpendicular to the transport direction, which, for a unidirectional transport regime, is also the predicted orientation when growth in height prevails.

Towards complex patterns   The recognizable shape and ubiquity of barchan dunes on Earth and Mars have made them a popular subject of study, so much so that models have been developed to explain 'seif dunes', *i.e.*, isolated longitudinal linear dunes on a starved bed, as morphological evolutions of this elemental dune [32, 178, 94, 179]. This approach is certainly partly motivated by the widespread observation of asymmetric barchans with an elongated arm. Four causes for barchan asymmetry have been identified [180, 92, 181]: dune collision, asymmetry of influx, inclined topography, and bidirectional winds. The autogenic processes of dune collision and asymmetry of influx are very common in barchan dune fields [115, 116] but only cause transitional dune asymmetry, localized in space and time.
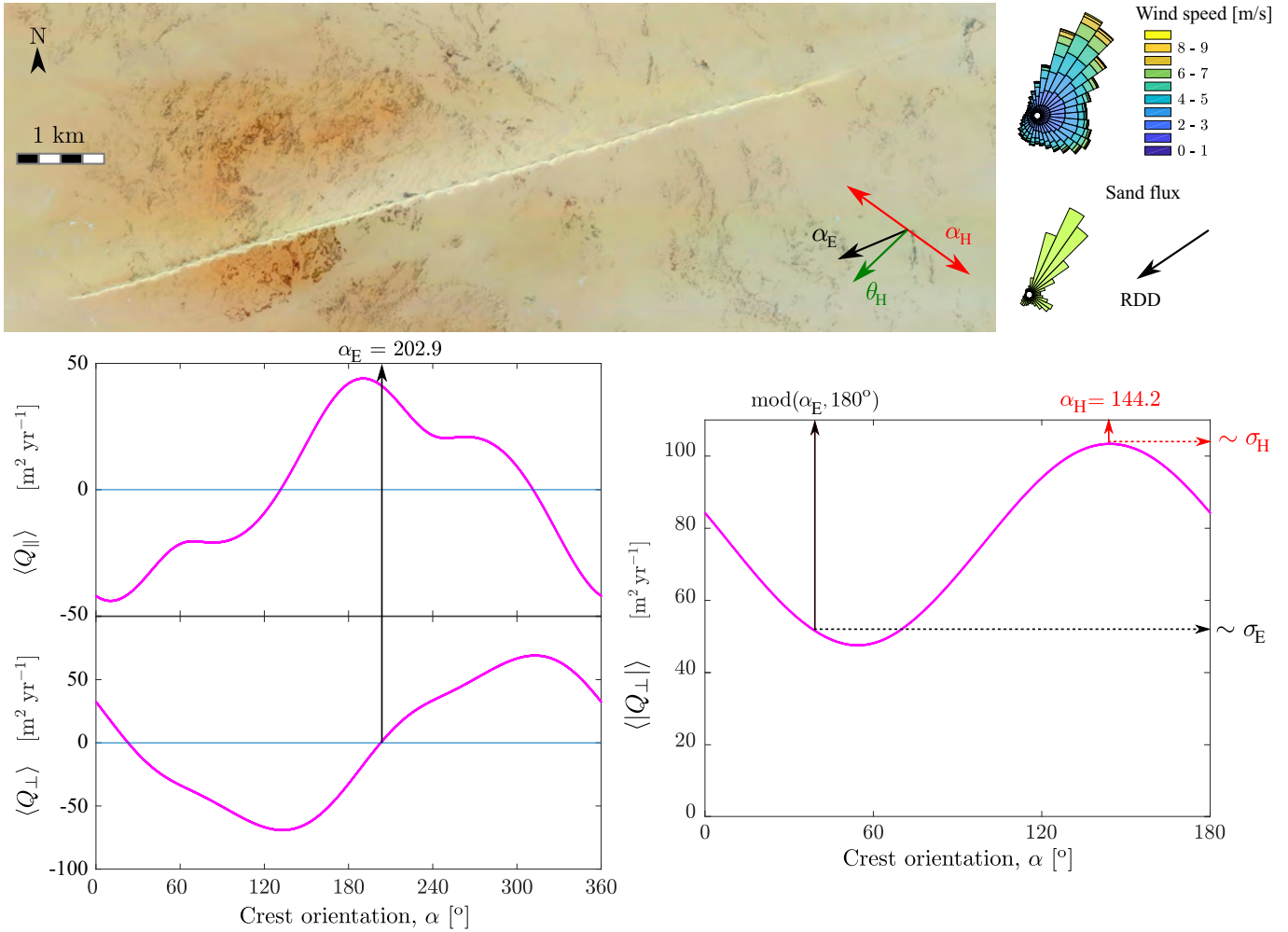
32

Figure 15: Isolated longitudinal linear dune on a starved bed in the Ténéré in Niger (18.8°N, 12.6°E). It extends downwind from an obstacle.

See caption of fig. 12 for an explanation of parameters and plots. It is worth noting that the direction of elongation does not generally correspond to the direction for which sand flux along crest is maximum but to the one for which crest-normal component of sand flux vanishes (no migration) and crest-parallel component is positive. There, the derivative of the crest-normal component is negative, which makes the elongation direction a stable equilibrium.

Along the Skeleton coast of Namibia, asymmetric barchans always have an elongated arm on the same side, which is ascribed to the bidirectional sand flux regime (Fig. 18). Only larger dunes have an elongated arm. This might be because smaller dunes are not large enough to integrate the entire period of wind reorientation. In this bidirectional regime of sand flux, the direction of sand flux for a dune that maximizes growth in height, θ_H, does not correspond to the direction of migration, θ_M. Here, the two directions differ by 7.5°, compared with 0.4° in the symmetric barchans example (Fig. 17). We believe this small difference drives an asymmetric sand redistribution between the two arms, which in this case leads to the elongation of the arm that is fed by the crest-parallel component of sand flux. In this example, the ratio $|\langle Q_\parallel(\alpha_H)\rangle/\langle Q_\perp(\alpha_H)\rangle|$ equals 0.13, which is significantly larger than the value for the symmetric barchans example (0.01, Fig. 17). Such asymmetric barchans with an elongated arm can also be seen as combinations of a migrating dune and an elongating dune at different scales. The barchan dune (large scale) has little sediment supply but is a source of sand for the elongated arm (smaller scale). As a result of dune migration, the orientation of the elongated arm is shifted in the opposite direction of the migration from that which would prevail for elongation without migration. Conversely, an elongating dune can be seen as an extremely asymmetric barchan, whose crescentic base is prevented from migrating. This picture is supported for example by the dune termination of one of the large linear longitudinal dunes on a partially starved bed observed in the bottom right corner of Fig. 16. The ratio $|\langle Q_\parallel(\alpha_H)\rangle/\langle Q_\perp(\alpha_H)\rangle|$ increases consistently with dune asymmetry in the three examples of symmetric
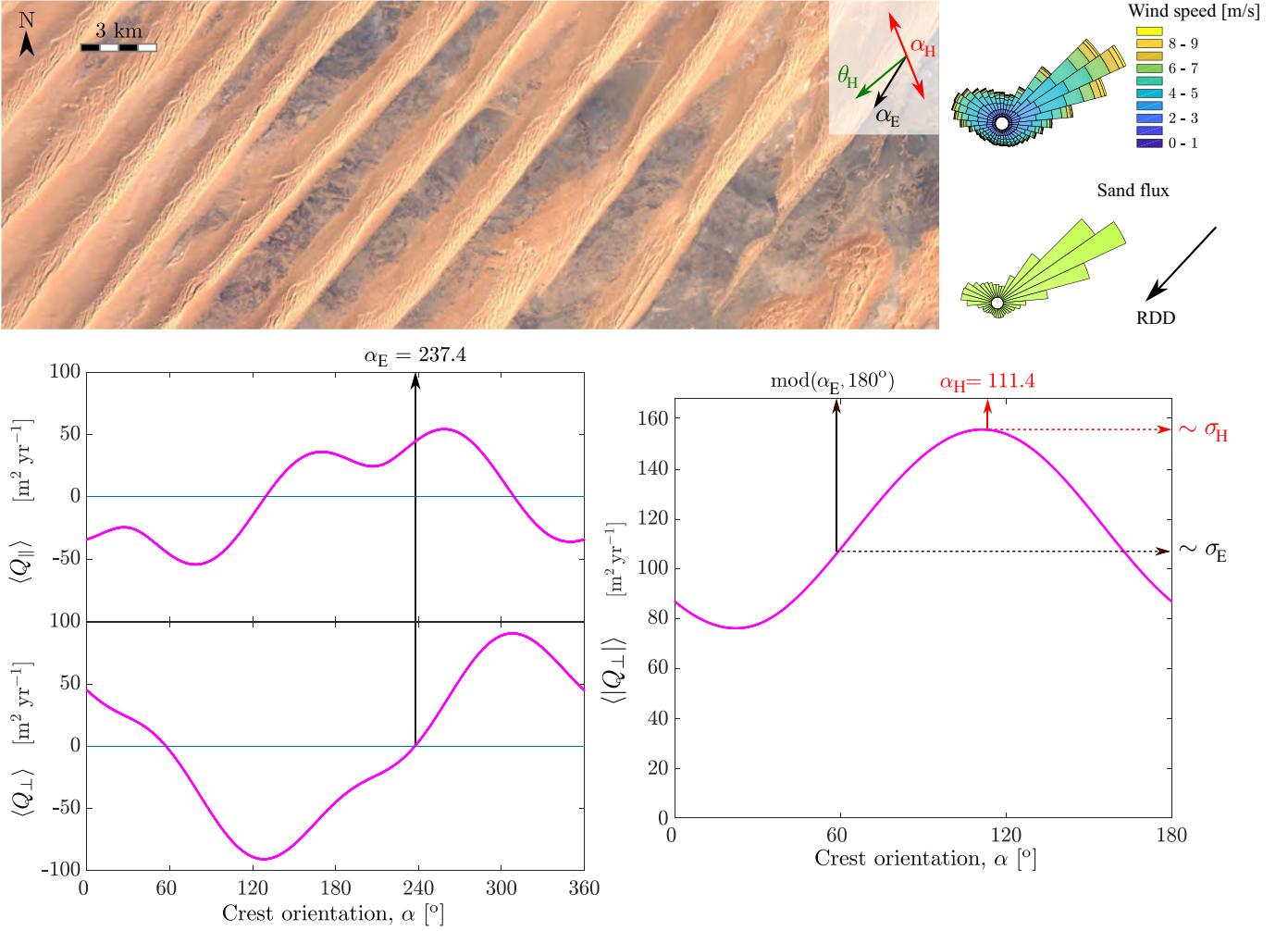
33

Figure 16: Periodic longitudinal linear dunes with partially starved interdune area in the Chech desert in Namibia (24.3°N, 4.4°E).
See caption of fig. 12 for an explanation of parameters and plots.

barchans, asymmetric barchans and large longitudinal linear dunes.

Asymmetric barchans are isolated structures, which clearly exemplify a coexistence of the different formative processes. Meanwhile, most sand seas exhibit complex dune patterns that may also result from such a coexistence. 'Raked linear dunes', such as those shown in Figure 19, are another example of this coexistence. These dunes, which lie on an armored bed composed of coarse grains, have a constant orientation for considerable distances and a marked asymmetry between a periodic pattern of semi-crescentic structures on one side and a continuous slope on the other. This semi-crescentic periodic pattern has been described as resulting from the development of superimposed dunes that grow in height and migrate in the bed instability mode on a linear dune that elongates [126]. The coexistence of these processes produces coupled primary and secondary patterns with similar height but with different shapes and orientations, which are oblique to each other. The orientation of primary linear ridges corresponds to the predicted orientation for dunes in the elongating mode, albeit σ_E/σ_H has an intermediate value. The tri-directional transport regime also enables the secondary raked pattern to develop on the leeward side of the primary linear ridges, in consistency with the predicted migration direction for dunes in the bed instability mode. Quantitatively predicting the occurrence of this pattern still remains challenging.

Finally, we examine an example of star dunes (Fig. 20), one of the most emblematic intricate dune patterns. In this example in the Namib desert, the bed is partially starved and, starting from dune summits, we observe three main directions for the arms: (i) towards the northeast, (ii) the northwest, and (iii) the southeast. Star dunes should be observed in zones where the migration process is muted and where elongation and/or growth in height may be promoted
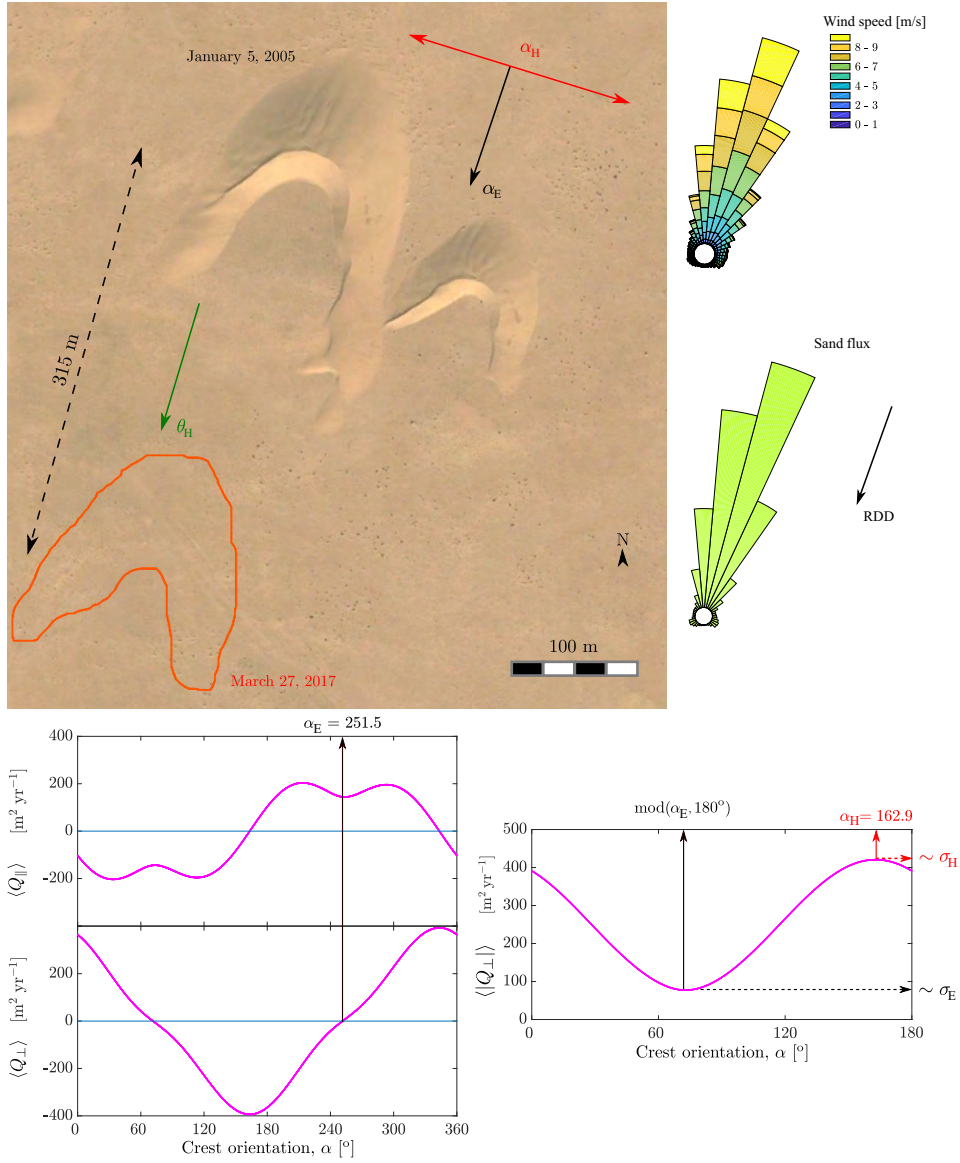
34

Figure 17: Barchan dune on a starved bed in Western Sahara in Morocco (27.5°N, 13.1°W). The red contour shows location of the main barchan 12 years after the snapshot was taken. See caption of fig. 12 for an explanation of parameters and plots.

in multiple directions. In this specific area, the ratio RDP/DP is close to zero so that dunes should barely migrate. The model shows three directions for elongation, which is made possible by taking into account the wind speed-up: towards the northeast ($\alpha_{E,1}$), the northwest ($\alpha_{E,2}$), and the southwest ($\alpha_{E,3}$). The predicted orientation for dunes that maximizes growth in height is very close to the northwest direction of elongation, $\alpha_{E,2}$. For this direction of elongation, the ratio σ_E/σ_H is very close to one. This is clearly the prevalent crest orientation in the field. However, an orientation close to $\alpha_{E,1}$ is observed, although the ratio $\sigma_E/\sigma_H = 0.23$ is significantly smaller than the theoretical threshold value of 0.6. On the other hand, the predicted orientation $\alpha_{E,3}$ is not observed, while the ratio σ_E/σ_H is larger (but still below the theoretical threshold value). Instead, we observe a direction towards the southeast, opposite to the other prevailing direction, which is towards the northwest. Both orientations could therefore correspond to the orientation that maximizes growth in height, which would be promoted by migration. We note that $\left|\langle|Q_\perp(\alpha_H)|\rangle/\langle Q_\perp(\alpha_H)\rangle\right|$ is much larger than any of the values of $\left|\langle|Q_\perp(\alpha_E)|\rangle/\langle Q_\parallel(\alpha_E)\rangle\right|$. Such a pattern with several orientations is still difficult to predict correctly. This could be partly due to the fact that the pattern is significantly different from the symmetric linear ridges assumed in calculations.
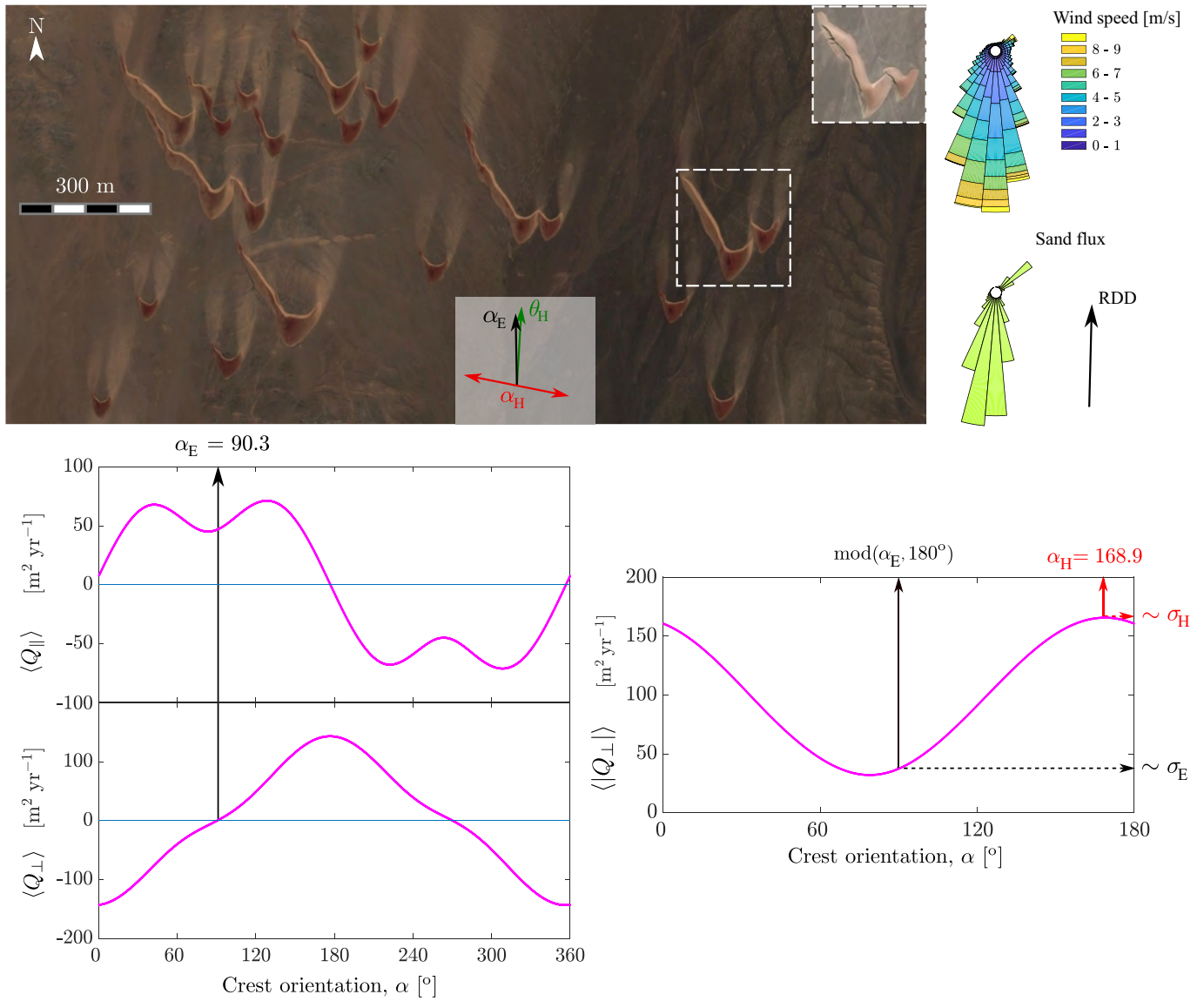
35

Figure 18: Asymmetric barchan dune with an elongated horn on a starved bed on the Skeleton coast in Namibia (20.1°S, 13.3°E).
The inset shows the dunes in the white dashed box after a secondary wind event. See caption of fig. 12 for an explanation of parameters and plots.

As demonstrated in the examples above, the proposed framework for dynamics-based dune classification appears promising. In most cases, it correctly predicts dune orientation. However, the definitive phase diagram of dune morphologies is still far from being developed, and the relevant parameters are only very partially determined. Such a comprehensive phase diagram requires a more exhaustive study than the few examples discussed here, for which we note that the values of the various dimensionless parameters are correlated. The model may also gain predictive power by further taking into account the coupling between dune morphology and sand transport. A first step could be to include the larger sand flux that occurs during crest reversals, as observed over the entire height of the elongated arm (inset in Fig. 18). Such a refinement of sand flux calculations requires consideration of the variation of the upwind slope with the time series of wind directions.
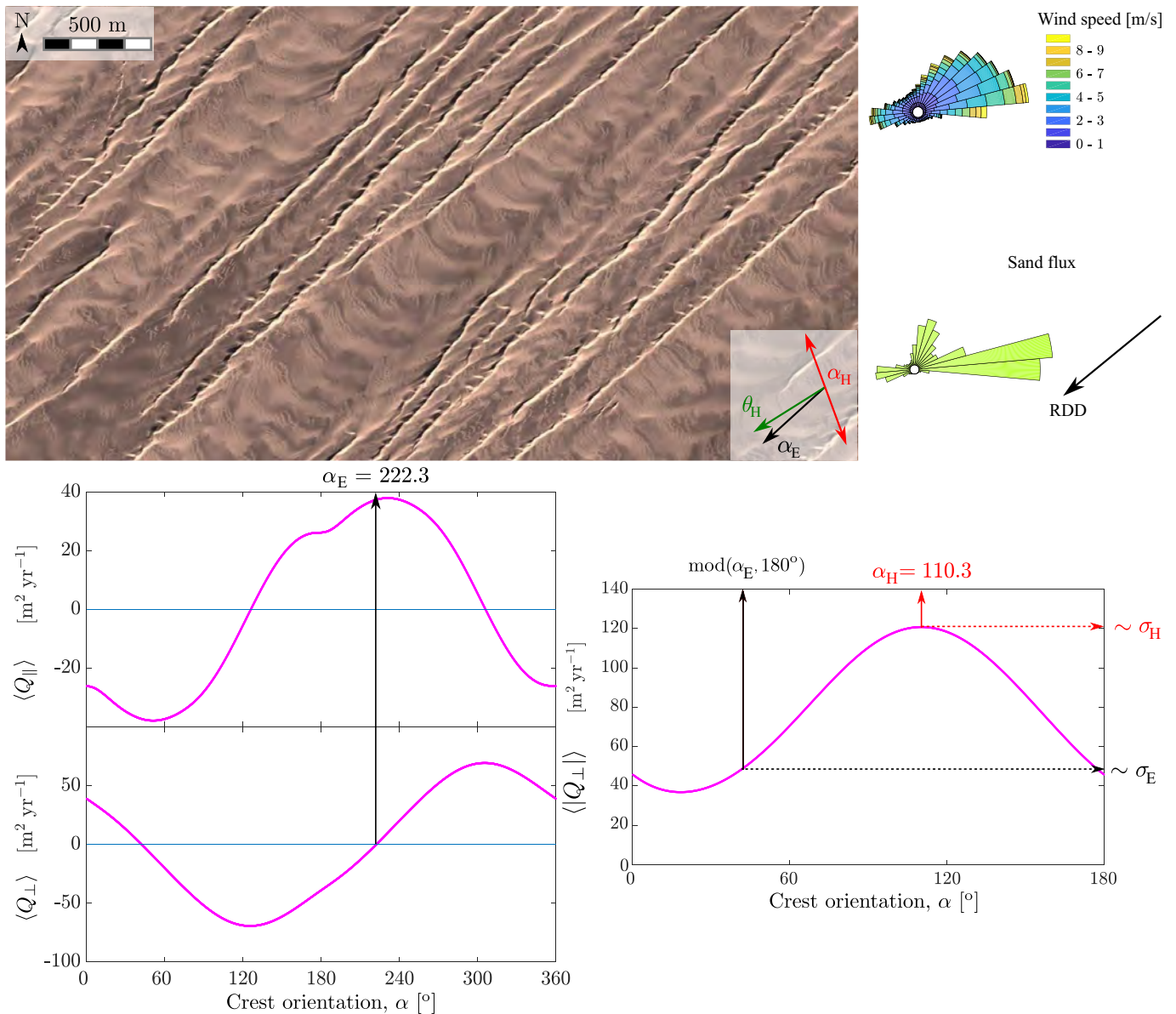
Figure 19: Raked linear dunes on an armored bed of coarse grains in Kumtagh desert in China (40.3°N, 92.7°E). See caption of fig. 12 for an explanation of parameters and plots.

5.3 Determining dune orientation relative to sand transport direction from morphology

The preceding discussion considers classification of dunes and characterization of formative mechanisms where wind measurements or sand transport measurements are available. As discussed in Section 2.3.2, however, some dynamic properties can be inferred even without such measurements. The long-crested examples in Figures 12-16, 19, and 21 can be used to test the approach of inferring dune orientation relative to the net transport direction based solely on morphology, as proposed in Table 2.3.2. In some of these examples dune morphology/asymmetry is unclear unless the image is rotated, so that the illumination comes from the top of the image. Except for Figure 16—in which the resolution is insufficient to determine the cross-sectional asymmetry of the main dunes and superimposed dunes—the examples are consistent with Table 2.3.2.

The dunes in Figures 12 and 21 are known from wind measurements to be transverse dunes, and in both cases this interpretation is demonstrable from morphology alone. The main dunes are asymmetrical, and the superimposed lee-side spurs are approximately symmetrical in cross-section (the spurs lack a steep lee side and gentle stoss side),
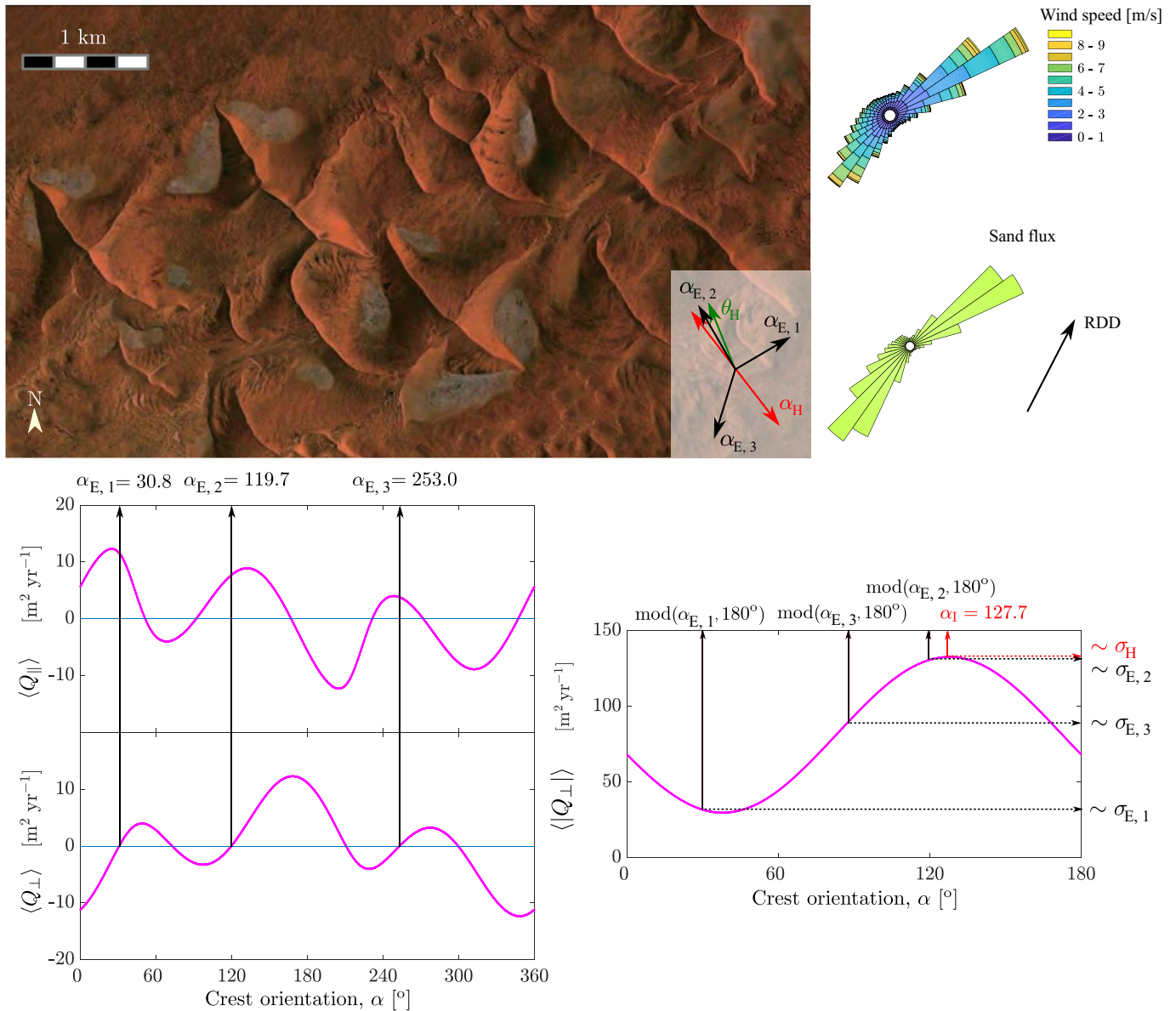
Figure 20: Star dunes on a partially starved bed in the Namib desert in Namibia (26.9°S, 15.9°E). See caption of fig. 12 for an explanation of parameters and plots.

demonstrating a lack of systematic migration and net transport parallel to the crests of the main dunes.

The dunes in Figure 13 are oblique to the resultant transport direction, and this can also be demonstrated from morphology. The main dunes have cross-sectional asymmetry indicating across-crest transport toward the southeast. Most of the dunes in the figure lack sufficient superimposed features to determine their migration direction, but the superimposed leeside spurs in the lower right corner of the image have slipfaces that preferentially dip in a direction parallel to the crests of the main dunes. This combination of across-crest transport and along-crest transport demonstrates obliquity of the main dunes, at least in this corner of the image.

Wind data show that the dunes in Figures 14, 15, and 19 are longitudinal dunes, which also can be demonstrated from morphology alone. The main dunes are relatively symmetrical in cross-section, and the superimposed dunes (Figs. 14 and 19) or sinuosities (Fig. 15), have consistent asymmetric cross-sections, thereby demonstrating systematic transport in an along-crest direction over the main dunes. The steeper lee sides of the superimposed features indicate net transport parallel to the crests of the main dunes toward the east southeast in Figure 14, and toward the west southwest in Figure 15. In Figure 19, the superimposed features resemble half-barchans migrating southwest along the lengths of the main dunes [126].
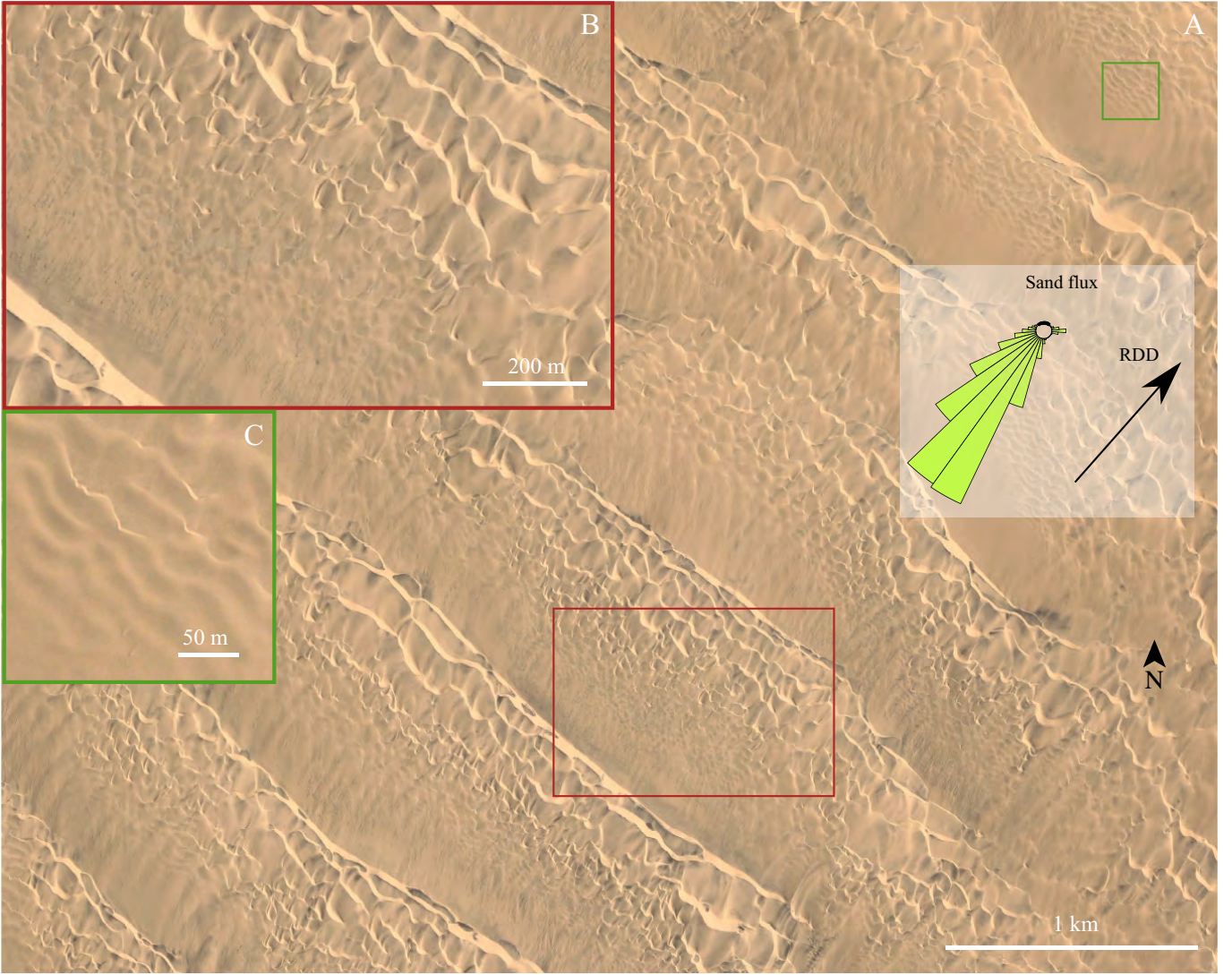
Figure 21: Illustration of the rough case with terrestrial dunes ($\mathcal{R}_r \simeq 80$). Photographs of a coastal dune field in southwest Angola (16.4°S, 11.9°E). Local winds are approximately unidirectional (see flux rose), and the dunes, with fairly straight crests perpendicular to the resultant drift direction (RDD), can be denominated as 'linear transverse'. Sand availability is high (no cohesive interdune). The dunes form at the elementary scale $\lambda_{\min} \simeq 20$ m (panel c, green frame), interact and coarsen in the course of their migration downwind (panel b, red frame) and the large-scale dune pattern has a wavelength $\lambda_{\max} \simeq 850$ m (panel a). Credit: Maxar Technologie (2022).

In summary, the migration directions superimposed topographic features relative to the main dunes can be used to determine whether the main dunes are transverse, oblique, or longitudinal and similarly to constrain the direction of net sand transport relative to the dunes. These inferences are qualitative and do not necessarily match the quantitative definition of Hunter et al. [38]. Nevertheless, this approach may be useful in interpretations of dunes where wind data or measurements of sand transport or dune migration are not available. This is often the case for other planets and is always the case for interpreting deposits of dunes in the stratigraphic record, the purpose for which this approach was initially developed (as discussed in Section 2.3.2).

5.4 Expected dune sizes in the solar system from fluid and sediment-transport mechanics

As environmental and boundary conditions significantly vary from one planetary body to another, dunes on their surfaces sample the different formation regimes.
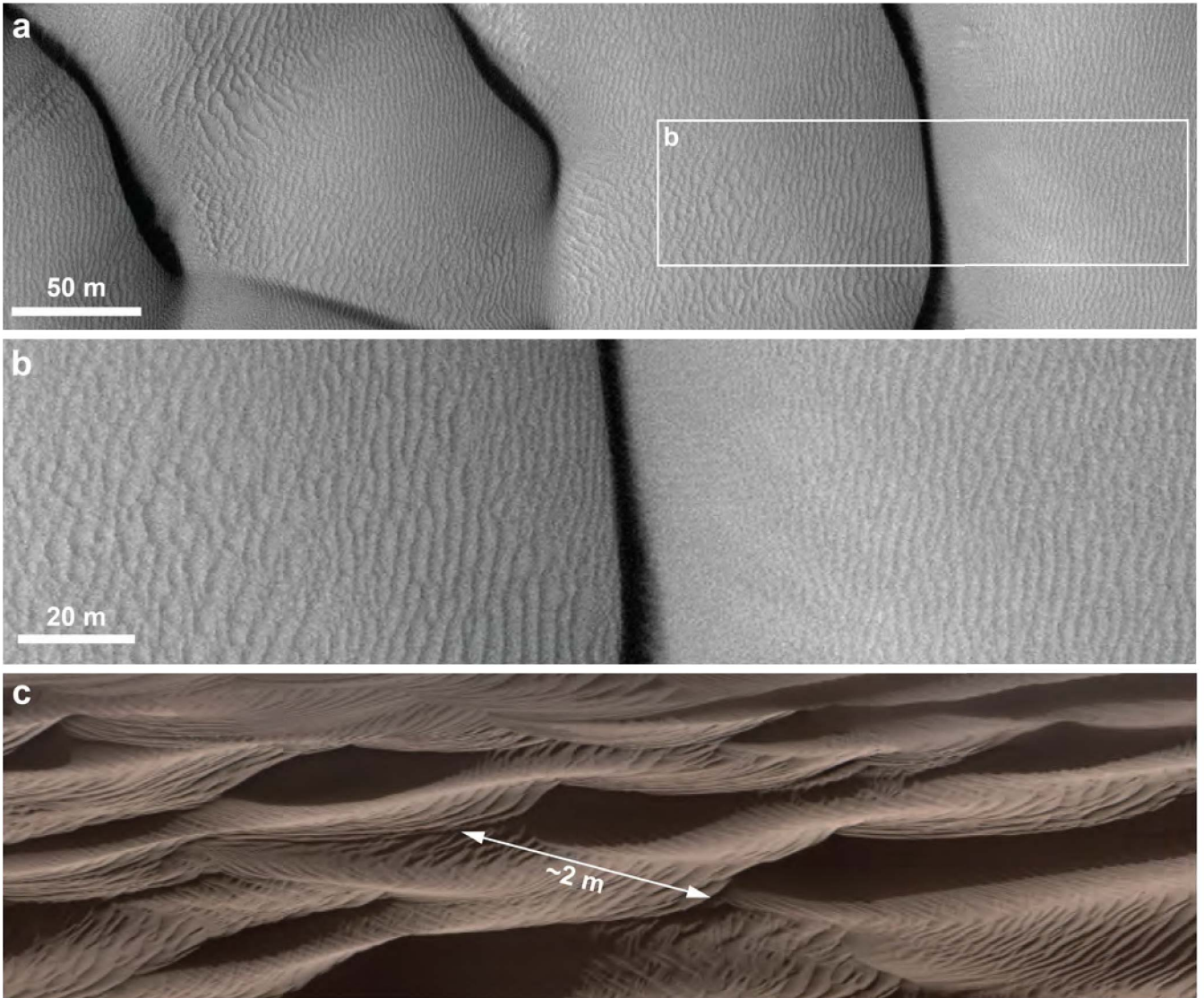
39

Figure 22: Illustration of dunes forming under aerodynamically smooth conditions, showing large martian ripples and dunes ($\mathcal{R}_r \simeq 1$). Dunes in Lyot (a,b) and Gale (c) craters. Martian bedforms display distinct scales. Dunes with hundred-meter-scale wavelengths (a) are mantled with meter-scale ripples (b). No bedforms with wavelengths between those two scales are observed. A closer look at a dune's surface with the Curiosity rover (here on 'Namib dune' within the Bagnold Dune Field) reveals smaller decimeter-scale bedforms, construed as impact ripples migrating on top of large ripples. Credit: (a-b), HiRISE image ESP_017605_2295; (c), NASA/JPL-Caltech/MSSS/Thomas Appere.

On Earth, typical grain sizes are about 200 μm, such that the thickness of the saltation layer is of the order of $20\,d \simeq 4\,\mathrm{mm}$ [182]. The height of aeolian impact ripples that mantle the surface of sand dunes is of similar, millimeter-scale. For an aerodynamic roughness, r, of that scale, and a typical shear velocity of the order of 0.4 m/s, one finds $\mathcal{R}_r \simeq 100$ (with $\nu = 1.5 \times 10^{-5}\,\mathrm{m^2/s}$), indicating that terrestrial saltation occurs in the rough regime. A smooth regime could possibly be observed for smaller grains and weak winds just above the transport threshold, for example. The typical value of the density ratio on Earth is $s \simeq 2200$ for quartz grains ($\rho_\mathrm{s} \simeq 2650\,\mathrm{kg/m^3}$) and air ($\rho_\mathrm{f} \simeq 1.2\,\mathrm{kg/m^3}$), which justifies the use of the transport law given in Eq. 2. The typical saturation length measured on Earth is of the order of 1 m, which yields a minimum dune wavelength in the order of 10 m, consistent with observations in nature [105, 183] and in a landscape scale field experiment [131].

Fig. 21 illustrates dunes forming in the aerodynamically rough regime, showing a coastal dune field in southwest Angola. The environment there closely matches the assumptions behind our classification, with a fairly unidirectional

40

wind blowing over a loose sand bed. Incipient dunes form with a scale $\lambda_{\min} \simeq 20$ m. Then, dunes coarsen as evidenced by a range of dune sizes, and display a consistent large-scale wavelength of the dune pattern, $\lambda_{\max} \simeq 850$ m. There, using ERA5-Land reanalysis data based on global atmospheric models ([167]), the thickness of ABL, Λ, is directly calculated as 300 m, or as 2 km using the same proxy as in [144].

For the low-pressure (*i.e.*, low-density, $\rho_{\mathrm{f}} \simeq 0.02\,\mathrm{kg/m^3}$) atmosphere of Mars, atmospheric kinematic viscosity is larger than on Earth, $\nu \simeq 10^{-3}\,\mathrm{m^2/s}$ and although uncertain, typical shear velocities are thought to be of the order of $u_* \simeq 1\,\mathrm{m/s}$ [12, 137, 184] so that $\mathcal{R}_r \sim 1$ for a millimeter-scale aerodynamic roughness. As a result, saltation occurs under an aerodynamically smooth regime on Mars, and two distinct ranges of dune sizes are expected if the ratio between the saturation length and the viscous length is smaller than about 1000. Saturation length has not been measured on Mars to date. With a larger density ratio than on Earth ($s \simeq 1.5 \times 10^5$ for basalt grains, $\rho_{\mathrm{s}} \simeq 3000\,\mathrm{kg/m^3}$), some models also predict a larger saturation length on Mars than on Earth [185]. Two distinct scales of bedforms larger than impact ripples are observed in monodisperse sand on Mars, as shown in fig. 22. Meter-scale ripples (distinct from smaller, decimeter-scale impact ripples) migrate on top of large hundred-meter-scale dunes [12, 102, 142, 186]. In that sense, large martian ripples and dunes are analogous to ripples superimposed on dunes in a subaqueous environment [12, 187, 137], where a smooth regime is expected as well. An alternative interpretation was proposed for these meter-scale ripples, under which they would simply be large impact ripples, growing to meter-scale wavelengths from their initial, decimeter-scale wavelengths [89]. However, that model cannot explain the absence of bedforms with wavelengths in the $\sim 20 - 80$ cm range in relatively well sorted sand [142]. Furthermore, the observed gap in bedform wavelengths between a large ripples and Mars' smallest dunes ($\lambda \sim 80$ m) matches the predictions of the Hanratty anomaly [139].

Dune formation regimes, and thus dune scales, on other planetary bodies remain highly uncertain (owing, *e.g.*, to large uncertainties in the materials that make up dune sand). On Titan, grains have been proposed to be made of complex hydrocarbons, water ice, or a combination of both; a density of $\rho_{\mathrm{s}} \simeq 1000\,\mathrm{kg/m^3}$ was proposed for porous organics that would form from a photochemical haze [188]. Although many uncertainties remain, a value of $s \simeq 200$ seems reasonable given current knowledge. For $u_* \simeq 0.1$ m/s, $\nu \simeq 10^{-6}\,\mathrm{m^2/s}$ and $r \simeq 10^{-3}$ m [189], one finds that $\mathcal{R}_r \simeq 100$, indicating that dunes on Titan would form under an aerodynamically rough regime, similar to terrestrial dunes. Linear dunes on Titan are observed around the equatorial region with a kilometer-scale, similar in scale to large linear dunes found on Earth [4]. Finally, on Venus, we consider the case of $u_* \simeq 5 \cdot 10^{-2}$ m/s, $\nu \simeq 5 \cdot 10^{-7}\,\mathrm{m^2/s}$ and $r \simeq 10^{-4}$ m [190], such that $\mathcal{R}_r \simeq 10$, *i.e.*, a value near the upper bound of the smooth regime.

6 Conclusion

Dunes are common landforms throughout the solar system that can teach us about past and current environmental conditions on Earth as well as on a variety of planetary bodies including Venus, Mars, Titan, and Pluto. Building a fundamental understanding of dune morphodynamics as well as predictive capabilities and mitigation strategies will require scientific collaboration across traditional field boundaries, and thus, a common language to describe sand dunes. Here, we synthesized existing terminology and distilled it into three independent but complementary dune classification schemes. First, we proposed a unifying description of dunes based on their morphology. This classification builds on a long legacy of existing terminology and solely requires observations of dune shapes as can be gathered from the ground, or from aerial or satellite imagery. Terminology can be further refined within that classification scheme when information about winds and dune migration is available. Second, we synthesized state-of-the-art models for dune morphodynamics, tying specific morphologic types with their formative dynamics as selected by wind regimes and boundary conditions. Third, we presented a classification of the various fluid dynamics regimes under which dunes may form, leading to different controls on initial and equilibrium dune sizes. This last scheme was developed for transverse dunes only, and encapsulates the complexity of variable boundary and environmental conditions that may be found across planetary bodies of the solar system. Together, these three classification schemes allow for variable levels of descriptive detail depending on available data, and encompass dune shape, dynamics, and scale as linked to their environmental conditions. Importantly, they offer a complete and unified framework, anchored in the mechanics of dune formation, for future studies to describe dunes on Earth and other planets.

7 Appendix – Concepts, models and methods

7.1 Dune size and timescale of wind-regime integration

We define the dune length scale as the square root of the dune cross-section, $\sqrt{HL/2}$, where H and L are the dune height and length. This approximates the dune profile to a triangle. To this dune size is associated a time scale $HL/(2Q)$ called the *dune turnover time*, which is the characteristic time to completely reshape the dune with a sand flux of norm Q [32]. Q is a volumetric flux per unit width (*i.e.*, it has the dimension of a length squared per time) and takes into account the dune compactness. This timescale sets the time duration over which one should consider the wind regime so that the dune integrates the whole complexity of the wind regime and is in a dynamical equilibrium over the considered period of time. A complex wind regime consists in a succession of wind events with different directions and strengths. We consider a flow sequence of duration τ_i between significant changes of sand flux direction. In a ideal scenario, the various flow sequences repeat periodically, defining a flow regime. The dunes integrate the wind regime if none of individual flow sequence completely reshapes the dune [62]. On the other hand one can expect that the dune has reached a dynamical equilibrium if the full considered period of time, τ_{tot}, is long enough to shape the dune. Thus, the size of the dune sets the period of time to consider (and vice versa) such that

$$\int_{\tau_i} Q(t)dt \ll HL/2 \leqslant \int_{\tau_{\mathrm{tot}}} Q(t)dt. \tag{1}$$

The boundary conditions should also not significantly change over the considered period of time. Note that Equation 1 does not take into account the direction of the sand flux because two winds with opposite directions contribute to build dunes. In principle, only the component of fluxes in line with the cross-section could be considered. In practice, it is difficult to obtain wind data for longer than the time required to build very large dunes. Shorter periods may be appropriate, but the duration should not be less than one period of the wind regime. Considering a shorter time period also enables to study whether the wind regime has changed [191, 192, 146]. The integral of the sand flux over a period of time T, $\int_T Q(t)dt$, where T is the duration of the wind regime, also defines the characteristic minimum cross-sectional area of dunes that integrates the wind regime. This concept of turnover time is derived from dimensional analysis and has never been systematically studied. It only sets a time scale as in principle, a dune can be fully reshaped without having to move all the sand it contains [99].

7.2 Sediment transport

7.2.1 Characterization of aeolian sediment transport

Sediment transport is coupled to fluid flow in the transport layer. It is characterized by a threshold (minimum) shear velocity (or basal shear stress), a saturated (maximum) sediment flux in steady state, the saturated flux, and a saturation length [193]. The saturation length corresponds to the spatial lag of the response of flux to a change in transport conditions, *i.e.*, how far downwind from a change in transport conditions (such as an increase of wind velocity) the sediment flux equilibrates with the new conditions. Three main parameters control sediment transport and saltation in particular.

First, the particle-to-fluid density ratio, $s = \rho_{\mathrm{s}}/\rho_{\mathrm{f}}$, encapsulates the reduced weight of particles in the fluid. Second, a commonly used parameter is the Shields number, $\Theta = u_*^2/[(s-1)gd]$ (where u_*, g, and d are the wind shear velocity, the gravitational acceleration and the grains diameter, respectively), which allows for comparisons of the basal shear stress on grains $(\rho_{\mathrm{f}} u_*^2)$ relative to the grains' apparent weight per unit of surface $(\sim (\rho_{\mathrm{s}} - \rho_{\mathrm{f}})gd)$. Third, the Galileo number, $\mathcal{G} = \sqrt{(s-1)gd^3}/\nu$ (where ν is the fluid viscosity), can be envisioned as the ratio of gravitational and viscous effects. It is the square root of a Reynolds number in which the length scale is taken as the grain size and the velocity scale as the Stokes limit of the grains' settling velocity. This parameter is useful to compare different environments regardless of flow velocity.

The dynamic threshold for sediment transport is defined by the minimum shear stress exerted by the fluid on the granular bed that can sustain transport in saltation. It is associated to a critical value of the Shields number, Θ_{t}. Θ_{t} varies with grain and flow properties, and is typically expressed as a function of grain size and apparent density or equivalent dimensionless parameters such as $\mathcal{G}$ and s [194, 195, 196, 184, 197].

The saturated sand flux at steady state, Q_{sat}, is proportional to the difference between the actual Shields number and its critical value. Such transport laws (*e.g.*, Eq. 2) are valid for saltation transport over a loose sand bed, when $s \gtrsim 100$. Under such conditions, the velocity of grains in saltation is independent of wind shear velocity, u_* (fig. 13 in [198]) due to coupling between the wind flow and sediment transport. If transport laws are fairly well established

and calibrated in steady and homogeneous conditions [198, 197, 199, 32, 200, 201, 202, 203, 204], threshold Shields numbers are much less constrained under extraterrestrial conditions, including on Mars [184, 205].

Some experimental data are available for the saturation length, L_{sat}, under terrestrial saltation (with L_{sat} typically between 0.5 and 1 m for sand grains in the range [100, 200 μm], [32, 206, 130, 132, 131]) as well as under subaqueous suspension [207], but significant knowledge gaps remain [185, 208, 209, 210] rendering predictions for saltation on Mars or Titan challenging. These knowledge gaps are particularly significant given that L_{sat} is a key parameter in dune-instability analysis [193, 141]. As the minimum length required to generate an effective coupling between the wind flow and sand transport, L_{sat} sets the characteristic wavelength of incipient dunes in most cases (Fig. 8).

7.2.2 Transport law – Saturated sand flux and onset of transport

There are many transport laws, which are more or less phenomenological, each with their own validity regime [182]. Here, we compute the saturated sand flux, Q_{sat}, (*i.e.*, maximum sand flux over a flat sand bed) using the relationship proposed in [211, 135], such that

$$Q_{sat} = \begin{cases} a_q \dfrac{\rho_f}{\rho_s g} u_t \left(u_*^2 - u_t^2 \right) \equiv a_q \dfrac{s-1}{s} d u_t \left(\Theta_*^2 - \Theta_t^2 \right) & \text{if } u_* > u_t, \\ 0 & \text{otherwise}, \end{cases} \tag{2}$$

where the dimensionless prefactor, $a_q \approx 8.33$, was calibrated in [135] and takes into account the dune compactness (~ 0.6) so that sand fluxes can be used directly for dunes dynamics. Equation 2 is a volumetric flux per unit width, *i.e.*, it has the dimension of length squared per time. In this formula, u_t is the threshold shear velocity for transport, which corresponds to the critical value of the Shields number, Θ_t, such that

$$u_t = \sqrt{\Theta_t} \sqrt{\frac{\rho_s - \rho_f}{\rho_f} g d}. \tag{3}$$

We take $\Theta_t^{1/2} = 0.082$ [212], so that u_t accounts for the dynamic (or impact) threshold, *i.e.*, the lowest shear velocity that can sustain saltation once it has been initiated [32]. For calculations, we use a constant threshold velocity of $u_t = 0.153$ m/s, which corresponds to quartz sand grains of diameter $d \simeq 160 \, \mu$m in air on Earth.

The transport law Eq. 2 is valid for transport in saltation over a mobile sand bed for moderate wind velocities above transport threshold. In such conditions, sand transport occurs in a few centimeters thick surface layer above the bed [203, 213]. In this law, first proposed by Ungar and Haff [201], the amount of transported grains is proportional to the difference between the basal shear stress and its threshold value, and the mean velocity of grains corresponds to the transport threshold wind velocity. Grains in saltation slow the wind in the transport layer, down to the transport threshold value when flux is saturated [135, 182].

7.2.3 Wind speed-up over a dune

The first source of complexity in morphodynamics of dunes relies in the coupling between wind flow, sand transport, and dune topography. Positive topography deflects the air flow and the compression of streamlines causes the wind speed close to the ground to be stronger over the obstacle than over a flat bed away from any topography, so that the sand flux over a dune depends on its shape. Usually defined as the *speed-up*, this is a critical ingredient that couples the dune topography and sand transport at all stages of the development of dunes, from the formation of incipient bedforms to the dynamics of major dune systems. It is often described in terms of a *fractional speed-up ratio* (or *relative speed-up ratio*), δ, which is the relative speed-up between the wind velocity at some elevation above the dune profile (u) and the wind velocity at the same elevation above a flat bed away from any topography (u_0) [170]:

$$\delta = \frac{u - u_0}{u_0}. \tag{4}$$

The value of δ varies with position along the dune profile, elevation above the bed, dune aspect ratio and aerodynamic roughness [170, 214]. In the field, measurements should be made in the transport layer to be relevant for flux variation and, if possible, under transport conditions because transport affects aerodynamic roughness. When measured close to the bed for different types of dunes on Earth, δ-values are reported to typically range between 0.4 and 1 for the maximum value, or for the one measured at the top of the dune [71, 215, 216, 217, 218]. In general, the wind velocity is not expected to be maximum at the top of the dune when measured sufficiently close to the ground, but slightly upwind (Section 7.4.1). However, on mature dunes the difference between the maximum wind velocity and wind

velocity at the dune top should be small.

Jackson and Hunt analyzed the theoretical response in 2D of a turbulent air flow in aerodynamically rough regime to the perturbation induced by a symmetric hump with small aspect ratio and curvature (Sections 4 & 7.4.1) [170]. They found that in this case the fractional speed-up, taken at its maximum or at top of the hump, is independent on wind velocity, depends only weakly on aerodynamic roughness, and is almost proportional to the hump aspect ratio [170] :

$$\delta \simeq \beta \frac{H}{L}, \tag{5}$$

where L and H are the characteristic length and height of the hump, and β a dimensionless coefficient that takes into account the aerodynamic roughness, position along the hump profile, and elevation above the bed. For typical values of aerodynamic roughness encountered in dunes on Earth, $\beta \simeq 6$ when considering the maximum of shear velocity, u_* [170, 141, 219] (Section 7.4.1).

The increase in wind shear velocity leads to an increase in saturated sand flux up the dune slope. Equivalently to the relative speed-up ratio, one can define a relative flux-up ratio [41, 219], $\gamma = (Q - Q_0)/Q_0$, which can be calculated for saturated flux with Equation 2 given a value for δ. Because of transport threshold in Equation 2, γ depends on wind velocity even if δ does not as in Equation 5, $e.g.$, γ goes to infinity if unperturbed wind velocity, u_0, is just below u_t [64].

The variation of wind shear velocity along the dune profile, which leads to variation of sand flux, is a key parameter to understand dune growth and dynamics (Section 4 & 7.4.1). Its dependency on the dune streamwise aspect ratio, H/L, which has been observed in the field for reversing dunes [220], also has a strong impact on dune dynamics in multidirectional wind regimes (Sections 5.2 & 7.3.3). The 3D shape of the dune and the orientation of wind relative to the dune ($e.g.$, the wind may not blow perpendicularly to crest line) can also deflect the sand flux direction above the dune [221, 222, 71, 223, 217, 224] by combined effects of wind streamline deflection and of gravity, because the dune topography gradient has components in both parallel and normal to (non-deflected) wind. The sand flux deflection by topography explains the 3D shapes of a barchan [225, 122] or the transverse instability [124, 125] in a unidirectional flow. Here, we do not take into account the sand flux deflection in calculations but only the primary effect of dune topography, which is wind-speed-up and its dependency on apparent dune aspect ratio.

7.3 Sand flux from wind data

7.3.1 Sand flux on a flat sand bed from wind data

We compute sand fluxes using the surface wind data from the ECMWF ERA5-Land reanalysis [166, 167]. This global weather forecasting model based on data assimilation aims to include all available measurements from weather stations, radiosondes, ships, and satellites. It provides numerical extrapolation of many parameters from the beginning of 1979 up to now (2023) with a horizontal spatial resolution of $0.1° \times 0.1°$ (about 11 km at the equator) and a time resolution of 1 hour. We denote t_i, $i \in [1; N]$ the different times, which are regularly spaced. We extract from data the wind direction, θ, relative to the east and wind speed, u, at a height $z = 10$ m and calculate the shear velocity, u_*, over a flat sand bed using the law of the wall:

$$u_*(t_i) = u(z, t_i) \frac{\kappa}{\ln(z/z_0)}, \tag{6}$$

where κ is the von-Kármán constant ($\kappa = 0.41$) and z_0 the aerodynamic roughness length scale, which is modified by grains in saltation in transport conditions. We take $z_0 = 1\,\mathrm{mm}$ for all calculations on Earth.

We define the mean shear velocity $\langle u_* \rangle$ as the shear velocity averaged over the time periods when transport is occuring:

$$\langle u_* \rangle = \frac{1}{\sum_{i=1}^{N} H_u} \sum_{i=1}^{N} H_u\, u_* \qquad \text{where} \qquad H_u = \begin{cases} 1 & \text{when } u_* > u_\mathrm{t}, \\ 0 & \text{else.} \end{cases} \tag{7}$$

Using the calculated shear velocity, $u_*(t_i)$, and extracted wind direction, $\theta(t_i)$, we compute the saturated sand flux over a flat sand bed, $\vec{Q}_0$, using the transport law in Eq. 2:

$$\vec{Q}_0(t_i) = \begin{pmatrix} Q_\mathrm{sat}(t_i) \cos[\theta(t_i)] \\ Q_\mathrm{sat}(t_i) \sin[\theta(t_i)] \end{pmatrix}, \tag{8}$$

44

which we integrate over the entire time period to calculate the resultant sand flux:

$$\langle \vec{Q}_0 \rangle = \frac{1}{N} \sum_{i=1}^{N} \vec{Q}_0. \tag{9}$$

7.3.2 Sand flux over dunes from wind data

To evaluate the characteristic growth, migration, and elongation rates of dunes in the field, we need to calculate the characteristic wind shear velocity and corresponding sand flux over dunes. This characteristic wind shear velocity takes into account the wind speed-up and is typically the maximum value, or the one at the top of the dune, which we take to be the same. Wind fractional speed-up ratio, δ (Eq. 4), depends on streamwise dune aspect ratio (Eq. 5). Considering a symmetric linear dune of uniform and steady aspect ratio H/L in cross section and orientation α, a wind of direction θ experiences an apparent dune aspect-ratio $H \left| \sin \left(\theta - \alpha \right) \right| / L$, so that the characteristic wind shear velocity, u_c, depends on the angle between wind direction and dune orientation:

$$u_\mathrm{c}(\alpha) = u_* \left(1 + \delta \left| \sin \left(\theta - \alpha \right) \right| \right), \qquad \text{where} \qquad \delta = \beta \frac{H}{L}. \tag{10}$$

In Eq. 10, u_* is the shear velocity over a flat sand bed (Eq. 6). For the calculations in field examples of Section 5.2, we use $\delta = 0.8$. Future improvements could include unsteady aspect ratios, which are probably important to better model reversing dunes, but here we only take into account the effect of dune orientation with respect to winds.

The corresponding characteristic sand flux over the dune, which we assume to be saturated, can be decomposed into crest-parallel and crest-normal components of transport:

$$\vec{Q}_\mathrm{c}(\alpha) = \begin{pmatrix} Q_\parallel(\alpha) \\ Q_\perp(\alpha) \end{pmatrix} = \begin{pmatrix} Q_\mathrm{sat}(u_\mathrm{c}) \cos \left(\theta - \alpha \right) \\ Q_\mathrm{sat}(u_\mathrm{c}) \sin \left(\theta - \alpha \right) \end{pmatrix}, \tag{11}$$

where Q_sat is calculated with Eq. 2 using u_c (Eq. 10). The effect of the topography on the saturated sand flux due to the wind speed-up is not directly integrated into the sand flux but into wind shear velocity to better account for the transport threshold. Sand can be transported at the dune top while shear velocity is below the threshold for transport where the bed is flat. However, our analysis assumes that wind velocity is above threshold where the bed is flat. $\vec{Q}_\mathrm{c}$, is the characteristic sand flux over the dune, which can be assimilated to the maximum value of the sand flux or the value at the dune top. In our analysis, we assume that the sand flux varies in line with the topography along the dune profile (and wind boundary layer detaches in the lee side), so that the averaged sand flux over a streamwise dune section is assumed to be proportional to Q_c, and the characteristic divergence of the sand flux is Q_c/L, where L is the streamwise length of the dune. This is not valid if transport occurs only at the dune top.

Then, the time-averaged components of these fluxes allow us to predict the orientation of dunes according to the prevailing growth mechanism.

7.3.3 Orientation of dunes in multidirectional flow regimes depending on the prevailing growth mechanism

Growth rate in height The growth rate in height of a dune is directly related to the sand deposition rate at the crest and erosion rate at the trough, which correspond to divergences of the sand flux at the crest and the trough, respectively. For long straight dunes with an avalanche face or large aspect ratio that are much larger than the minimum dune size (Section 4), we assume that the sand flux typically varies over a length proportional to the streamwise dune length, L, between a maximum value Q_max upwind of the crest and zero downwind of the crest, because the wind boundary layer detaches in the lee side. Thus, the characteristic growth rate is:

$$\sigma = \frac{Q_\mathrm{max}}{HL}, \tag{12}$$

where H is the dune height. Dunes that exhibit smaller streamwise lengths have larger growth rate.

When growth in height is the prevailing growth mechanism, like in the bed instability mode, the orientation of the dune crestline is such that the growth rate is maximum. In a multidirectional wind regime, a dune should then have an orientation α_H that minimizes the different streamwise lengths, so that it experiences the *Maximum Gross Bedform-Normal Transport* (MGBNT) [40], which we consider to be equivalent to the maximum of $\langle |Q_\perp| \rangle$. The absolute value reflects that transport in both directions across the crest contribute to dune growth [40, 41]. Using signed values of transport subtracts transport in opposing directions, even though they both contribute to dune growth.

MGBNT yields good agreement with experiments on wind ripples [40], centimetric and decimetric sand bedforms under water [62, 122, 41], numerical simulations [119, 63, 64], and field measurements for bimodal flow regimes [165, 131] in full mobilized bed conditions.

Elongation without migration The direction of elongation is the direction of sand net transport as experienced by the dune. The direction α_F of an elongating dune correspond to a null perpendicular to crest net transport ($\langle Q_\perp \rangle = 0$) and a positive along crest net transport ($\langle Q_\parallel \rangle > 0$). This is the predicted orientation for dunes on a starved bed if they do not migrate. Prediction of several directions of elongation within a same wind regime is made possible by taking into account the dependency of wind speed-up on dune orientation.

The predicted orientation for elongating dunes is in good agreement with experiments on centimetric sand bedforms under water [41], numerical simulations [64] and field measurements [226] for bimodal flow regimes. This rule also correctly predicts the multiple directions of elongation observed for star dunes on a starved bed in numerical simulations when the flow regime is multidirectional with a null RDP [90].

7.4 Wind flow over incipient free dunes

7.4.1 Turbulent flow model

Wind flow over a flat bottom or topography with a small aspect ratio can be divided in different regions above the bed (or layers) in which the transfer of fluid momentum is dominated by different processes. Sediment transport takes place in an *inner layer* where the flow is turbulent (high Reynolds number) and is characterized by velocity fluctuations and intermittent flow structures that transport the fluid momentum to the bed, where the flow is slowed by wall friction. In the outer layer, the fluid is comparable to a perfect fluid. In a sublayer, just above the bed, viscous effects are dominant.

Turbulent stress in the inner layer can be described by means of an *eddy viscosity* characterized by a *mixing length*. There is no characteristic length scale intrinsic to turbulence and the mixing length is a local quantity, usually similar to the distance to the obstacle that is causing the momentum transfer. Under this model for a stationary outer flow, the time-averaged velocity profile, $u(z)$, inside the inner layer above a flat wall is known as the law of the wall:

$$u(z) = \frac{u_*}{\kappa} \ln \left(\frac{z}{z_0} \right), \tag{13}$$

where u_* is the shear velocity, $\kappa \simeq 0.41$ the von Kármán constant, z the distance from the wall, and z_0 is the distance at which the velocity as given by Eq. (13) goes to zero and relates to *aerodynamic roughness*. The shear velocity is defined from the basal shear stress τ, such that $\tau = \rho_f u_*^2$, where ρ_f is the fluid density. The law of the wall is well supported by experimental data [227, 228, 133]. The length z_0 is either set by the characteristic roughness length scale of the wall, r, or by the thickness of the viscous sublayer when it is larger than roughness. The characteristic thickness of the viscous sublayer is ν/u_*, where ν is the fluid kinematic viscosity. The roughness Reynolds number, $\mathcal{R}_r = r u_*/\nu$, compares that two length scales. When $\mathcal{R}_r > 100$, flow is aerodynamically rough ; conversely, when $\mathcal{R}_r$ is smaller than a few units, flow is aerodynamically smooth, and the thickness of the viscous sublayer sets the characteristic length z_0 [133].

For a wavy bed, the thicknesses of the boundary layers are modulated by topography. They are thinner where flow velocity spatially increases, and thicker where flow velocity decreases. In order to study the formation of incipient dunes from a flat sand bed, we consider the linear response of the flow to a small sinusoidal perturbation of the bed topography of wavelength λ and low amplitude h_0 ($h_0/\lambda \ll 1$), such that

$$h(x) = h_0 \sin(2\pi x/\lambda). \tag{14}$$

In this case, the perturbation of the basal shear stress is proportional to the aspect ratio of the topographic perturbation, and can be expressed as the sum of two components: one that is in phase with topography, with a weight denoted $\mathcal{A}$, and one that is in phase quadrature, with a weight denoted $\mathcal{B}$, *i.e.*,

$$\tau(x) = \tau_0 \left[1 + \frac{2\pi h_0}{\lambda} \left(\mathcal{A} \sin(2\pi x/\lambda) + \mathcal{B} \cos(2\pi x/\lambda) \right) \right], \tag{15}$$

where τ_0 is the unperturbed (flat bed) shear stress. In principle, coefficient $\mathcal{A}$ accounts for dune migration, whereas coefficient $\mathcal{B}$ accounts for dune growth [193, 229, 219]. Within this framework, the ratio of the relative increase in
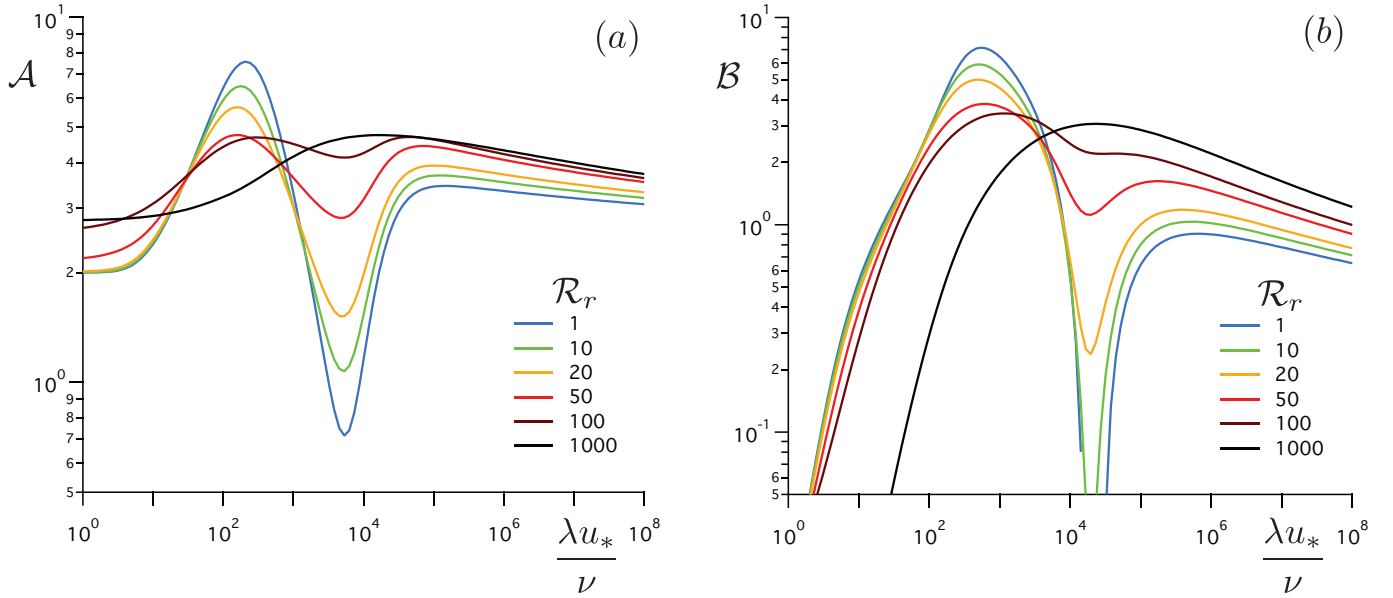
Figure 23: Response of the flow to a sinusoidal perturbation of wavelength λ for different boundary Reynolds numbers $\mathcal{R}_r$, *i.e.*, r (adapted from [134]). The coefficients $\mathcal{A}$ (a) and $\mathcal{B}$ (b) are the weight coefficients of the perturbation of the basal shear stress for the in-phase and in-phase-quadrature components, respectively. They are plotted as a function of wavelength, normalized by the viscous length, *i.e.*, a bedform-scale Reynolds number.

shear-stress at the tops of the sinusoidal bed equals $\mathcal{A}(2\pi h_0/\lambda)$. In the limit of small perturbations, the relative speed-up of shear velocity is half of that (because $\tau \propto u_*^2$) and the fractional speed-up ratio is $\delta = (\mathcal{A}/2)(2\pi h_0/\lambda)$ at the tops of the bed. However, wind shear velocity and shear stress are not maximum at the tops of the bed but are phase-shifted. The phase shift, $\phi = \arctan(\mathcal{B}/\mathcal{A})$, is positive if τ is maximum upwind of the top of the bed. There, the maximum fractional speed-up ratio of shear velocity is $\delta = (\sqrt{\mathcal{A}^2 + \mathcal{B}^2}/2)(2\pi h_0/\lambda)$.

Under the above framework, the flow response to a small perturbation was calculated by Jackson and Hunt [170] in the rough case (constant z_0, $\mathcal{R}_r \to \infty$). In that limit, $\mathcal{A}$ and $\mathcal{B}$ weakly (logarithmically) vary with the wavelength of the bed perturbation (Fig. 23). More importantly, in rough conditions, $\mathcal{B}$ and the phase shift are always positive, favoring the development of the dune instability at all wavelengths [193, 230].

This positive shift can be explained as follows. In the outer region of the flow, well above the bed, the flow behaves as a potential flow, in which inertia and pressure gradient balance each other. Therefore, the flow is in phase with the topography, such that wind velocity is maximum over topographic highs and minimum over troughs. According to Bernoulli's principle, pressure is in turn minimal over topographic highs and maximum over troughs. Thus, along a streamline, the pressure gradient is minimum (and negative) where the velocity increases the most, above the maximum slope. It is in phase quadrature with topography. In contrast, flow velocity is reduced due to friction in the inner turbulent layer, and fluid inertia is therefore reduced. In the inner layer, the flow is driven by the transverse turbulent transport of momentum from the outer region to the inner layer (in phase) and by the longitudinal (streamwise) pressure gradient inherited from the outer flow and that is maintained in the inner layer (in phase quadrature). Therefore, fluid velocity and shear stress peak upwind of the maximum of topography. This positive offset was measured in the field on dunes with small aspect ratios [218, 131].

Under aerodynamically smooth conditions, both the turbulent and viscous boundary layers are modulated by topography and coupled. Regarding the turbulent mixing, the usual correction relative to the rough conditions over a flat bed is modeled as a decrease in both the mixing length and the turbulent viscosity near the bed, with a characteristic length scale proportional to the thickness of the viscous boundary layer [231]. Such corrections are important when considering, *e.g.*, the development of dissolution and melting patterns (Section 7.4.2). More importantly for dunes, the shear stress on the bed is controlled by the viscous boundary layer. A larger shear stress goes with a thinner viscous boundary layer, which thins out when the (negative) pressure gradient decreases. To model unusual experimental measurements of the shear stress on a wavy bed in a water channel [232, 233], Hanratty assumed a spatial lag between the effective pressure gradient inside the viscous boundary layer and the outer pressure gradient proportional to the

characteristic thickness of the viscous boundary layer [138, 234]. Under this assumption, it follows that the factors $\mathcal{A}$ and $\mathcal{B}$ in particular abruptly decrease for a range of wavelengths (fig. 23). This sharp transition can explain the dissolution pattern [235, 134]. Although not directly evidenced by experimental data, this model interestingly predicts a negative phase shift between shear stress and topography for a range of wavelengths set by the characteristic thickness of the viscous boundary layer (Fig. 23). If this prediction is correct, dunes with these wavelengths can not develop [141, 137]. This prediction is consistent with the general absence of dunes with wavelengths from a few to a few tens of meters on Mars, where the kinematic viscosity of the atmosphere is larger than on Earth [187, 102, 137]. The fundamental origin of this anomalous flow regime is an active area of research, and is likely associated with a laminar-to-turbulent transition [232, 234].

7.4.2 Dissolution and melting patterns as evidence for the Hanratty anomaly

Transverse patterns may form on an ice sheet under deep flows when the ice sublimates in air or melts under water. Similar patterns are also observed in soluble rocky substrates dissolving under water flow. These erosion patterns can only appear if the rate of substrate erosion (sublimation, melting, or dissolution) is greater in the troughs than on the bumps. Dissolution increases the concentration of solutes at the solid/fluid interface, and sublimation or melting extracts heat from the fluid, which decreases temperature at the solid/fluid interface. To sustain the melting or dissolution process, heat or solute concentration must be transported towards or away from the interface. This transport may be buoyancy-driven by melting or dissolution themselves, leading to density stratification into the fluid caused by gradients in temperature or concentration [236, 237, 238, 239, 240]. In the case of a stable density stratification, differential erosion between bumps and troughs is explained by the coupling between flow and topography, which modulates the thicknesses of boundary layers (analogously to the case of dunes discussed above) and the turbulent transport of heat and concentration [235, 134]. The existence of dissolution patterns suggests that the turbulent viscosity and diffusion of heat or concentration are more significant in troughs than over bumps.

Such patterns were reproduced experimentally in laboratory flumes over plaster [241, 242, 243] or ice [244, 245, 246] beds and under turbulent flows. Based on these studies, the initial and mature patterns have wavelengths that scale with the inverse of flow velocity, *i.e.*, that are proportional to the characteristic thickness of the viscous boundary layer [247, 248]. Furthermore, mature patterns reach a stationary state with constant amplitude and wavelength. This pattern saturation seems to coincide with a smooth-to-rough regime transition, at which point bedform amplitude becomes much greater than the thickness of the boundary layer. These experimental observations support the existence of a particular turbulent flow regime in the smooth case for a range of wavelengths, the Hanratty anomaly.

7.5 Possible confinement by the atmospheric boundary layer

A planetary atmosphere, like Earth's, displays a vertical structure. As radiation from the sun heats the ground, it leads to an unstable density stratification (with warmer, less dense air at the bottom), which in turn drives convection in the atmospheric boundary layer (ABL). Above the ABL, in the free atmosphere, density stratification is stable (*i.e.,*, air density decreases with altitude). The height of the ABL, Λ, depends on the heat flux from the ground to the atmosphere and varies spatially due to, *e.g.*, lateral variations in ground albedo, and in time, *e.g.*, due to seasonal changes in sun radiative flux. Such fluctuations make it challenging to determine a characteristic height of the ABL that is relevant to dune formation, especially as giant dunes integrate flows over a long period, but only under conditions that are conducive to active sediment transport [145]. Shear stresses in excess of threshold values for sand transport tend to occur during strong diurnal convection within the boundary layer over dune fields—this convection is associated with high Λ values [249].

Another challenge lies in modeling wind flow over a dune under ABL confinement. In the subaqueous case, there is a coupling between the bottom topography and the water free surface, which can deform and where waves can propagate due to the gravitational restoring force. In particular, this coupling causes a transition between downstream-moving dunes and upstream-moving antidunes when the flow over the dune exceeds the velocity of water waves. In this case, flow regime is controlled by the Froude number, a dimensionless number that relates flow velocity to speed of shallow water waves. Like in the subaqueous case, gravity waves can also propagate at the interface between the ABL and the free atmosphere, where a density jump, $\Delta\rho_f$, occurs. One can thus define a Froude number, $\mathcal{F} = U/\sqrt{g\Lambda\Delta\rho_f/\rho_f}$, where U is the flow velocity at altitude Λ [250, 251, 252, 253].

A second Froude number, $\mathcal{F}_N$, can be defined from the strength of the vertical density stratification in the free atmosphere, $\partial_z\rho_f$. Stable stratification in the free atmosphere sets a characteristic oscillation frequency of fluid particles, the Brunt-Väisälä frequency, $N = \sqrt{-g\partial_z\rho_f/\rho_f}$, such that $\mathcal{F}_N = U/(\Lambda N)$ [250, 251, 252, 253]. The coupling between dune dynamics and the ABL, and its dependence on these Froude numbers, remain largely unexplored. In

addition to the ABL, flow confinement can result from other phenomena, such as katabatic winds. Each specific confinement scenario is likely to be characterized by different controls on Λ. Cross-wind or secondary dune patterns could possibly be induced by such confinement effects [101].

Acknowledgement

References

[1] David B Loope, Clinton M Rowe, and R Matthew Joeckel. Annual monsoon rains recorded by jurassic dunes. *Nature*, 412(6842):64–66, 2001.

[2] Frank Preusser, Dirk Radies, and Albert Matter. A 160,000-year record of dune development and atmospheric circulation in southern arabia. *Science*, 296(5575):2018–2020, 2002.

[3] Hiroki Shozaki and Hitoshi Hasegawa. Development of longitudinal dunes under pangaean atmospheric circulation. *Climate of the Past*, 18(7):1529–1539, 2022.

[4] Ralph D Lorenz, S Wall, Jani Radebaugh, G Boubin, Erwan Reffet, M Janssen, E Stofan, R Lopes, R Kirk, Charles Elachi, et al. The sand seas of titan: Cassini radar observations of longitudinal dunes. *Science*, 312(5774):724–727, 2006.

[5] Lori K Fenton. Dune migration and slip face advancement in the rabe crater dune field, mars. *Geophysical Research Letters*, 33(20), 2006.

[6] Rosalyn K Hayward, Timothy N Titus, Timothy I Michaels, Lori K Fenton, Anthony Colaprete, and Philip R Christensen. Aeolian dunes as ground truth for atmospheric modeling on mars. *Journal of Geophysical Research: Planets*, 114(E11), 2009.

[7] J. Radebaugh, R. Lorenz, T. Farr, P. Paillou, C. Savage, and C. Spencer. Linear dunes on titan and earth: Initial remote sensing comparisons. *Geomorphology*, 121(1–2):122–132, 2010.

[8] Mary C Bourke, Nick Lancaster, Lori K Fenton, Eric JR Parteli, James R Zimbelman, and Jani Radebaugh. Extraterrestrial dunes: An introduction to the special issue on planetary dune systems. *Geomorphology*, 121(1-2):1–14, 2010.

[9] L.K. Fenton, T.I. Michaels, and R.A. Beyer. Inverse maximum gross bedform-normal transport 1: How to determine a dune-constructing wind regime using only imagery. *Icarus*, 2013.

[10] Antoine Lucas, Sébastien Rodriguez, Clément Narteau, Benjamin Charnay, Sylvain Courrech du Pont, Tetsuya Tokano, Amandine Garcia, Mélanie Thiriet, Alexander G Hayes, Ralph D Lorenz, et al. Growth mechanisms and dune orientation on titan. *Geophysical Research Letters*, 41(17):6093–6100, 2014.

[11] Benjamin Charnay, Erika Barth, Scot Rafkin, Clément Narteau, Sébastien Lebonnois, Sébastien Rodriguez, Sylvain Courrech du Pont, and Antoine Lucas. Methane storms as a driver of titan's dune orientation. *Nature Geoscience*, 8(5):362–366, 2015.

[12] Mathieu GA Lapotre, Ryan C Ewing, MP Lamb, WW Fischer, JP Grotzinger, David M Rubin, KW Lewis, MJ Ballard, M Day, S Gupta, et al. Large wind ripples on mars: A record of atmospheric evolution. *Science*, 353(6294):55–58, 2016.

[13] Laura Fernandez-Cascales, Antoine Lucas, Sébastien Rodriguez, Xin Gao, Aymeric Spiga, and Clément Narteau. First quantification of relationship between dune orientation and sediment availability, olympia undae, mars. *Earth and Planetary Science Letters*, 489:241–250, 2018.

[14] DM Rubin, MAG Lapôtre, Andrew W Stevens, MP Lamb, CM Fedo, JP Grotzinger, S Gupta, KM Stack, AR Vasavada, SG Banham, et al. Ancient winds, waves, and atmosphere in gale crater, mars, inferred from sedimentary structures and wave modeling. *Journal of Geophysical Research: Planets*, 127(4):e2021JE007162, 2022.

[15] Amelia J Couldrey, Thomas Benson, Michiel AF Knaapen, Kerry V Marten, and Richard JS Whitehouse. Morphological evolution of a barchan dune migrating past an offshore wind farm foundation. *Earth Surface Processes and Landforms*, 45(12):2884–2896, 2020.

[16] Robert R Sokal. Classification: Purposes, principles, progress, prospects: Clustering and other new techniques have changed classificatory principles and practice in many sciences. *Science*, 185(4157):1115–1123, 1974.

[17] Ian Livingstone, Andrew Warren, et al. *Aeolian geomorphology: an introduction.* Addison Wesley Longman Ltd, 1996.

[18] Edwin Dinwiddie McKee. A study of global sand seas. *Geological Survey Professional Paper*, 1052, 1979.

[19] K. Pye and H. Tsoar. *Aeolian Sand And Sand Dunes.* Unwin Hyman, London, 1990.

[20] Nicholas Lancaster. Star dunes. *Progress in Physical Geography*, 13(1):67–91, 1989.

[21] P.A. Hesp and I.J. Walker. Coastal dunes v2. In J.J.F. Shroder, editor, *Treatise on Geomorphology*, volume 7, pages 540–591. Elsevier Inc., 2021.

[22] Nikolaj A Sokolòw. *Die Dünen: Bildung, Entwickelung und innerer Bau.* Springer, 1894. German translation from Russian assisted A. Arzruni.

[23] Frank A Melton. A tentative classification of sand dunes its application to dune history in the southern high plains. *The Journal of Geology*, 48(2):113–174, 1940.

[24] HTU Smith. Dune morphology and chronology in central and western nebraska. *The Journal of Geology*, 73(4):557–578, 1965.

[25] William S Cooper. Coastal sand dunes of oregon and washington. *Mem. Geol. Soc. of America*, 72:169, 1958.

[26] William S Cooper. Coastal dunes of california. 104:131, 1967.

[27] Monique Mainguet. A classification of dunes based on aeolian dynamics and the sand budget. In *Deserts and arid lands*, pages 31–58. Springer, 1984.

[28] Léon Aufrère. Essai sur les dunes du sahara algérien. *Geografiska Annaler*, pages 481–500, 1935.

[29] John T Hack. Dunes of the western navajo country. *Geographical Review*, 31(2):240–263, 1941.

[30] Ronald Greeley and James D Iversen. *Wind as a geological process: on Earth, Mars, Venus and Titan.* Number 4. CUP Archive, 1987.

[31] A. Warren Cooke, R. and A. Goudie. *Desert Geomorphology.* UCL press., 1993.

[32] R. A. Bagnold. *The physics of blown sand and desert dunes.* Chapman and Hall, London., 1941.

[33] R.J. Wasson and R. Hyde. Factors determining desert dune type. *Nature*, 304:337–339, Jul 1983.

[34] Joanna E Bullard and Ian Livingstone. Interactions between aeolian and fluvial systems in dryland environments. *Area*, 34(1):8–16, 2002.

[35] Steven R Bishop, Hiroshi Momiji, Ricardo Carretero-González, and Andrew Warren. Modelling desert dune fields based on discrete dynamics. *Discrete Dynamics in Nature and Society*, 7(1):7–17, 2002.

[36] Nicholas Lancaster. *Geomorphology of desert dunes.* Routledge, 2013.

[37] Nicholas Lancaster. Dune morphology and dynamics. In *Geomorphology of desert environments*, pages 474–505. Springer, 1994.

[38] Ralph E Hunter, Bruce M Richmond, and TAU Rho Alpha. Storm-controlled oblique dunes of the oregon coast. *Geological Society of America Bulletin*, 94(12):1450–1465, 1983.

[39] D. M. Rubin and R. E. Hunter. Why deposit of longitudinal dunes are rarely recognised in the geologic record. *Sedimentology*, 32:147–157, 1985.

[40] D. M. Rubin and R. E. Hunter. Bedform alignment in directionally varying flows. *Science*, 237:276–278, 1987.

[41] Sylvain Courrech du Pont, Clément Narteau, and Xin Gao. Two modes for dune orientation. *Geology*, 42(9):743–746, 2014.

[42] Patrick A Hesp. Conceptual models of the evolution of transgressive dune field systems. *Geomorphology*, 199:138–149, 2013.

[43] KJ Page. Riverine source bordering sand dune. *Australian Geographer*, 11(6):603–605, 1971.

[44] Donald Belcher, Joseph Veverka, and Carl Sagan. Mariner photography of mars and aerial photography of earth: Some analogies. *Icarus*, 15(2):241–252, 1971.

[45] JA Cutts and RSU Smith. Eolian deposits and dunes on mars. *Journal of Geophysical Research*, 78(20):4139–4154, 1973.

[46] Serina Diniega, Mikhail Kreslavsky, Jani Radebaugh, Simone Silvestro, Matt Telfer, and Daniela Tirsch. Our evolving understanding of aeolian bedforms, based on observation of dunes on different worlds. *Aeolian research*, 26:5–27, 2017.

[47] Rosalyn K Hayward, Kevin F Mullins, Lori K Fenton, Trent M Hare, Timothy N Titus, Mary C Bourke, Anthony Colaprete, and Philip R Christensen. Mars global digital dune database and initial science results. *Journal of Geophysical Research: Planets*, 112(E11), 2007.

[48] Paul Hesse. Sand seas. *Aeolian Geomorphology: A New Introduction*, pages 179–208, 2019.

[49] Giles Wiggs. Desert dunes: Form and process. *Aeolian Geomorphology: A New Introduction*, pages 133–155, 2019.

[50] Ryan C Ewing and G Kocurek. Aeolian dune-field pattern boundary conditions. *Geomorphology*, 114(3):175–187, 2010.

[51] Gary Kocurek and Ryan C Ewing. Trickle-down and trickle-up boundary conditions in eolian dune-field pattern formation. *SEPM special publication: Autogenic dynamics and self-organization in sedimentary systems*, 106:18–39, 2016.

[52] MW Telfer, PP Hesse, M Perez-Fernandez, RM Bailey, S Bajkan, and N Lancaster. Morphodynamics, boundary conditions and pattern evolution within a vegetated linear dunefield. *Geomorphology*, 290:85–100, 2017.

[53] Mohammed A Al-Masrahy and Nigel P Mountney. Remote sensing of spatial variability in aeolian dune and interdune morphology in the rub?al-khali, saudi arabia. *Aeolian Research*, 11:155–170, 2013.

[54] Xunming Wang, Zhibao Dong, Jiawu Zhang, and Guangting Chen. Geomorphology of sand dunes in the northeast taklimakan desert. *Geomorphology*, 42(3-4):183–195, 2002.

[55] G Kocurek, M Townsley, E Yeh, KG Havholm, and ML Sweet. Dune and dune-field development on padre island, texas, with implications for interdune deposition and water-table-controlled accumulation. *Journal of Sedimentary Research*, 62(4):622–635, 1992.

[56] Joanna M Nield and Giles FS Wiggs. The application of terrestrial laser scanning to aeolian saltation cloud measurement and its response to changing surface moisture. *Earth Surface Processes and Landforms*, 36(2):273–278, 2011.

[57] Hicham Elbelrhiti. Initiation and early development of barchan dunes: A case study of the moroccan atlantic sahara desert. *Geomorphology*, 138(1):181–188, 2012.

[58] Pauline Delorme, JM Nield, GFS Wiggs, MC Baddock, NR Bristow, JL Best, KT Christensen, and Philippe Claudin. Field evidence for the initiation of isolated aeolian sand patches. *Geophysical Research Letters*, page e2022GL101553, 2023.

[59] Donald August HOLM. Dome-shaped dunes of the central nejd, saudi arabia. *Comptes Rendus*, 7:107–112, 1953.

[60] A Warren. Dunes in the tenere desert. *Geographical Journal*, pages 458–461, 1971.

[61] A Warren. Observations on dunes and bi-modal sands in the ténéré desert. *Sedimentology*, 19(1-2):37–44, 1972.

[62] David M Rubin and Hiroshi Ikeda. Flume experiments on the alignment of transverse, oblique, and longitudinal dunes in directionally varying flows. *Sedimentology*, 37(4):673–684, 1990.

[63] E.J.R. Parteli, O. Duràn, H. Tsoar, V. Schwämmle, and H.J. Herrmann. Dune formation under bimodal winds. *PNAS*, 1106(52):22085–22089, 2009.

[64] Xin Gao, Clément Narteau, Olivier Rozier, and Sylvain Courrech du Pont. Phase diagrams of dune shape and orientation depending on sand availability. *Scientific reports*, 5(1):1–12, 2015.

[65] David M Rubin. A unifying model for planform straightness of ripples and dunes in air and water. *Earth-science reviews*, 113(3-4):176–185, 2012.

[66] Thomas S Ahlbrandt and Steven G Fryberger. Eolian deposits in the nebraska sand hills. 1980.

[67] Haim Tsoar. Sand dunes mobility and stability in relation to climate. *Physica A: Statistical Mechanics and its Applications*, 357(1):50–56, 2005.

[68] Andreas CW Baas and JM Nield. Modelling vegetated dune landscapes. *Geophysical Research Letters*, 34(6), 2007.

[69] Joanna M Nield and Andreas CW Baas. Investigating parabolic and nebkha dune formation using a cellular automaton modelling approach. *Earth Surface Processes and Landforms*, 33(5):724–740, 2008.

[70] Patrick A Hesp and Thomas AG Smyth. Nebkha flow dynamics and shadow dune formation. *Geomorphology*, 282:27–38, 2017.

[71] SM Arens and GEM Van der Lee. Saltation sand traps for the measurement of aeolian transport into the foredunes. *Soil Technology*, 8(1):61–74, 1995.

[72] Patrick Hesp. Foredunes and blowouts: initiation, geomorphology and dynamics. *Geomorphology*, 48(1-3):245–268, 2002.

[73] Luis Hernández-Calvento, Derek WT Jackson, Andrew Cooper, and Emma Pérez-Chacón. Island-encapsulating eolian sedimentary systems of the canary and cape verde archipelagos. *Journal of Sedimentary Research*, 87(2):117–125, 2017.

[74] Patrick A Hesp, Luis Hernández-Calvento, Juan B Gallego-Fernández, Graziela Miot da Silva, Antonio I Hernández-Cordero, Marie-Helene Ruz, and Levi García Romero. Nebkha or not?-climate control on foredune mode. *Journal of Arid Environments*, 187:104444, 2021.

[75] PD Jungerius. A simulation model of blowout development. *Earth surface processes and landforms*, 9(6):509–512, 1984.

[76] Edwin S Hills. The lunette, a new land form of aeolian origin. *Australian Geographer*, 3(7):15–21, 1940.

[77] Jim M Bowler. Clay dunes: their occurrence, formation and environmental significance. *Earth-Science Reviews*, 9(4):315–338, 1973.

[78] A Goudie and DSG Thomas. Lunette dunes in southern africa. *Journal of Arid Environments*, 10(1):1–12, 1986.

[79] Samantha E Saye, Kenneth Pye, and Lars B Clemmensen. Development of a cliff-top dune indicated by particle size and geochemical characteristics: Rubjerg knude, denmark. *Sedimentology*, 53(1):1–21, 2006.

[80] Ian Livingstone and Andrew Warren. *Aeolian Geomorphology: A New Introduction.* John Wiley & Sons, 2019.

[81] Ralph D Lorenz and James R Zimbelman. *Dune worlds: How windblown sand shapes planetary landscapes.* Springer Science & Business Media, 2014.

[82] Matt W Telfer, Eric JR Parteli, Jani Radebaugh, Ross A Beyer, Tanguy Bertrand, François Forget, Francis Nimmo, Will M Grundy, Jeffrey M Moore, S Alan Stern, et al. Dunes on pluto. *Science*, 360(6392):992–997, 2018.

[83] Pan Jia, Bruno Andreotti, and Philippe Claudin. Giant ripples on comet 67p/churyumov–gerasimenko sculpted by sunset thermal wind. *Proceedings of the National Academy of Sciences*, 114(10):2509–2514, 2017.

[84] George D McDonald, Joshua Méndez Harper, Lujendra Ojha, Paul Corlies, Josef Dufek, Ryan C Ewing, and Laura Kerber. Aeolian sediment transport on io from lava–frost interactions. *Nature communications*, 13(1):1–9, 2022.

[85] Rosalyn K Hayward, LK Fenton, and Timothy N Titus. Mars global digital dune database (mgd3): Global dune distribution and wind pattern observations. *Icarus*, 230:38–46, 2014.

[86] Mackenzie Day and Gary Kocurek. Pattern similarity across planetary dune fields. *Geology*, 46(11):999–1002, 2018.

[87] Matt Balme, Daniel C Berman, Mary C Bourke, and James R Zimbelman. Transverse aeolian ridges (tars) on mars. *Geomorphology*, 101(4):703–720, 2008.

[88] Daniel C Berman, Matthew R Balme, Scot CR Rafkin, and James R Zimbelman. Transverse aeolian ridges (tars) on mars ii: distributions, orientations, and ages. *Icarus*, 213(1):116–130, 2011.

[89] R Sullivan, JF Kok, I Katra, and H Yizhaq. A broad continuum of aeolian impact ripple morphologies on mars is enabled by low wind dynamic pressures. *Journal of Geophysical Research: Planets*, 125(10):e2020JE006485, 2020.

[90] Dong Zhang, Clément Narteau, Olivier Rozier, and Sylvain Courrech du Pont. Morphology and dynamics of star dunes from numerical modelling. *Nature Geoscience*, 2012.

[91] K. Taniguchi, N. Endo, and H. Sekiguchi. The effect of periodic changes in wind direction on the deformation and morphology of isolated sand dunes based on flume experiments and field data from the western sahara. *Geomorphology*, 179:286–299, 2012.

[92] Eric JR Parteli, Orencio Durán, Mary C Bourke, Haim Tsoar, Thorsten Pöschel, and Hans Herrmann. Origins of barchan dune asymmetry: Insights from numerical simulations. *Aeolian Research*, 12:121–133, 2014.

[93] David M Rubin, S Courrech du Pont, Clement Narteau, Claire E Newman, Nathan Bridges, and Mathieu Gaetan Andre Lapotre. Interpretation of wind regime of bagnold dunes in gale crater, guided by third-generation models of dune formation. In *AGU Fall Meeting Abstracts*, volume 2016, pages EP43D–05, 2016.

[94] Haim Tsoar and Eric JR Parteli. Bidirectional winds, barchan dune asymmetry and formation of seif dunes from barchans: a discussion. *Environmental Earth Sciences*, 75(18):1–10, 2016.

[95] DM Rubin and Ralph E Hunter. Reconstructing bedform assemblages from compound crossbedding. In *Developments in sedimentology*, volume 38, pages 407–427. Elsevier, 1983.

[96] David M Rubin and Carissa L Carter. *Bedforms 4.0: MATLAB code for simulating bedforms and cross-bedding.* US Geological Survey, 2005.

[97] Zhibao Dong, Zhenhai Wei, Guangqiang Qian, Zhengcai Zhang, Wanyin Luo, and Guangyin Hu. ?raked? linear dunes in the kumtagh desert, china. *Geomorphology*, 123(1-2):122–128, 2010.

[98] David M Rubin and Carissa L Carter. *Bedforms and cross-bedding in animation.* Number 2. SEPM (Society for Sedimentary Geology), 2006.

[99] DM Rubin and DS McCulloch. Single and superimposed bedforms: a synthesis of san francisco bay and flume observations. *Sedimentary Geology*, 26(1-3):207–231, 1980.

[100] Orencio Durán, Veit Schwämmle, Pedro G Lind, and Hans J Herrmann. The dune size distribution and scaling relations of barchan dune fields. *Granular Matter*, 11(1):7–11, 2009.

[101] Cyril Gadal, Pauline Delorme, Clément Narteau, Giles FS Wiggs, Matthew Baddock, Joanna M Nield, and Philippe Claudin. Local wind regime induced by giant linear dunes: comparison of era5-land reanalysis with surface measurements. *Boundary-Layer Meteorology*, 185(3):309–332, 2022.

[102] MGA Lapôtre, RC Ewing, CM Weitz, KW Lewis, MP Lamb, BL Ehlmann, and DM Rubin. Morphologic diversity of martian ripples: Implications for large-ripple formation. *Geophysical Research Letters*, 45(19):10–229, 2018.

[103] Dana Derickson, Gary Kocurek, Ryan C Ewing, and Charlie Bristow. Origin of a complex and spatially diverse dune-field pattern, algodones, southeastern california. *Geomorphology*, 99(1-4):186–204, 2008.

[104] Ryan C Ewing, George D McDonald, and Alex G Hayes. Multi-spatial analysis of aeolian dune-field patterns. *Geomorphology*, 240:44–53, 2015.

[105] Cyril Gadal, Clément Narteau, Ryan C Ewing, Andrew Gunn, Douglas Jerolmack, Bruno Andreotti, and Philippe Claudin. Spatial and temporal development of incipient dunes. *Geophysical Research Letters*, 47(16):e2020GL088919, 2020.

[106] CH Hugenholtz and SA Wolfe. Biogeomorphic model of dunefield activation and stabilization on the northern great plains. *Geomorphology*, 70(1-2):53–70, 2005.

[107] Carrie Beveridge, Gary Kocurek, Ryan C Ewing, Nicholas Lancaster, P Morthekai, Ashok K Singhvi, and Shannon A Mahan. Development of spatially diverse and complex dune-field patterns: Gran desierto dune field, sonora, mexico. *Sedimentology*, 53(6):1391–1409, 2006.

[108] Zhiwei Xu, Joseph A Mason, and Huayu Lu. Vegetated dune morphodynamics during recent stabilization of the mu us dune field, north-central china. *Geomorphology*, 228:486–503, 2015.

[109] Gary Kocurek, Ryan C Ewing, and David Mohrig. How do bedform patterns arise? new views on the role of bedform interactions within a set of boundary conditions. *Earth surface processes and landforms*, 35(1):51–63, 2010.

[110] Erin Eastwood, Joanna Nield, Andreas Baas, and Gary Kocurek. Modelling controls on aeolian dune-field pattern evolution. *Sedimentology*, 58(6):1391–1406, 2011.

[111] M Colin Marvin, Mathieu GA Lapôtre, Andrew Gunn, Mackenzie Day, and Alejandro Soto. Dune interactions record changes in boundary conditions. *Geology*, 2023.

[112] Stacey L Worman, A Brad Murray, Ryan Littlewood, Bruno Andreotti, and Philippe Claudin. Modeling emergent large-scale structures of barchan dune fields. *Geology*, 41(10):1059–1062, 2013.

[113] Noritaka Endo, Keisuke Taniguchi, and Atsunari Katsuki. Observation of the whole process of interaction between barchans by flume experiments. *Geophysical Research Letters*, 31(12), 2004.

[114] Pascal Hersen and Stéphane Douady. Collision of barchan dunes as a mechanism of size regulation. *Geophysical Research Letters*, 32(21), 2005.

[115] Hicham Elbelrhiti, Bruno Andreotti, and Philippe Claudin. Barchan dune corridors: field characterization and investigation of control parameters. *Journal of Geophysical Research: Earth Surface*, 113(F2), 2008.

[116] Mathieu Génois, Sylvain Courrech du Pont, Pascal Hersen, and Guillaume Grégoire. An agent-based model of dune interactions produces the emergence of patterns in deserts. *Geophysical Research Letters*, 40(15):3909–3914, 2013.

[117] Mathieu Génois, Pascal Hersen, Sylvain Courrech du Pont, and Guillaume Grégoire. Spatial structuring and size selection as collective behaviours in an agent-based model for barchan fields. *The European Physical Journal B*, 86:1–13, 2013.

[118] Mathieu Génois, Pascal Hersen, Eric Bertin, Sylvain Courrech du Pont, and Guillaume Grégoire. Out-of-equilibrium stationary states, percolation, and subcritical instabilities in a fully nonconservative system. *Physical Review E*, 94(4):042101, 2016.

[119] BT Werner and G Kocurek. Bed-form dynamics: Does the tail wag the dog? *Geology*, 25(9):771–774, 1997.

[120] Andreas CW Baas. Complex systems in aeolian geomorphology. *Geomorphology*, 91(3-4):311–331, 2007.

[121] Cyril Gadal, Clément Narteau, Sylvain Courrech du Pont, Olivier Rozier, and Philippe Claudin. Incipient bedforms in a bidirectional wind regime. *Journal of Fluid Mechanics*, 862:490–516, 2019.

[122] Erwan Reffet, Sylvain Courrech du Pont, Pascal Hersen, and Stéphane Douady. Formation and stability of transverse and longitudinal sand dunes. *Geology*, 39(6):491–494, 2010.

[123] Xin Gao, Cyril Gadal, Olivier Rozier, and Clément Narteau. Morphodynamics of barchan and dome dunes under variable wind regimes. *Geology*, 46(9):743–746, 2018.

[124] E.J.R. Parteli, J.S. Andrade, and H.J. Herrmann. Transverse instability of dunes. *Phys. Rev. Lett.*, 107:188001, 2011.

[125] L. Guignier, H. Niiya, H. Nishimori, D. Lague, and A. Valance. Sand dunes as migrating strings. *Phys. Rev E*, 87:052206, 2013.

[126] Ping Lü, Clément Narteau, Zhibao Dong, Olivier Rozier, and Sylvain Courrech du Pont. Unravelling raked linear dunes to explain the coexistence of bedforms in complex dunefields. *Nature communications*, 8(1):1–9, 2017.

[127] Felix M Exner. *Zur physik der dünen.* Hölder, 1920.

[128] Felix M Exner. *Über die Wechselwirkung zwischen Wasser und Geschiebe in Flüssen: Gedr. mit Unterstützg aus d. Jerome u. Margaret Stonborough-Fonds.* Hölder-Pichler-Tempsky, A.-G., 1925.

[129] Chris Paola and Vaughan R Voller. A generalized exner equation for sediment mass balance. *Journal of Geophysical Research: Earth Surface*, 110(F4), 2005.

[130] Bruno Andreotti, Philippe Claudin, and Olivier Pouliquen. Measurements of the aeolian sand transport saturation length. *Geomorphology*, 123(3-4):343–348, 2010.

[131] Ping Lü, Clément Narteau, Zhibao Dong, Philippe Claudin, Sébastien Rodriguez, Zhishan An, Laura Fernandez-Cascales, Cyril Gadal, and Sylvain Courrech du Pont. Direct validation of dune instability theory. *Proceedings of the National Academy of Sciences*, 118(17), 2021.

[132] Houssam Selmani, Alexandre Valance, A Ould El Moctar, Pascal Dupont, and Rabeh Zegadi. Aeolian sand transport in out-of-equilibrium regimes. *Geophysical Research Letters*, 45(4):1838–1844, 2018.

[133] Mohammadreza Kadivar, David Tormey, and Gerard McGranaghan. A review on turbulent flow over rough surfaces: Fundamentals and theories. *International Journal of Thermofluids*, 10:100077, 2021.

[134] Philippe Claudin, Orencio Durán, and Bruno Andreotti. Dissolution instability and roughening transition. *Journal of Fluid Mechanics*, 832, 2017.

[135] O. Duràn, P. Claudin, and B. Andreotti. On aeolian transport: Grain-scale interactions, dynamical mechanisms and scaling laws. *Aeolian Research*, 3:243–270, 2011.

[136] M Bordiec, S Carpy, O Bourgeois, C Herny, M Massé, L Perret, P Claudin, S Pochat, and Sylvain Douté. Sublimation waves: Geomorphic markers of interactions between icy planetary surfaces and winds. *Earth-Science Reviews*, 211:103350, 2020.

[137] Orencio Durán Vinent, Bruno Andreotti, Philippe Claudin, and Christian Winter. A unified model of ripples and dunes in water and planetary environments. *Nature Geoscience*, 12(5):345–350, 2019.

[138] Thomas J Hanratty. Stability of surfaces that are dissolving or being formed by convective diffusion. *Annual Review of Fluid Mechanics*, 13(1):231–252, 1981.

[139] Lior Rubanenko, Mathieu GA Lapôtre, Ryan C Ewing, Lori K Fenton, and Andrew Gunn. A distinct ripple-formation regime on mars revealed by the morphometrics of barchan dunes. *Nature Communications*, 13(1):7156, 2022.

[140] Philippe Claudin and Bruno Andreotti. A scaling law for aeolian dunes on mars, venus, earth, and for subaqueous ripples. *Earth and Planetary Science Letters*, 252:30, 2006.

[141] François Charru, Bruno Andreotti, and Philippe Claudin. Sand ripples and dunes. *Annual Review of Fluid Mechanics*, 45:469–493, 2013.

[142] Mathieu GA Lapôtre, Ryan C Ewing, and Michael P Lamb. An evolving understanding of enigmatic large ripples on mars. *Journal of Geophysical Research: Planets*, 126(2):e2020JE006729, 2021.

[143] BT Werner and G Kocurek. Bedform spacing from defect dynamics. *Geology*, 27(8):727–730, 1999.

[144] Bruno Andreotti, Antoine Fourriere, Fouzia Ould-Kaddour, Brad Murray, and Philippe Claudin. Giant aeolian dune size determined by the average depth of the atmospheric boundary layer. *Nature*, 457(7233):1120–1123, 2009.

[145] Andrew Gunn, Giampietro Casasanta, Luca Di Liberto, Federico Falcini, Nicholas Lancaster, and Douglas J Jerolmack. What sets aeolian dune height? *Nature Communications*, 13(1):2401, 2022.

[146] Andrew Gunn. Formation and reorganization time scales of aeolian landscapes. *Geology*, 51(4):351–355, 2023.

[147] Nicholas Lancaster, Gary Kocurek, Ashok Singhvi, V Pandey, Max Deynoux, Jean-Francois Ghienne, and Khalidou Lô. Late pleistocene and holocene dune activity and wind regimes in the western sahara desert of mauritania. *Geology*, 30(11):991–994, 2002.

[148] Andreas CW Baas and Lucie A Delobel. Desert dunes transformed by end-of-century changes in wind climate. *Nature Climate Change*, 12(11):999–1006, 2022.

[149] Joseph A Mason, James B Swinehart, Paul R Hanson, DB Loope, Ronald J Goble, Xiaodong Miao, and Rebecca L Schmeisser. Late pleistocene dune activity in the central great plains, usa. *Quaternary Science Reviews*, 30(27-28):3858–3870, 2011.

[150] Patrick A Hesp and Thomas AG Smyth. Anchored dunes. *Aeolian geomorphology: a new introduction*, pages 157–178, 2019.

[151] A. C. Benjumea-Lopez and Patrick A Hesp. Evolution of a coastal transgressive dunefield to a parabolic dunefield, canunda dunes, south australia. *Geomorphology*, 430:108653, 2023.

[152] EDWIN D McKEE. Structures of dunes at white sands national monument, new mexico (and a comparison with structures of dunes from other selected areas) 1. *Sedimentology*, 7(1):3–69, 1966.

[153] Steven G Fryberger. Geological overview of white sands national monument. *A viable from: http://www. nps. gov/whsa*, 2000.

[154] Gary Kocurek, Mary Carr, Ryan Ewing, Karen G Havholm, YC Nagar, and AK Singhvi. White sands dune field, new mexico: age, dune dynamics and recent accumulations. *Sedimentary Geology*, 197(3-4):313–331, 2007.

[155] Ryan C Ewing. White sands. *Inland Dunes of North America*, pages 207–237, 2020.

[156] Vance T Holliday, Matthew Cuba, Wayne Lee, Jason Windingstad, Brendan Fenerty, and David Bustos. Onset of dune construction based on archaeological evidence, white sands, new mexico. *Quaternary Research*, pages 1–9, 2023.

[157] JD Phillips, RC Ewing, R Bowling, Bradley A Weymer, P Barrineau, JA Nittrouer, and ME Everett. Low-angle eolian deposits formed by protodune migration, and insights into slipface development at white sands dune field, new mexico. *Aeolian Research*, 36:9–26, 2019.

[158] O. Duràn and H. Herrmann. Modeling of saturated sand flux. *Journal of Statistical Mechanics: Theory and Experiment*, 2006.

[159] Meredith D Reitz, Douglas J Jerolmack, Ryan C Ewing, and Raleigh L Martin. Barchan-parabolic dune pattern transition from vegetation stability threshold. *Geophysical Research Letters*, 37(19), 2010.

[160] Douglas J Jerolmack, Ryan C Ewing, Federico Falcini, Raleigh L Martin, Claire Masteller, Colin Phillips, Meredith D Reitz, and Ilya Buynevich. Internal boundary layer model for the evolution of desert dune fields. *Nature Geoscience*, 5(3):206–209, 2012.

[161] Richard P Langford, Jessica M Rose, and Diane E White. Groundwater salinity as a control on development of eolian landscape: An example from the white sands of new mexico. *Geomorphology*, 105(1-2):39–49, 2009.

[162] Andrew Gunn, Phillip Schmutz, Matt Wanker, DA Edmonds, RC Ewing, and Douglas J Jerolmack. Macroscopic flow disequilibrium over aeolian dune fields. *Geophysical Research Letters*, 47(18):e2020GL088773, 2020.

[163] RWG Carter, PA Hesp, and K Nordstrom. Geomorphology of erosional dune landscapes. *Coastal dunes: Processes and morphology*, pages 217–250, 1990.

[164] Thomas E Barchyn and Chris H Hugenholtz. Reactivation of supply-limited dune fields from blowouts: A conceptual framework for state characterization. *Geomorphology*, 201:172–182, 2013.

[165] Lü Ping, Clément Narteau, Zhibao Dong, Zhengcai Zhang, and Sylvain Courrech du Pont. Emergence of oblique dunes in a landscape-scale experiment. *Nature Geoscience*, 7(2):99–103, 2014.

[166] Hans Hersbach, W Bell, P. Berrisford, A. Horányi, J. Muñoz-Sabater, J. Nicolas, R. Radu, D. Schepers, A. Simmons, C. Soci, and D. Dee. Global reanalysis: goodbye ERA-Interim, hello ERA5. *ECMWF Newsl*, pages 17–24, 04 2019.

[167] Joaquín Muñoz-Sabater, Emanuel Dutra, Anna Agustí-Panareda, Clément Albergel, Gabriele Arduini, Gianpaolo Balsamo, Souhail Boussetta, Margarita Choulga, Shaun Harrigan, Hans Hersbach, et al. Era5-land: A state-of-the-art global reanalysis dataset for land applications. *Earth System Science Data*, 13(9):4349–4383, 2021.

[168] Steven G Fryberger and Gary Dean. Dune Forms and Wind Regime. *A Study of Global Sand Seas*, 1052:137–169, 1979.

[169] Kim I Pearce and Ian J Walker. Frequency and magnitude biases in the 'Fryberger' model, with implications for characterizing geomorphically effective winds. *Geomorphology*, 68(1):39–55, 2005.

[170] P.S. Jackson and J.C.R. Hunt. Turbulent wind flow over a low hill. *Quart. J. R. Met. Soc.*, 101:929–955, 1975.

[171] Antoine Lucas, Clément Narteau, Sébastien Rodriguez, Olivier Rozier, Yann Callot, Amandine Garcia, and S. Courrech du Pont. Sediment flux from the morphodynamics of elongating linear dunes. *Geology*, 43:1027–1030, 2015.

[172] Pascal Hersen. Flow effects on the morphology and dynamics of aeolian and subaqueous barchan dunes. *Journal of Geophysical Research: Earth Surface*, 110(F4), 2005.

[173] Olivier Rozier, Clément Narteau, Cyril Gadal, Philippe Claudin, and Sylvain Courrech du Pont. Elongation and stability of a linear dune. *Geophysical Research Letters*, 46(24):14521–14530, 2019.

[174] Serge Kiki Sandoungout. *Caractérisation de la morphologie des dunes dans des écoulements unidirectionnels et alternatifs*. PhD thesis, Université de Bretagne occidentale-Brest, 2019.

[175] Xin Gao, Clément Narteau, and Cyril Gadal. Migration of reversing dunes against the sand flow path as a singular expression of the speed-up effect. *Journal of Geophysical Research: Earth Surface*, 126(5):e2020JF005913, 2021.

[176] Sachi Nakao-Kusune, Takahiro Sakaue, Hiraku Nishimori, and Hiizu Nakanishi. Stabilization of a straight longitudinal dune under bimodal wind with large directional variation. *Physical Review E*, 101(1):012903, 2020.

[177] Cyril Gadal, Clément Narteau, Sylvain Courrech du Pont, Olivier Rozier, and Philippe Claudin. Periodicity in fields of elongating dunes. *Geology*, 48(4):343–347, 2020.

[178] H Tsoar. The formation of seif dunes from barchans-a discussion. *Zeitschrift fur Geomorphologie*, 28(1):99–103, 1984.

[179] Ping Lv, Zhibao Dong, Clement Narteau, and Olivier Rozier. Morphodynamic mechanisms for the formation of asymmetric barchans: improvement of the bagnold and tsoar models. *Environmental Earth Sciences*, 75:1–9, 2016.

[180] Mary C Bourke. Barchan dune asymmetry: Observations from mars and earth. *Icarus*, 205(1):183–197, 2010.

[181] Zhengcai Zhang, Zhibao Dong, Guangyin Hu, and Eric JR Parteli. Migration and morphology of asymmetric barchans in the central hexi corridor of northwest china. *Geosciences*, 8(6):204, 2018.

[182] Alexandre Valance, Keld Rømer Rasmussen, Ahmed Ould El Moctar, and Pascal Dupont. The physics of aeolian sand transport. *Comptes Rendus Physique*, 16(1):105–117, 2015.

[183] Pauline Delorme, Giles FS Wiggs, Matthew C Baddock, Philippe Claudin, Joanna M Nield, and Andrew Valdez. Dune initiation in a bimodal wind regime. *Journal of Geophysical Research: Earth Surface*, 125(11):e2020JF005757, 2020.

[184] Bruno Andreotti, Philippe Claudin, Jens Jacob Iversen, Jonathan P Merrison, and Keld R Rasmussen. A lower-than-expected saltation threshold at martian pressure and below. *Proceedings of the National Academy of Sciences*, 118(5):e2012386118, 2021.

[185] Thomas Pähtz, Jasper F Kok, Eric JR Parteli, and Hans J Herrmann. Flux saturation length of sediment transport. *Physical review letters*, 111(21):218002, 2013.

[186] Ryan C Ewing, Mathieu GA Lapotre, KW Lewis, M Day, N Stein, David M Rubin, R Sullivan, S Banham, MP Lamb, NT Bridges, et al. Sedimentary processes of the bagnold dunes: Implications for the eolian rock record of mars. *Journal of Geophysical Research: Planets*, 122(12):2544–2573, 2017.

[187] Mathieu GA Lapotre, Michael P Lamb, and Brandon McElroy. What sets the size of current ripples? *Geology*, 45(3):243–246, 2017.

[188] Xinting Yu, Sarah M Hörst, Chao He, Patricia McGuiggan, and Bryan Crawford. Where does titan sand come from: insight from mechanical properties of titan sand candidates. *Journal of Geophysical Research: Planets*, 123(9):2310–2321, 2018.

[189] S Rodriguez, Stéphane Le Mouélic, Jason W Barnes, JF Kok, SCR Rafkin, Ralph D Lorenz, B Charnay, J Radebaugh, C Narteau, Thomas Cornet, et al. Observational evidence for active dust storms on titan at equinox. *Nature Geoscience*, 11(10):727–732, 2018.

[190] R Greeley, J Iversen, R Leach, J Marshall, B White, and S Williams. Windblown sand on venus: Preliminary results of laboratory simulations. *Icarus*, 57(1):112–124, 1984.

[191] Andrew Warren and David Allison. The palaeoenvironmental significance of dune size hierarchies. *Palaeogeography, Palaeoclimatology, Palaeoecology*, 137(3-4):289–303, 1998.

[192] Gary Kocurek and Ryan C Ewing. Aeolian dune field self-organization–implications for the formation of simple versus complex dune-field patterns. *Geomorphology*, 72(1-4):94–105, 2005.

[193] Klaus Kroy, Gerd Sauermann, and Hans J Herrmann. Minimal model for aeolian sand dunes. *Physical Review E*, 66(3):031302, 2002.

[194] WS Chepil. Dynamics of wind erosion: Ii. initiation of soil movement. *Soil science*, 60(5):397, 1945.

[195] R Greeley, R Leach, B White, J Iversen, and J Pollack. Threshold windspeeds for sand on mars: Wind tunnel simulations. *Geophysical Research Letters*, 7(2):121–124, 1980.

[196] C Swann, DJ Sherman, and RC Ewing. Experimentally derived thresholds for windblown sand on mars. *Geophysical Research Letters*, 47(3):e2019GL084484, 2020.

[197] Thomas Pähtz and Orencio Durán. Unification of aeolian and fluvial sediment transport rate from granular physics. *Physical Review Letters*, 124(16):168001, 2020.

[198] Orencio Durán, Bruno Andreotti, and Philippe Claudin. Numerical simulation of turbulent sediment transport, from bed load to saltation. *Physics of Fluids*, 24(10):103306, 2012.

[199] Raleigh L Martin and Jasper F Kok. Wind-invariant saltation heights imply linear scaling of aeolian saltation flux with shear stress. *Science advances*, 3(6):e1602569, 2017.

[200] P.R. Owen. Saltation of uniform grains in air. *J. Fluid Mech.*, 20:225–242, 1964.

[201] J.E. Ungar and P.K. Haff. Steady state saltation in air. *Sedimentology*, 34:289–299, 1987.

[202] Keld Rømer Rasmussen, James D Iversen, and Patrik Rautahemio. Saltation and wind-flow interaction in a variable slope wind tunnel. *Geomorphology*, 17(1-3):19–28, 1996.

[203] Mathieu Creyssels, Pascal Dupont, A Ould El Moctar, Alexandre Valance, Isabelle Cantat, James Thomas Jenkins, José Miguel Pasini, and Keld Rømer Rasmussen. Saltating particles in a turbulent boundary layer: experiment and theory. *Journal of Fluid Mechanics*, 625:47–74, 2009.

[204] Tuan Duc Ho, Alexandre Valance, Pascal Dupont, and A Ould El Moctar. Scaling laws in aeolian sand transport. *Physical Review Letters*, 106(9):094501, 2011.

[205] Andrew Gunn and Douglas J Jerolmack. Conditions for aeolian transport in the solar system. *Nature Astronomy*, pages 1–7, 2022.

[206] Yaping Shao and MR Raupach. The overshoot and equilibration of saltation. *Journal of Geophysical Research: Atmospheres*, 97(D18):20559–20564, 1992.

[207] Philippe Claudin, François Charru, and Bruno Andreotti. Transport relaxation time and length scales in turbulent suspensions. *Journal of Fluid Mechanics*, 671:491–506, 2011.

[208] Thomas Pähtz, Eric JR Parteli, Jasper F Kok, and Hans J Herrmann. Analytical model for flux saturation in sediment transport. *Physical Review E*, 89(5):052213, 2014.

[209] Thomas Pähtz, Amir Omeradžić, Marcus V Carneiro, Nuno AM Araújo, and Hans J Herrmann. Discrete element method simulations of the saturation of aeolian sand transport. *Geophysical Research Letters*, 42(6):2063–2070, 2015.

[210] Thomas Pähtz and Orencio Durán. Fluid forces or impacts: What governs the entrainment of soil particles in sediment transport mediated by a newtonian fluid? *Physical Review Fluids*, 2(7):074303, 2017.

[211] Jasper F Kok, Eric JR Parteli, Timothy I Michaels, and Diana Bou Karam. The physics of wind-blown sand and dust. *Reports on progress in Physics*, 75(10):106901, 2012.

[212] James D Iversen and Keld Rømer Rasmussen. The effect of surface slope on saltation threshold. *Sedimentology*, 41(4):721–728, 1994.

[213] Zhibao Dong, Ping Lv, Zhengcai Zhang, Guangqiang Qian, and Wanyin Luo. Aeolian transport in the field: A comparison of the effects of different surface treatments. *Journal of Geophysical Research: Atmospheres*, 117(D9), 2012.

[214] RE Britter, JCR Hunt, and KJ Richards. Air flow over a two-dimensional hill: studies of velocity speed-up, roughness effects and turbulence. *Quarterly Journal of the Royal Meteorological Society*, 107(451):91–110, 1981.

[215] Giles FS Wiggs, Ian Livingstone, and Andrew Warren. The role of streamline curvature in sand dune dynamics: evidence from field and wind tunnel measurements. *Geomorphology*, 17(1):29–46, 1996.

[216] I.J. Walker and W.G. Nickling. Simulation and measurement of surface shear stress over isolated and closely spaced transverse dunes in a wind tunnel. *Earth Surface Processes and Landforms*, 28:1111–1124, 2003.

[217] I.J. Walker, P.A. Hesp, R.G.D. Davidson-Arnott, B.O. Bauer, S.L. Namikas, and J. Ollerhead. Response of three-dimensional flow to variations in the angle of incident wind and profile form of dunes: Greenwich dunes, prince edward island, canada. *Geomorphology*, 105:127–138, 2009.

[218] Philippe Claudin, GFS Wiggs, and Bruno Andreotti. Field evidence for the upwind velocity shift at the crest of low dunes. *Boundary-layer meteorology*, 148(1):195–206, 2013.

[219] Sylvain Courrech du Pont. Dune morphodynamics. *Comptes Rendus Physique*, 16(1):118–138, 2015.

[220] C McKenna Neuman, N Lancaster, and WG Nickling. Relations between dune morphology, air flow, and sediment flux on reversing dunes, Silver Peak, Nevada. *Sedimentology*, 44(6):1103–1111, 1997.

[221] H. Tsoar. Dynamic processes acting on a longitudinal (seif) sand dune. *Sedimentology*, 30(4):567–578, 1983.

[222] H. Tsoar and Yaalon D.H. Deflection of sand movement on a sinuous longitudinal (self) dune: use of fluorescent dye as tracer. *Sedimentary Geology*, 36:25–39, 1983.

[223] I.J. Walker and W.G. Nickling. Dynamics of secondary airflow and sediment transport over and in the lee of transverse dunes. *Progress in Physical Geography*, 26:47–75, 2002.

[224] I.J. Walker and D.H. Shugar. Secondary flow deflection in the lee of transverse dunes with implications for dune morphodynamics and migration. *Earth Surface Processes and Landforms*, 2013.

[225] Pascal Hersen. On the crescentic shape of barchan dunes. *The European Physical Journal B-Condensed Matter and Complex Systems*, 37:507–514, 2004.

[226] Ping Lü, Clément Narteau, Zhibao Dong, Philippe Claudin, Sébastien Rodriguez, Zhishan An, Cyril Gadal, and Sylvain Courrech du Pont. Coexistence of two dune growth mechanisms in a landscape-scale experiment. *Geophysical Research Letters*, 49(11):e2021GL097636, 2022.

[227] Michael P Schultz and Karen A Flack. Turbulent boundary layers on a systematically varied rough wall. *Physics of Fluids*, 21(1):015104, 2009.

[228] Karen A Flack and Michael P Schultz. Review of hydraulic roughness scales in the fully rough regime. *Journal of fluids engineering*, 132(4), 2010.

[229] B. Andreotti, P. Claudin, and S. Douady. Selection of dune shapes and velocities part 2: A two-dimensional modeling. *The european physical Journal B*, 28:341–352, 2002.

[230] Antoine Fourriere, Philippe Claudin, and Bruno Andreotti. Bedforms in a turbulent stream: formation of ripples by primary linear instability and of dunes by nonlinear pattern coarsening. *Journal of Fluid Mechanics*, 649:287–328, 2010.

[231] Edward R Van Driest. On turbulent flow near a wall. *Journal of the aeronautical sciences*, 23(11):1007–1011, 1956.

[232] Daniel P Zilker, Gerald W Cook, and Thomas J Hanratty. Influence of the amplitude of a solid wavy wall on a turbulent flow. part 1. non-separated flows. *Journal of Fluid Mechanics*, 82(1):29–51, 1977.

[233] Jonathan Abrams and Thomas J Hanratty. Relaxation effects observed for turbulent flow over a wavy surface. *Journal of Fluid Mechanics*, 151:443–455, 1985.

[234] Kenneth Arthur Frederick and Thomas J Hanratty. Velocity measurements for a turbulent nonseparated flow over solid waves. *Experiments in fluids*, 6(7):477–486, 1988.

[235] Charles B Thorsness and Thomas J Hanratty. Stability of dissolving or depositing surfaces. *AIChE Journal*, 25(4):697–701, 1979.

[236] Timothy S Sullivan, Yuanming Liu, and Robert E Ecke. Turbulent solutal convection and surface patterning in solid dissolution. *Physical Review E*, 54(1):486, 1996.

[237] Florence Haudin, Luis Atilio Riolfo, Bernard Knaepen, GM Homsy, and Anne De Wit. Experimental study of a buoyancy-driven instability of a miscible horizontal displacement in a hele-shaw cell. *Physics of fluids*, 26(4):044102, 2014.

[238] Caroline Cohen, Michael Berhanu, Julien Derr, and Sylvain Courrech du Pont. Erosion patterns on dissolving and melting bodies. *Physical Review Fluids*, 1(5):050508, 2016.

[239] Benjamin Favier, Jhaswantsing Purseed, and Laurent Duchemin. Rayleigh–bénard convection with a melting boundary. *Journal of Fluid Mechanics*, 858:437–473, 2019.

[240] Caroline Cohen, Michael Berhanu, Julien Derr, and Sylvain Courrech du Pont. Buoyancy-driven dissolution of inclined blocks: Erosion rate and pattern formation. *Physical Review Fluids*, 5(5):053802, 2020.

[241] JRL Allen. Bed forms due to mass transfer in turbulent flows: a kaleidoscope of phenomena. *Journal of Fluid Mechanics*, 49(1):49–63, 1971.

[242] Paul N Blumberg and Rane L Curl. Experimental and theoretical studies of dissolution roughness. *Journal of Fluid Mechanics*, 65(4):735–751, 1974.

[243] Benoit Villien, Ying Zheng, and Derek Lister. Surface dissolution and the development of scallops. *Chem. Eng. Comm.*, 192(1):125–136, 2005.

[244] George D Ashton and John F Kennedy. Ripples on underside of river ice covers. *Journal of the Hydraulics Division*, 98(9):1603–1624, 1972.

[245] RR Gilpin, T Hirata, and KC Cheng. Wave formation and heat transfer at an ice-water interface in the presence of a turbulent flow. *Journal of Fluid Mechanics*, 99(3):619–640, 1980.

[246] Mitchell Bushuk, David M Holland, Timothy P Stanton, Alon Stern, and Callum Gray. Ice scallops: a laboratory investigation of the ice–water interface. *Journal of fluid mechanics*, 873:942–976, 2019.

[247] Rane L Curl. Scallops and flutes. 1966.

[248] Rane L Curl. Deducing flow velocity in cave conduits from scallops. 1974.

[249] Andrew Gunn, Matthew Wanker, Nicholas Lancaster, Douglas A Edmonds, Ryan C Ewing, and Douglas J Jerolmack. Circadian rhythm of dune-field activity. *Geophysical Research Letters*, 48(5):e2020GL090924, 2021.

[250] Roland B Stull. *An introduction to boundary layer meteorology*, volume 13. Springer Science & Business Media, 1988.

[251] SB Vosper. Inversion effects on mountain lee waves. *Quarterly Journal of the Royal Meteorological Society: A journal of the atmospheric sciences, applied meteorology and physical oceanography*, 130(600):1723–1748, 2004.

[252] Qingfang Jiang. Applicability of reduced-gravity shallow-water theory to atmospheric flow over topography. *Journal of the Atmospheric Sciences*, 71(4):1460–1479, 2014.

[253] JCR Hunt, GG Vilenski, and ER Johnson. Stratified separated flow around a mountain with an inversion layer below the mountain top. *Journal of Fluid Mechanics*, 556:105–119, 2006.